Politechnika Wrocławska

WYDZIAŁ PODSTAWOWYCH PROBLEMÓW TECHNIKI

ILOŚCIOWA ANALIZA EEG PACJENTÓW Z NAPADAMI NIEŚWIADOMOŚCI

PAWEŁ GŁĄBA

Rozprawa doktorska wykonana pod kierunkiem

dra hab. Mirosława Łątki, prof. uczelni

Czerwiec 2023

Wrocław

Serdecznie dziękuję

Panu dr. hab. Mirosławowi Łątce, prof. uczelni

za szansę, zaufanie, wyrozumiałość,

poświęcony mi czas

oraz ogromne zaangażowanie.

Dr n. med. Małgorzacie Krauze

oraz mgr inż. Marcie Kuryło za owocną współpracę

oraz bezcenną bazę zapisów EEG.

Rodzinie, w szczególności żonie oraz rodzicom,

za cierpliwość i wsparcie w trudnych momentach.

1. Spis treści

2. Streszczenie

Napady nieświadomości są to spontaniczne, krótkie (trwające od kilku do kilkunastu sekund), uogólnione napady epileptyczne. Ich charakterystyczną manifestacją jest utrata świadomości oraz obecność w zapisie EEG kompleksów iglica-fala wolna (SWD, z ang. spike and wave discharges). Takie wyładowania w przypadku napadów nieświadomości są regularne (około 3 Hz), symetryczne i ich obecność jest ważnym kryterium diagnostycznym. Według oficjalnej definicji Międzynarodowej Ligi Przeciwko Epilepsji napady nieświadomości można podzielić na dziecięce napady nieświadomości (CAE z ang. childhood absence epilepsy), młodzieńcze napady nieświadomości (JAE z ang. juvenile absence epilepsy), oraz rzadsze młodzieńcze mioklonicznе napady nieświadomości (JME z ang. juvenile myoclonic epilepsy) i uogólnione toniczno-mioklonicznе napady nieświadomości (GTCA z ang. generalized tonic clonic seizure). W przypadku nieleczonych pacjentów mogą one zostać wywołane przez hiperwentylację, deprywację snu czy gry wideo.

W niniejszej pracy przedstawiono problemy związane z diagnozą napadów nieświadomości i ich automatyczną detekcją w zapisach elektroencefalograficznych (EEG). Przedyskutowano możliwości monitorowania postępów farmakoterapii oraz ilościowej charakteryzacji morfologii napadów nieświadomości. Wyniki badań zostały szczegółowo omówione w trzech opublikowanych artykułach.

Pierwsza praca *Changes in Interictal Pretreatment and Posttreatment EEG in Childhood Absence Epilepsy* [1] poświęcona została zmianom w międzynapadowych fragmentach zapisów EEG u pacjentów z napadami nieświadomości. Do badań wykorzystano transformatę falkową z funkcją bazową Morleta. W pracy wykazano znaczące różnice mocy falkowej pacjentów w paśmie beta oraz theta w porównaniu do grupy kontrolnej. Ponadto sformułowano hipotezę głoszącą, że podniesiona moc falkowa w paśmie theta i beta jest odpowiednio wynikiem ponadnormatywnej aktywności mózgu i skłonności do generowania iglic padaczkowych. Wyniki te są zgodne z teorią nadpobudliwości kory mózgowej tłumaczącą patofizjologię napadów nieświadomości. Analiza sygnałów EEG pacjentów po leczeniu wykazała istotny

spadek wartości mocy falkowych, zwłaszcza w niskich częstotliwościach. Jest to pierwszy krok w opracowaniu metody monitorowania postępów farmakoterapii z możliwością indywidualnego miareczkowania leków.

Druga publikacja *Absence Seizure Detection Algorithm for Portable EEG Devices* [2] przedstawia możliwości automatycznej detekcji napadów nieświadomości przy użyciu mobilnego urządzenia EEG. Wykrywanie oparto o właściwości ciągłej transformaty falkowej w paśmie delta oraz beta. Wykorzystując zaledwie cztery odprowadzenia, uzyskano skuteczność na poziomie 97,6% z zaledwie 0,7 fałszywymi detekcjami na godzinę. Pojawienie się niedrogich, przenośnych urządzeń EEG utorowało drogę do długoterminowego, zdalnego monitorowania pacjentów z CAE i JAE. Potencjalne korzyści z tego rodzaju monitorowania to ułatwienie diagnozy, spersonalizowane miareczkowanie leków oraz określenie czasu trwania farmakoterapii.

Ostatnia praca *EEG phase synchronization during absence seizures* opisuje zmiany synchronizacji EEG podczas napadów nieświadomości. Do analizy wykorzystano jednosekundowe okna z półsekundowym krokiem. Współczynnik synchronizacji obliczany był za pomocą ciągłej transformaty falkowej z funkcją bazową Morleta. Dla 19 kanałowego EEG, klasyfikator k-NN (z ang. k-nearest neighbors), który wykorzystywał współczynnik synchronizacji i znormalizowaną amplitudę EEG jako cechy wykrył 99,2% napadów nieświadomości. Pokrycie segmentów sklasyfikowanych jako napadowe z zarejestrowanymi napadami wyniosło jedynie 82,9%. Niepełne pokrycie wynika z trywialnego efektu skończonej rozdzielczości segmentacji EEG, ale przede wszystkim, z fragmentacji napadów nieświadomości. To drugie zjawisko zostało po raz pierwszy ilościowo opisane i może posłużyć do lepszego rozróżnienia CAE i JAE.

3. Abstract

Typical absence seizures are spontaneous, short (lasting several seconds), and generalized epileptic seizures. Their characteristic manifestations are the loss of consciousness and the presence of spike and wave discharges (SWD) complexes in the EEG record. These are regular (about 3 Hz), and symmetrical discharges which are the main diagnostic criterion. According to the official definition of the International League Against Epilepsy, absence seizures can be divided into childhood absence epilepsy (CAE), juvenile absence seizures (JAE), the less common juvenile myoclonic absence seizures (JME), and generalized tonic-myoclonic absence seizures (GTCA). In untreated patients, they can be provoked by hyperventilation, sleep deprivation or video games.

This doctoral thesis summarizes the results presented in three scientific papers [1-3] published in the international journals. In particular, I discuss the problems in diagnosis of absence seizures, their automatic detection in electroencephalographic recordings, assessment of the efficacy of pharmacotherapy, and quantitative characterization of the morphology of seizures.

In the first paper *Changes in Interictal Pretreatment and Posttreatment EEG in Childhood Absence Epilepsy* [1] I employed the Morlet wavelet transform to show significant differences in the power of the beta and theta bands in the patients and control group. In addition, a hypothesis was formulated that the increased power in these bands observed in the patients results from abnormal brain activity and the propensity to generate epileptic spikes, respectively. These results are consistent with the theory of cortical focus theory explaining the pathophysiology of absence seizures. The increased wavelet power in the above-mentioned bands could be treated as a biomarker of absence seizure epilepsy. The analysis of follow-up EEG records showed a significant decrease in wavelet powers, especially in low frequencies**.** This is the first step in developing a method for monitoring the progress of pharmacotherapy with the possibility of personalized drug titration.

The second publication *Absence Seizure Detection Algorithm for Portable EEG Devices* [2] explores the possibilities of automatic detection of absence seizures

using a mobile EEG device. The detection was based on the properties of the continuous wavelet transform in the delta and beta bands. Using only four electrodes, 97.6% of ictal EEG was correctly identified with the false detection rate equal to 0.7 per hour. The appearance of low-cost, portable EEG devices has paved the way for long-term, remote monitoring of CAE and JAE patients. Potential benefits of this type of monitoring include facilitating diagnosis, personalized drug titration, and determining the duration of pharmacotherapy.

The last paper in the series, *EEG phase synchronization during absence seizures* [3], describes changes in EEG synchronization index during absence seizures. A one-second windows with a half-second overlap were used to calculate the Morlet wavelet phase synchronization index. For the 19-channel EEG, the k-NN classifier which employed the synchronization index and the normalized EEG amplitude as the features detected 99.2% of the seizures. Interestingly enough, the overlap of the segments classified as ictal with the actual seizures was equal to only 82.9%. The incomplete overlap is due to the trivial effect of finite resolution of EEG segmentation and, most importantly, fragmentation of absence seizures. This phenomenon has been quantitatively described for the first time and could be used to distinguish CAE and JAE.

4. Wstęp

Epilepsja jest najczęściej występującą chorobą mózgu dotykającą ponad 46 milionów ludzi na świecie (Beghi et al., 2019). Szacuje się, że w samej Europie cierpi na nią 5% dzieci (Pediaditis et al., 2012). Około 40% pacjentów nie może być leczonych farmakologicznie lub operacyjnie, co przy dużym odsetku błędnie zdiagnozowanych przypadków stanowi wyzwanie zarówno dla lekarzy, jak i inżynierów biomedycznych (Beghi et al., 2019). Dziecięce napady nieświadomości CAE występują u 9,6/100 000 dzieci poniżej piętnastego roku życia. Badania przebiegu farmakoterapii napadów nieświadomości (Glauser et al., 2013) wykazały, że u zaledwie 37% pacjentów efekt farmakoterapii po pierwszym roku leczenia można uznać za zadawalający. Kliniczne monitorowanie napadów padaczkowych wykorzystuje się do diagnozy, optymalizacji terapii oraz opracowywania nowych leków. Do niedawna długoterminowe monitorowanie napadów opierało się głównie na wynikach zgłaszanych przez pacjentów lub opiekunów w połączeniu z okazjonalnym, krótkim badaniem EEG. Należy podkreślić, że zaledwie mała część napadów nieświadomości (w przybliżeniu 6%) jest zauważana przez rodziców bądź opiekunów (Keilson et al., 1987; Akman et al., 2009). Obecnie proces diagnozy oparty jest na retrospektywnej analizie wideo EEG przez wykwalifikowanych neurologów.

5. Cel oraz zakres pracy

Rozprawa doktorska podsumowuje wyniki cyklu trzech publikacji poświęconych ilościowej analizie EEG pacjentów z napadami nieświadomości. Głównymi problemami badawczymi są:

1) Problem prawidłowej diagnozy pacjentów z dziecięcymi i młodzieńczymi napadami nieświadomości.
2) Opracowanie algorytmu automatycznej detekcji napadów nieświadomości, który pozwoli na długookresowe monitorowanie stanu pacjentów.
3) Opracowanie metody pozwalającej na spersonalizowaną kontrolę procesu farmakoterapii.

Prawidłowa diagnostyka różnicowa CAE i JAE jest niezwykle ważna. W okresie dojrzewania około 60% pacjentów z CAE przechodzi w remisję (Morse et al., 2019). U pacjentów z JAE dożywotnia terapia jest regułą (Vorderwülbecke et al., 2017). W związku z krótkim czasem trwania napadu (zazwyczaj od 2 do 10 sekund) i trudnością z jego wykryciem, mogą minąć miesiące, a nawet lata, zanim zostanie wprowadzone leczenie farmakologiczne (Siren et al., 2002). Badania wykazały, że dzieci z napadami nieświadomości mają specyficzne trudności ze skupieniem uwagi (Fedio and Mirsky, 1969), pamięcią wzrokową (Jambaqué et al., 1993; Pavone et al., 2001) oraz zaburzeniami motoryki (Henkin et al., 2005). Prawidłowa farmakoterapia, w wyniku której powstrzymano napady nieświadomości, może wspomóc neurokognitywny rozwój dziecka (Sirén et al., 2007). Badania przebiegu leczenia napadów nieświadomości (Glauser et al., 2013) wykazały, że zaledwie 37% pacjentów pozytywnie reaguje na początkową farmakoterapię. Proces ten jest wciąż oparty na doświadczeniu neurologa i próbach odstawienia leku po pewnym okresie braku napadów. Nie znaleziono klinicznego czynnika, który byłby przydatny w dokładnym przewidywaniu oporności na leki przy diagnozie (Walker et al., 2015). Precyzyjna terapia oparta na patogenezie i mechanizmach działania leków przeciwpadaczkowego zwykle nie jest możliwa, ponieważ te mechanizmy nie są w pełni poznane (Orsini et al., 2018). Potrzeba implementacji automatycznego

i niezawodnego algorytmu wykrywania napadów nieświadomości została już opisana w przeszłości (Faust et al., 2015). Taki algorytm wraz z mobilnym urządzeniem EEG ma tworzyć system długookresowego monitorowania stanu pacjenta, co ma wspomóc nie tylko diagnozę, ale również przyspieszyć proces farmakoterapii pomagając w spersonalizowanym miareczkowaniu leków i określeniu momentu, w którym można podjąć próbę odstawienia leków.

Prezentowane wyniki dotyczące detekcji napadów nieświadomości oparte są na jednym z największych zbiorów zapisów EEG (36 pacjentów z CAE i 29 z JAE) pozyskanych z trzech niezależnych ośrodków: Dolnośląskiego Szpitala Specjalistycznego im. T. Marciniaka we Wrocławiu, Uniwersyteckiego Szpitala Dziecięcego w Krakowie oraz Kliniki Neurologii i Epileptologii „Pomnik Centrum Zdrowia Dziecka".

W niniejszej pracy doktorskiej postawiono hipotezę, że na podstawie zmian międzynapadowej mocy falkowej w różnych pasmach oraz zmian jej synchronizacji możliwe jest opracowanie nowej metody diagnostyki pacjentów z napadami nieświadomości, jak również monitorowania postępu farmakoterapii. Opracowany algorytm detekcji napadów nieświadomości ma na celu wsparcie wyżej wymienionych procesów. Jakościowy opis fragmentacji napadów nieświadomości jest pierwszym krokiem do zbadania możliwości skutecznego różnicowania pacjentów z CAE i JAE.

6. Napady nieświadomości

Napady nieświadomości, również znane jako napady *petit mal* są szczególnym typem epilepsji. Ich kliniczną manifestacją jest krótka i niespodziewana utrata świadomości. Takie zdarzenia nie są bezpośrednim zagrożeniem życia pacjenta, ale w pewnych okolicznościach, jak przechodzenie przez jezdnię, pływanie czy praca na wysokości mogą doprowadzić do tragicznego w skutkach wypadku. W zapisie encefalograficznym charakteryzują się uogólnionymi, rytmicznymi i zsynchronizowanymi wyładowaniami z zespołem iglicy i fali wolnej (SWD) o częstotliwości wynoszącej około 3 Hz. Nieleczona choroba prowadzi do zaburzeń w neurokognitywnym rozwoju dzieci (Sirén et al., 2007).

Międzynarodowa Liga Przeciwko Epilepsji (ILAE) w 2017 roku opisała genetyczne uogólnione epilepsje (GGE z ang. generalized genetic epilepsy), w skład których wchodzą idiopatyczne uogólnione epilepsje (IGEs z ang. idiopathic generalized epilepsies) (Hirsch et al., 2022). Te z kolei zostały podzielone na 4 syndromy: dziecięce napady nieświadomości (CAE), młodzieńcze napady nieświadomości (JAE), młodzieńcze, mioklioniczne napady nieświadomości (JME) oraz uogólnione, toniczno-kloniczne napady nieświadomości (GTCA). Rozpoznanie idiopatycznych uogólnionych epilepsji jako specjalnego podtypu genetycznych jest pomocne, ponieważ niesie ze sobą konsekwencje w postaci prognozy i przebiegu farmakoterapii.

Badania populacyjne dzieci i dorosłych wykazały, że odpowiednio 23% i 43% pacjentów ma uogólnioną padaczkę (Camfield and Camfield, 2015), z czego 53%-58% cierpi na jeden z czterech syndromów IGE (Wirrell et al., 2011). Typ napadów nieświadomości jest związany z wiekiem pacjenta, jednakże nie może stanowić samodzielnego kryterium diagnostycznego. CAE występuje u pacjentów w wieku 2-13 lat, JAE w wieku 8-20 lat natomiast JME oraz GTCA w wieku 5-40 lat (Hirsch et al., 2022).

Powszechnie uważano, że uogólnione wyładowania iglica-fala wolna mają nagły początek z normalnego zapisu EEG. Jednakże ostatnie badania wykazują obecność lokalnych i szybko rozprzestrzeniających się wyładowań padaczkowych, które prowokują właściwy napad (Zenteno, 2007). W niektórych przypadkach wizualna inspekcja może ujawnić zmiany w częstotliwości i amplitudzie sygnału na kilka sekund przed napadem (Inouye et al., 1990). W celu odkrycia mechanizmów neuronalnych, przyczyniających się do generowania napadów konieczna wydaje się bardziej zaawansowana analiza.

Synchronizacja lub sprzężenie sieci neuronowych w mózgu jest tematem, który wzbudza duże zainteresowanie (Le Van Quyen et al., 1998; Martinerie et al., 1998; Lopes da Silva et al., 2003b; Aarabi et al., 2008). Ataki padaczkowe są uważane za nadmiernie zsynchronizowaną aktywność neuronów w mózgu (Fisher et al., 2005). Jednym z ostatnich problemów badawczych jest odpowiedź na pytanie, czy ta

nadmierna synchronizacja prowadzi do napadu, czy jest jego wynikiem? (Majumdar et al., 2014). Badania prowadzą do różnych koncepcji, niektórzy badacze zaobserwowali zmniejszoną synchronizację przed wystąpieniem ataku (Chavez et al., 2003; Mormann et al., 2003; Wang et al., 2011; Zheng et al., 2014). Głównym celem znalezienia biomarkera napadu jest jego przewidywanie i zapobieganie (Lopes da Silva et al., 2003a; Mormann et al., 2007).

Pojawienie się komercyjnych, przenośnych urządzeń EEG zapoczątkowało prace nad zbadaniem możliwości długoterminowego zdalnego monitorowania pacjentów z napadami nieświadomości (Krigolson et al., 2017). Potencjalnymi korzyściami wynikającymi z tego rodzaju monitorowania pacjentów są ułatwienie diagnozy, spersonalizowane miareczkowanie leków oraz bardziej precyzyjne określenie czasu trwania farmakoterapii. Algorytm detekcji napadów nieświadomości powinien wykorzystywać niewielką liczbę elektrod, być zoptymalizowany pod kątem kosztu obliczeniowego oraz wykazywać odporność na artefakty ruchowe.

Analiza skuteczności farmakoterapii napadów nieświadomości (Glauser et al., 2013) wykazała, że zaledwie 37% pacjentów pozytywnie reaguje na leczenie. Najczęściej lekarze wykorzystują trzy leki – kwas walproinowy, etosuksymid oraz lamotryginę. Wybór zależy od tego czy, czy występują inne rodzaje napadów uogólnionych oraz od reakcji niepożądanych. Do najczęstszych efektów ubocznych można zaliczyć zmęczenie, senność, nudności, zawroty głowy, zaburzenia równowagi, bóle głowy, zmiany nastroju czy wymioty. Farmakologiczna kontrola napadów nieświadomości przy zadawalającym poziomie efektów ubocznych jest osiągana dla około połowy dzieci z CAE (Glauser et al., 2013). Monoterapia dowolnym z wymienionych leków nie powinna być porzucana do czasu, zanim nie osiągnie się maksymalnej tolerowanej dawki (Panayiotopoulos, 2005). Kombinacja wyżej wymienionych leków może być stosowana w przypadku cięższych przypadków. Remisja u większości dzieci z napadami nieświadomości występuje po kilku latach farmakoterapii. W przypadku nawrotu choroby proces farmakoterapii zostaje wznawiany i może trwać przez całe życie (Guerrini, 2006).

6.1 Dziecięce napady nieświadomości (CAE)

Dziecięce napady nieświadomości odpowiadają za 18% przypadków dziecięcych epilepsji (Cavazzuti, 1980). Średni czas trwania napadu wynosi 10 s i może pojawić się od kilku do nawet kilkudziesięciu razy podczas dnia (Schomer and Lopes da Silva, 2018). Co warto podkreślić, większość neurologów zalicza wszystkie przypadki napadów nieświadomości występujących przed dziesiątym rokiem życia jako CAE (Bouma et al., 1996). Pacjenci zazwyczaj dobrze reagują na leczenie (Covanis, 2010). W okresie dojrzewania, około 60% dzieci przechodzi w remisję (Morse et al., 2019). W pozostałych przypadkach syndrom rozwija się do innych zespołów padaczkowych. Nie wiadomo, jaka jest zależność między EEG przed leczeniem oraz w trakcie farmakoterapii (Dlugos et al., 2013). Szczególne cechy zapisu EEG mogłyby pomóc w próbie zróżnicowania CAE i JAE.

Międzynapadowy zapis elektroencefalograficzny nie wykracza poza granicę normy (Lopes da Silva et al., 2003a). Mogą się pojawić krótkie paroksyzmy o częstotliwości od 2,5 do 4 Hz w postaci uogólnionych wyładowań iglica-fala wolna. Podczas snu, takie wyładowania mogą być zdezorganizowane (Elmali et al., 2020).

Zapis napadów charakteryzuje się regularnymi wyładowaniami SWD. U 21% pacjentów mają częstotliwość 2,5Hz. Wyładowania o częstotliwości 4Hz występują u 43% pacjentów (Sadleir et al., 2006). Fragmentacje napadów zdefiniowane jako krótkie zakłócenia rytmu ictalnego lub wyładowania o innej od typowej morfologii występują około 8-krotnie rzadziej niż u pacjentów z JAE (Sadleir et al., 2009). Napady nieświadomości u nieleczonych dzieci mogą być efektywnie prowokowane przez hiperwentylację (Rozenblat et al., 2020).

6.2 Młodzieńcze napady nieświadomości (JAE)

JAE odpowiada za zaledwie 2,4%-3.1% nowo zdiagnozowanych epilepsji u dzieci i młodzieży (Wirrell et al., 2011). Charakteryzuje się bardziej subtelnymi napadami nieświadomości, które zazwyczaj występują u nieleczonych pacjentów rzadziej niż raz dziennie. Jest to jeden z powodów, dla których liczba chorych może

być niedoszacowana (Jallon and Latour, 2005). Uogólnione toniczno-kloniczne napady są widoczne u ponad 90% przypadków.

Zazwyczaj JAE dotyka pacjentów w wieku od 9 do 13 lat (zakres od 8 do 20 lat). W niektórych przypadkach może występować również u dorosłych (Marini et al., 2003). Przeważnie pacjenci dobrze reagują na leczenie, ale może być wymagana dożywotnia terapia (Vorderwülbecke et al., 2017). Cierpiący na JAE, są bardziej narażeni na dodatkowe schorzenia takie jak ADHD, depresję, problemy w nauce czy stany lękowe (Abarrategui et al., 2018; Gruenbaum et al., 2021). W przypadku diagnozy pacjentów w wieku poniżej dziesiątego roku życia odróżnienie JAE od CAE może być trudne. Pomimo podobieństw, u pacjentów z JAE napady mogą mieć nieznacznie wyższą częstotliwość wyładowań ≥ 3 Hz (w zakresie od 3 do 5,5 Hz), które dodatkowo są w większym stopniu nieregularne (Elmali et al., 2020).

6.3 Biomarkery EEG do identyfikowania epilepsji

Diagnoza napadów nieświadomości polega na ich prowokowaniu i rejestracji zapisu EEG. Pacjenci są poddawani hiperwentylacji i fotostymulacji, aby wywołać napad padaczkowy. W trudniejszych przypadkach stosuje się również deprywację snu. Jest to jednak kosztowny i czasochłonny proces, który dodatkowo wpływa negatywnie na komfort pacjentów, którymi są głównie dzieci. Co dziesiąta osoba mogła doświadczyć w ciągu swojego życia napadu padaczkowego jako objawu innej choroby jak np. ciężkiej hiponatremii (Gallotto and Seeck, 2023). Z tego powodu, trudno jest postawić prawidłową diagnozę po wystąpieniu pierwszego napadu (Krumholz, 2009). Bardziej przydatne diagnostycznie biomarkery powinny zatem pochodzić z nienapadowego EEG (Engel et al., 2018).

Ze wszystkich do tej pory zaproponowanych biomarkerów EEG, międzynapadowe wyładowania padaczkowe (IED z ang. interictal epileptic discharges) zdefiniowane jako krótkie wyładowania obejmujące iglice, kompleksy ostrej fali czy pojedyncze kompleksy iglica-fala wolna są najbardziej znaczące (Engel et al., 2018). Jednakże u pacjentów z rozpoznaną chorobą, ale z negatywnym, rutynowym badaniem EEG zakłada się obecność ukrytych IED (Gallotto and Seeck, 2023). Takie wyładowania nie mogą zostać zidentyfikowane przez neurologów

podczas opisu EEG. Powodem mogą być zbyt słabe wyładowania bądź niemożność zarejestrowania wyładowań mających swoje źródło z głęboko położonych obszarów mózgu przez standardowe aparat encefalograficzny.

W zapisach EEG pacjentów cierpiących na epilepsję zaobserwowano krótkie, wysokoczęstotliwościowe oscylacje (HFOs z ang. high-frequency oscillations) w zakresie 80 – 600Hz. Badania wykazały, że taka aktywność może być rozważana za biomarker (Jacobs et al., 2009) oraz miarę intensywności epilepsji (Zijlmans et al., 2009). Dodatkowo można ją wykorzystywać do lokalizowania obszarów mózgu, które generują napady epileptyczne w celu resekcji (Engel and da Silva, 2012). Mimo, że są to jedne z najbardziej obiecujących biomarkerów to należy w kolejnych badaniach potwierdzić ich wiarygodność (Engel et al., 2018). Głównym ograniczeniem wykorzystania wysokoczęstotliwościowych oscylacji jako biomarkera epilepsji jest konieczność użycia aparatu EEG mogącego rejestrować sygnał z wysoką częstotliwością.

Niska rozdzielczość przestrzenna EEG utrudnia lokalizację obszaru kory mózgowej, który jest zaangażowany w generację napadów ogniskowych. Zaproponowano jednak nowe metody oparte na analizie połączeń funkcjonalnych, które próbują przezwyciężyć ten problem (van Mierlo et al., 2019). Analiza sygnału EEG w tym kontekście pozwala na lokalizowanie obszarów, w których rozpoczyna się napad padaczkowy (Wilke et al., 2011) oraz selekcję kandydatów do zabiegu neurochirurgicznego (van Mierlo et al., 2019). Analiza połączeń w paśmie theta, beta oraz alfa umożliwiła klasyfikować zdrowych i cierpiących na padaczkę skroniową na podstawie międzynapadowych fragmentów zapisów EEG (Verhoeven et al., 2018). Jednakże nie wiele wiadomo na temat tego, czy zmiany są już obecne na początku choroby, czy występują dopiero, gdy epilepsja jest rozwinięta (Gallotto and Seeck, 2023).

Kolejnym potencjalnym biomarkerem, który znalazł zastosowanie w diagnozie napadów nieświadomości jest mikrostan (Gallotto and Seeck, 2023). Koncept mikrostanu wywodzi się z założenia, że aktywność mózgu w stanie spoczynkowym nie jest całkowicie losowa ani chaotyczna, ale może być opisana za

pomocą skończonej liczby map, które zmieniają się w czasie, pozostając przez krótki czas (ok. 50-150 milisekund) stabilne. Chociaż znaleziono kilka konfiguracji mikrostanów, większość badań wykazała, że za pomocą podstawowych czterech wzorców można opisać do 70% całego EEG (Khanna et al., 2015). Rozdzielczość czasowa na poziomie milisekund pozwala na wykrywanie szybkich zmian w sieciach mózgowych umożliwiając badanie ich odchyleń w różnych grupach pacjentów (Ahmadi et al., 2020). Dla chorych z napadami nieświadomości przejście z jednego mikrostanu do kolejnego trwało znacznie dłużej niż w grupie zdrowych co sugeruje, że czas trwania określonego stanu może być biomarkerem choroby (Liu et al., 2018).

7. Detekcja i predykcja napadów nieświadomości

Elektroencefalografia jest powszechnie stosowaną techniką pomiaru patologicznej aktywności bioelektrycznej mózgu w celu diagnozowania napadów padaczkowych (Yuan et al., 2019). Pomiary wykonywane są w laboratoriach i placówkach klinicznych przy użyciu wysokiej jakości, drogiego sprzętu, który jednocześnie wymaga do obsługi wykwalifikowanego personelu (Sugden et al., 2023). W ostatnich latach na rynku pojawiło się wiele przenośnych urządzeń EEG, które są małe, lekkie i zasilane na baterie, a koszt zakupu jest przynajmniej o rząd wielkości mniejszy (Casson, 2019). Stwarza to nowe możliwości zdalnego przeprowadzania wielogodzinnych badań EEG.

Obecnie Internet Rzeczy (IoT z ang. Internet of Things) rozumiany jako system połączonych przedmiotów mogących rejestrować, przetwarzać i wymieniać dane odgrywa coraz większą rolę w opiece medycznej. Ta technologia pozwala na ciągły monitoring stanu pacjentów w czasie rzeczywistym wykorzystując urządzenia mobilne. W połączeniu z przechowywaniem danych w chmurze i wykorzystaniu sztucznej inteligencji IoT może stać się potężnym narzędziem rozwiązującym wiele obecnych problemów służby zdrowia wpisując się w koncept medycyny personalizowanej (precyzyjnej) (YIN et al., 2016).

W ostatnich latach opublikowano wiele prac poświęconych detekcji napadów nieświadomości w celu wsparcia automatycznego systemu diagnozy. W tym kontekście, implementacja takich algorytmów ma za zadanie odciążyć lekarzy

w uciążliwej pracy oraz wspomóc zarówno proces diagnozy jak i farmakoterapii (van Luijtelaar et al., 2016).

Już przed rozpoczęciem napadu mogą występować zmiany aktywności centralnego układu nerwowego, co definiuje fazę przednapadową zapisu EEG (Ein Shoka et al., 2023). Przewidywanie nadchodzącego napadu polega na wykryciu subtelnych zmian wspomnianej aktywności bioelektrycznej mózgu podczas przejścia z międzynapadowego fragmentu zapisu do fazy przednapadowej (Singh and Malhotra, 2019). W rezultacie proces wczesnego rozpoznania napadów na etapie przednapadowym podnosi komfort pacjentów (Abualsaud et al., 2018; Li et al., 2019), a w szczególnych okolicznościach może uratować życie umożliwiając im podjęcie środków ostrożności. W połączeniu z neurostymulacja pozwala to na regulację oraz modyfikację objawów epilepsji (Fisher and Velasco, 2014), a w przyszłości może doprowadzić do aktywnego powstrzymywania napadów (Dümpelmann, 2019).

8. Publikacja 1 – *Changes in Interictal Pretreatment and Posttreatment EEG in Childhood Absence Epilepsy*

Pierwsza publikacja opisuje zmiany mocy falkowej w interictalnych fragmentach EEG u dzieci z napadami nieświadomości. Porównując do grupy kontrolnej, zaobserwowano zwiększoną moc falkową w paśmie theta oraz beta. Dodatkowo możliwym było zaprezentowanie wpływu farmakoterapii na wartości mocy, która dla większości przypadków znacząco spadała. Jest to pierwszy krok do opracowania metody pozwalającej na monitorowanie postępu farmakoterapii, spersonalizowanego miareczkowania leków oraz precyzyjnego określenia momentu zakończenia procesu leczenia. Na podstawie uzyskanych wyników, sformułowano hipotezę, że wzrost mocy falkowej w paśmie theta oraz beta wynika odpowiednio z nadmiernej pobudliwości kory mózgowej i skłonności do generowania iglic padaczkowych. Twierdzimy, że charakterystyczne cechy widma mocy falkowej mogą być wykorzystane do zdefiniowania biomarkera napadów nieświadomości.

Zgodnie z oświadczeniem o współautorstwie mój procentowy wkład do niniejszej pracy wynosi 60%. Współuczestniczyłem w sformułowanie programu badawczego i przygotowaniu manuskryptu. Przeprowadziłem wszystkie obliczenia.

frontiers in Neuroscience

BRIEF RESEARCH REPORT
published: 13 March 2020
doi: 10.3389/fnins.2020.00196

Changes in Interictal Pretreatment and Posttreatment EEG in Childhood Absence Epilepsy

Pawel Glaba[1], Miroslaw Latka[1], Małgorzata J. Krause[2], Marta Kuryło[2], Wojciech Jernajczyk[3], Wojciech Walas[4] and Bruce J. West[5]*

[1] Department of Biomedical Engineering, Wroclaw University of Science and Technology, Wroclaw, Poland, [2] Department of Pediatric Neurology, T. Marciniak Hospital, Wroclaw, Poland, [3] Clinical Neurophysiology, Institute of Psychiatry and Neurology, Warszawa, Poland, [4] Neonatal and Pediatric Intensive Care Unit, University Hospital in Opole, Opole, Poland, [5] Mathematics and Information Science Directorate, Army Research Office, Durham, NC, United States

Spike and wave discharges (SWDs) are a characteristic manifestation of childhood absence epilepsy (CAE). It has long been believed that they unpredictably emerge from otherwise almost normal interictal EEG. Herein, we demonstrate that pretreatment closed-eyes theta and beta EEG wavelet powers of CAE patients (20 girls and 10 boys, mean age 7.4 ± 1.9 years) are much higher than those of age-matched healthy controls at multiple sites of the 10–20 system. For example, at the C4 site, we observed a 100 and 63% increase in power of theta and beta rhythms, respectively. We were able to compare the baseline and posttreatment wavelet power in 16 patients. Pharmacotherapy brought about a statistically significant decrease in delta and theta wavelet power in all the channels, e.g., for C4 the reduction was equal to 45% (delta) and 63% (theta). The less pronounced attenuation of posttreatment beta waves was observed in 13 channels (36% at C4 site). The beta and theta wavelet power were positively correlated with the percentage of time in seizure (defined as the ratio of the duration of all absences which patients experienced to the duration of recording) for majority of channels. We hypothesize that the increased theta and beta powers result from cortical hyperexcitability and propensity for epileptic spike generation, respectively. We argue that the distinct features of CAE wavelet power spectrum may be used to define an EEG biomarker which could be used for diagnosis and monitoring of patients.

Keywords: childhood absence epilepsy, EEG, wavelets, biomarker, cortical excitability

OPEN ACCESS

Edited by:
Francisco Ciruela, University of Barcelona, Spain

Reviewed by:
Peter Halasz, Hungarian Society for Sleep Medicine, Hungary
Vadim Valerievich Grubov, Saratov State Technical University, Russia

****Correspondence:***
Miroslaw Latka
miroslaw.latka@pwr.edu.pl

Specialty section:
This article was submitted to Neuropharmacology, a section of the journal Frontiers in Neuroscience

Received: *25 July 2019*
Accepted: *24 February 2020*
Published: *13 March 2020*

Citation:
Glaba P, Latka M, Krause MJ, Kuryło M, Jernajczyk W, Walas W and West BJ (2020) Changes in Interictal Pretreatment and Posttreatment EEG in Childhood Absence Epilepsy. Front. Neurosci. 14:196. doi: 10.3389/fnins.2020.00196

INTRODUCTION

Childhood absence epilepsy (CAE) is the most common pediatric epileptic syndrome. It has a prevalence of 10–15% in childhood epilepsies and an incidence of 1.3–6 per 100,000 in children under the age of 16 years (Covanis, 2010). The disorder is most likely multifactorial, resulting from interactions between genetic and acquired factors (Gallentine and Mikati, 2012).

The ictal EEG of a typical absence seizure demonstrates rhythmic ∼3 Hz bilateral, synchronous and symmetrical spike and wave discharges (SWDs) with a median duration of approximately 10 s, which may appear several times per day, sometimes as often as dozens of times per day (Schomer and Lopes da Silva, 2018). It has long been believed that SWDs are unpredictable and emerge from

otherwise almost normal interictal EEG (Lopes da Silva et al., 2003). Interictal EEG abnormalities include sparse fragments of SWDs and focal discharges as well as posterior bilateral delta activity (Sadleir et al., 2006).

The response to monotherapy (valproic acid, ethosuximide, and lamotrigine) is generally good. As many as 75–85% of treated patients are seizure free and have a normal EEG (Covanis, 2010). The rest usually respond to a combination of drugs such as valproic acid and ethosuximide. Pharmacological seizure control with acceptable side effects is achieved for slightly more than half of the children. The relationship between pretreatment EEG and response to therapy is unknown (Dlugos et al., 2013). In general, CAE carries a good prognosis. Seizures spontaneously cease with ongoing maturation.

The cortical focus theory postulates that an absence seizure originates from a focus in the somatosensory cortex which is in a specific state conducive to seizure propagation. At the beginning of the seizure, it is the cortex that drives the thalamus, but prominent generalized spike-wave discharges result from their subsequent mutual interaction (Meeren et al., 2005). Considering the principal role of the cortex in absence seizure generation, we hypothesize that in CAE, interictal EEG manifests distinct features that can be detected even in routine, rest EEG recordings.

MATERIALS AND METHODS

We retrospectively analyzed a routine, anonymized pretreatment video EEG recording (average duration 37 ± 13 min) of n = 30 CAE patients (20 girls and 10 boys) with a mean age of 7.4 ± 1.9 years. The analysis was approved by the ethics committee and the board of the T. Marciniak Hospital in Wrocław, Poland. CAE epilepsy syndrome was established based on of history, age at onset, clinical, and EEG findings as well as neuroimaging. In this cohort, we observed 173 seizures, 6 ± 3 per patient on average. The median seizure duration was 12 ± 4 s. On average, the ratio of the duration of all absences which patients experienced to the duration of EEG recording was 4 ± 2%. We refer to this ratio as the percentage of time in seizure (PTS). In nine cases, the first seizure occurred during hyperventilation, on average 130 ± 55 s after its onset. The control group (15 girls and 15 boys) was age matched (7.3 ± 1.9 years) to the patients. EEG was recorded using the Elmiko Digitrack system with a BRAINTRONICS B.V. ISO-1032CE amplifier. The sampling frequency was equal to 250 Hz. The 10–20 international standard was used to position 19 Ag/AgCl electrodes (impedances were below 5 kΩ). The ground electrode was placed at the patients' forehead. The average reference electrode montage was used for time-frequency calculations. All the EEG recordings were performed between 2008 and 2018 by the same certified EEG technician.

After diagnosis, the pharmacotherapy of 16 out of 30 patients was administered by the outpatient neurology department of T. Marciniak Hospital. Valproic acid (two daily dosages of 244 ± 58 mg and 311 ± 111 mg) was used in 75% of the cases and 19% of the patients were treated with ethosuximide (two daily dosages of 250 mg). A combination of valproic acid (250 mg twice a day) and ethosuximide (150 mg twice a day) was used in 6% of the patients. The treatment response was evaluated with routine EEG with hyperventilation and photostimulation.

For each patient we extracted five closed-eyes (CE) motion artifact free pretreatment EEG segments: interictal (preceding the seizure by 226 ± 122 s), preictal A (beginning 31 s before the seizure), preictal B (beginning 16 s before the seizure), postictal A (beginning 1 s after seizure), and postictal B (beginning 16 s after the seizure). The average length of the interictal segments was: 84 ± 32 s. Due to the presence of motion artifacts and/or eye openings the length of the preictal and postictal segments slightly varied. Their average length was equal to 15 ± 2 s, 15 ± 3 s, 16 ± 1 s, and 14 ± 2 s for preictal A, preictal B, postictal A, and postictal B, respectively. The chosen length of pre- and postictal segments assured that data from all subjects could be included in analysis. For the controls, the average length of selected CE EEG segments was 55 ± 27 s. We also analyzed the most recent follow-up EEG which on average was recorded 1.5 ± 2 years after the video EEG used for diagnosis. The average length of CE segments selected for analysis from the follow-up EEG was 28 ± 15 s. There were no seizures in the follow-up EEGs.

We calculated the continuous wavelet transform (CWT) of EEG using the complex Morlet mother function. We analyzed the statistical properties of instantaneous wavelet power $w(f, t_0)$ (square of the modulus of complex wavelet coefficients) and temporal average $W(f) = < w(f, t_0) >_{t0}$ over the selected EEG segment. We used the mother function with the center frequency f_c = 1 and bandwidth f_b = 1.8 (Latka et al., 2003). For these parameters, the transform was computed for three frequencies f: 6.5, 9, and 15 Hz. **Figure 1A** elucidates the rationale for such a choice of frequencies. The dashed red line in this figure represents the percentage difference between the C4 wavelet spectrum $W(f)$ of patients and controls. The difference curve has two distinct local maxima at 6.5 and 15 Hz. These frequencies were used to analyze theta and beta rhythms, respectively. The spectra of patients and controls have the maxima around 9 Hz and consequently such frequency was used for analysis of alpha waves. **Figure 1B** shows that the chosen wavelet calculated for 15 Hz may be used for detection of epileptic spikes. In other words, we focus on this part of the beta band which may be involved in the genesis of epileptic spikes. The spectacular increase of beta wavelet power in the vicinity of the epileptic spikes in **Figure 1B** can be employed in the simple but highly effective SWD detector which we describe elsewhere. The wavelet with f_c = 1 and bandwidth f_b = 1.5 calculated for frequency 3 Hz was used to quantify delta waves.

We used the Shapiro–Wilk test to determine whether the analyzed data were normally distributed. We compared the pretreatment and posttreatment values of $W(f)$ as well as the values of the controls with the Kruskal–Wallis test (with Tukey's *post-hoc* comparisons). The same test was used to analyze the changes in wavelet power in preictal and postictal segments. The patients' pretreatment wavelet power averaged over all channels was compared with that of controls using also a non-parametrical statistical testing (Maris and Oostenveld, 2007). The reported p-values for this test correspond to 1×10^5 random

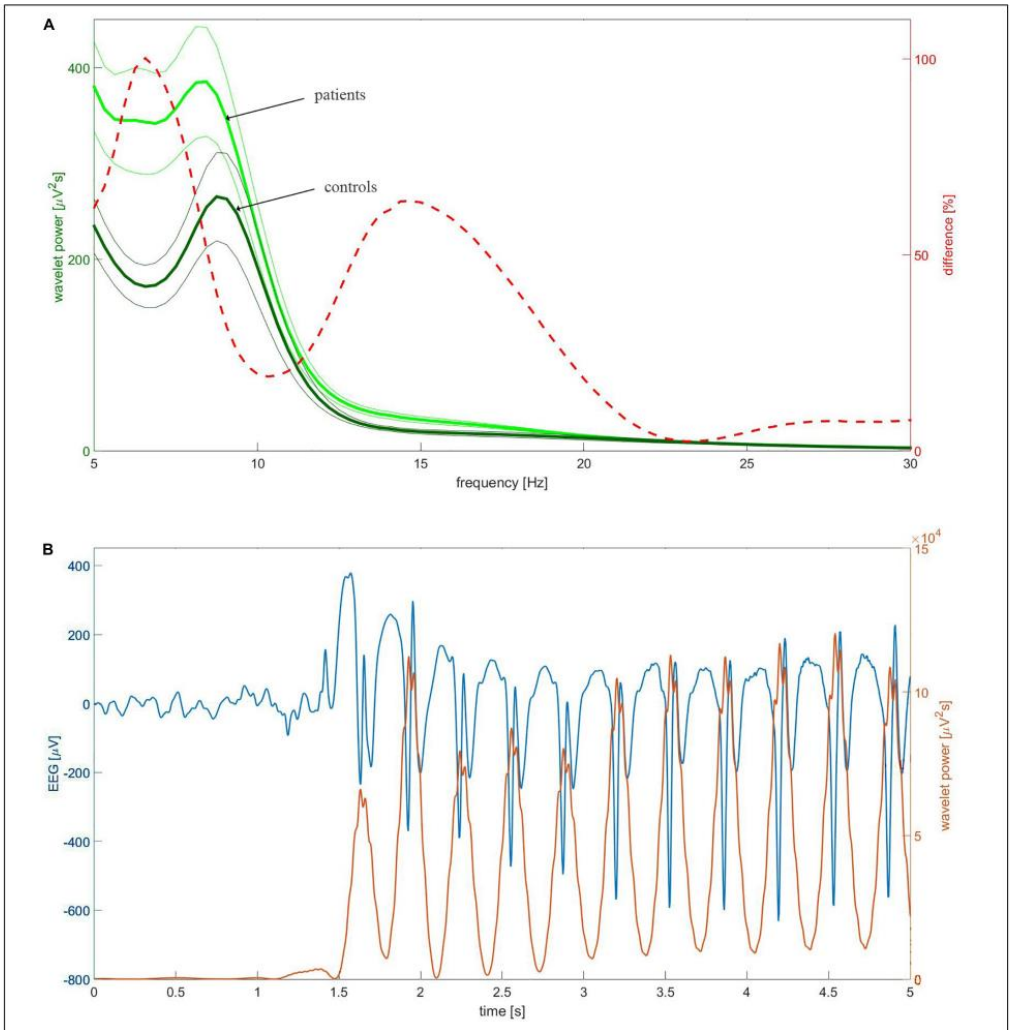

FIGURE 1 | (A) The group-averaged wavelet power spectrum in C4 channel of patients (thick light green) and controls (thick dark green). The complex Morlet wavelet (f_c = 1, f_b = 1.8) was used as a mother function. The thin lines which bracket the averages represent standard error of the mean (SEM). The percentage difference between the patients and controls was drawn with the red dashed line. **(B)** Example of childhood absence epilepsy seizure. The presented section of EEG (blue curve) was extracted from EEG of a 7-year-old girl (patient BZ). The instantaneous power of the complex Morlet wavelet (f_c = 1, f_b = 1.8) calculated for 15 Hz was drawn with the red curve.

draws. The area under the receiver operating characteristic curve (AUC) was used to quantify differences in $W(f)$ between patients and controls. AUC was also calculated for pretreatment and posttreatment values of W. The values of AUC, sensitivity and specificity were reported for selected channels. The correlation between the values of $W(f)$ for all four EEG bands and the percentage of time in seizure was examined for all 19 EEG channels using Pearson's correlation coefficient. The significance threshold for all the statistical tests was set to 0.05. The wavelet and statistical analyses were done with MATLAB R2015A.

We employed classifiers implemented in Weka software (version 3.8)[1] to discriminate between patients and controls using theta and beta wavelet power $W(f)$. Out of 38 such attributes, we used only these with non-zero gain ratio (entropic measure). Machine learning was performed with 10-fold cross-validation.

RESULTS

Figure 2 shows that the pretreatment interictal closed-eyes theta and beta EEG wavelet powers of CAE patients are much higher than those of age-matched controls at multiple sites of the 10–20 system. For the theta band, we observed a 100% increase in patients' wavelet power W at C4 site (343 ± 296 $\mu V^2 s$ vs. 172 ± 118 $\mu V^2 s$, $p = 9 \times 10^{-3}$, AUC = 0.87, sensitivity = 0.87, specificity = 0.63). For the beta band, the power in the patients was 63% greater than in the controls (32 ± 18 $\mu V^2 s$ vs. 20 ± 13 $\mu V^2 s$, $p = 4 \times 10^{-3}$, AUC = 0.77, sensitivity = 0.77, specificity = 0.73). With the exception of channel Fz, there was no statistically significant difference between the pretreatment patients and the controls for alpha rhythm. For the delta band, the increased pretreatment wavelet power was observed only at the occipital channels.

The value of $W(f)$ averaged over all 19 EEG channels was higher for pretreatment patients both for theta and beta bands. The corresponding p-values for Kruskall-Wallis test were equal to 4×10^{-3} and 1×10^{-3}. For non-parametric testing, $p = 8 \times 10^{-4}$ and $p = 1 \times 10^{-4}$ for theta and beta rhythms, respectively. Kruskall-Wallis test did not detect differences in alpha and delta power between untreated patients and controls. Non-parametric testing showed the differences in the delta band with $p = 2 \times 10^{-2}$.

In **Figure 3** we present the probability density function (PDF) of instantaneous interictal theta and beta wavelet power $w(f,t_0)$ in channel C4 for the controls (light green) and the pretreatment patients (dark green). For both cohorts, we aggregated the values of $w(f,t_0)$ from all their members. It is apparent that the tail of the PDF is much longer for the pretreatment cohort. The insets in both subplots show the boxplots of time-averaged values of the pretreatment and posttreatment wavelet power W as well as that of the controls. It is apparent from **Figure 3A** that pharmacotherapy suppressed the elevated pretreatment theta power that dropped 63% from 343 ± 296 $\mu V^2 s$ to 127 ± 123 $\mu V^2 s$ with *post-hoc* $p = 2 \times 10^{-4}$ (AUC = 0.87, sensitivity = 0.75, specificity = 0.87). The patients' posttreatment C4 theta power was not statistically different from that of the controls ($p = 0.26$). **Figure 3B** shows that the influence of treatment on C4 beta power was weaker. In that case the power was reduced 36% from 32 ± 18 $\mu V^2 s$ to 21 ± 22 $\mu V^2 s$ with *post-hoc* $p = 3 \times 10^{-3}$ (AUC = 0.78, sensitivity = 0.81, specificity = 0.70).

For the alpha band, there were no statistically significant differences between the wavelet power in interictal segments and those in preictal and postictal ones. The W of theta and beta rhythms was statistically greater than the interictal value only in postical A segments (channels Fp1, Fp2, F7, F8, and Fp1, F7, respectively). Such increases in theta wavelet power were not observed in postictal B segments. For preictal B and postictal A segments (adjacent to the absence seizure) the delta wavelet power was statistically greater than the interictal values in all 19 EEG channels. For example, at the C4 site, patients' wavelet power in preictal B segment was 367% greater than in the controls ($1{,}259 \pm 1{,}973$ $\mu V^2 s$ vs. 269 ± 136 $\mu V^2 s$, $p = 3 \times 10^{-5}$, AUC = 0.82, sensitivity = 0.76, specificity = 0.83) and 212% greater than the average value in the interictal segments 403 ± 276 $\mu V^2 s$ ($p = 2 \times 10^{-2}$, AUC = 0.82, sensitivity = 0.69, specificity = 0.73). Postictal A wavelet power W at C4 for the delta band was 651% greater than in the controls ($2{,}020 \pm 3{,}837$ $\mu V^2 s$ vs. 269 ± 136 $\mu V^2 s$, $p = 1 \times 10^{-5}$, AUC = 0.83, sensitivity = 0.76, specificity = 0.83) and 402% greater than that for interictal segments ($p = 1 \times 10^{-2}$, AUC = 0.74, sensitivity = 0.69, specificity = 0.77). There were no statistically significant differences in the interictal and postictal B delta wavelet power. Thus, the increase in postictal theta and delta wavelet power subsides within 30 s after the absence seizure.

Both for the theta and beta bands, the interictal wavelet power W was positively correlated with the percentage of time in seizure PTS in majority of channels. For theta waves, there were 17 such channels and the average value of Pearson's correlation coefficient r was equal to 0.51 ± 0.11 (range 0.26–0.66, maximum at T3 and minimum at P4). For beta rhythm, we found 16 channels where correlations were significant (average value $r = 0.51$, range 0.19–0.66, maximum at P3 and minimum at O2). No statistically significant relationship between W and PTS was observed for alpha waves.

One can see in **Figure 4** that pharmacotherapy primarily attenuates the low-frequency part of EEG spectrum. For all the channels, the values of interictal posttreatment delta and theta power are smaller than the pretreatment ones. In particular, for the delta band, W for C4 channel fell 45% from 394 ± 280 $\mu V^2 s$ to 218 ± 328 $\mu V^2 s$ ($p = 7 \times 10^{-3}$, AUC = 0.90, sensitivity = 0.75, specificity = 0.84). The less pronounced decrease in posttreatment beta power was observed in 13 channels. The fact that there is no increase of posttreatment alpha wavelet power implies that the attenuation of theta rhythm does not result from EEG maturation but is caused by treatment.

For channel C4, the reduction of W was observed in 100 and 81% patients for the theta and beta band, respectively. The data presented in **Figures 4E,F** are representative of the downward trend in the wavelet power during pharmacotherapy. For theta rhythm, a reduction was observed in all patients for channel C4, and all but one in channels: F7, T5, T6, P3, P4, and Pz. Upon averaging of all channels, both for theta and beta waves the reduction of W was observed in 94% cases.

Out of 38 potential attributes, only 13 had non-zero gain ratio. For theta rhythm: C4 (0.28), Cz (0.28), P3 (0.24), O1 (0.22), Fz (0.21), Pz(0.21), C3 (0.20), For beta waves: Pz (0.29), P3(0.28), P4 (0.28), O1 (0.26), O2 (0.21), C4 (0.19). The Bayesian network classifier (with default parameters) turned out to be the most balanced. It achieved accuracy of 78%, specificity 79%, and sensitivity 77%. The classification was based on only six channels: C4, Cz, Fz for theta band and Pz, P3, O1 for beta band.

[1]https://www.cs.waikato.ac.nz/ml/weka/

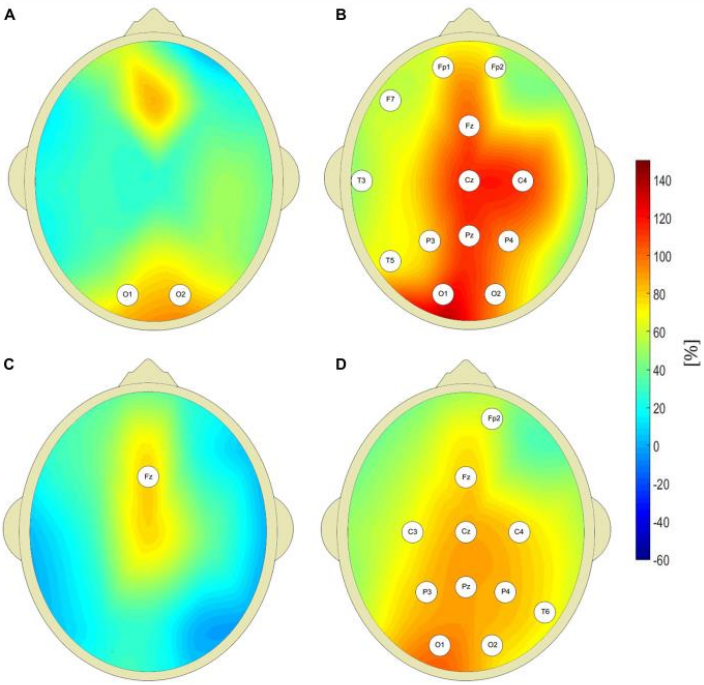

FIGURE 2 | Percentage differences between wavelet power of closed-eyes interictal pretreatment EEG of CAE patients and the controls (with respect to controls) for: delta **(A)**, theta **(B)**, alpha **(C)**, and beta **(D)** rhythms. The EEG channel labels indicate sites for which the differences were statistically significant.

DISCUSSION

GAERS and the WAG/Rij rodent models have paved the way for the understanding of pathophysiology of human CAE seizures (Akman et al., 2010). Lüttjohann and Van Luijtelaar reviewed animal studies and the translation of research results from rodent models to humans (Lüttjohann and Van Luijtelaar, 2015). According to the cortical focus theory of Meeren et al. (2005) the genesis of absence seizure starts with a single spike which rapidly spreads over the hyperexcited cortex. The formation of prominent SWDs is possible only due to interaction with the thalamus which acts as a resonant circuit. The rapid generalization of spike-wave activity over the cortex is due to short-range intracortical fibers and to a subpopulation of cells that have long-range association fibers. These fibers run under the cortex in the white matter, making extensive connections with other cortical areas.

In rats, SWDs emerge from the cortical focus which is located either within the perioral somatosensory cortex (WAG/Rij) or the secondary somatosensory cortex (GAERS) and subsequently propagate via the corticothalamocortical loop. Polack et al. demonstrated that blockade of action potential discharge and synaptic activities in facial somatosensory cortical neurons (by topical application of tetrodotoxin) prevents the formation of SWDs (Polack et al., 2009). In contrast, pharmacological inhibition of a remote motor cortical region does not suppress ictal activities. Westmijse et al. discovered, using a beamforming source localization technique, that in humans the sources of spikes from a train of SWDs were at the frontal lateral, central and medial parietal cortices (Westmijse et al., 2009). The involvement of the thalamus in the generation of SWDs was demonstrated in combined EEG-fMRI (Granert et al., 2008; Moeller et al., 2010) and MEG (Tenney et al., 2013) studies. The differences between rat and human data are in the frequencies of SWDs (6–11 Hz vs. 2.5–4 Hz) and the location of the early local cortical activity which is quite variable in humans. The location may even change during a seizure (Westmijse et al., 2009) and is predominantly, but not exclusively, located in the frontal-central/parietal areas. The low variability of the position of cortical focus in the rats can easily be explained by the fact that both epileptic strains are fully inbred, and the animals are homozygous.

Herein, we found that the pretreatment closed-eyes theta wavelet power of CAE patients was much higher than that of age-matched controls at multiple sites of the 10–20 system.

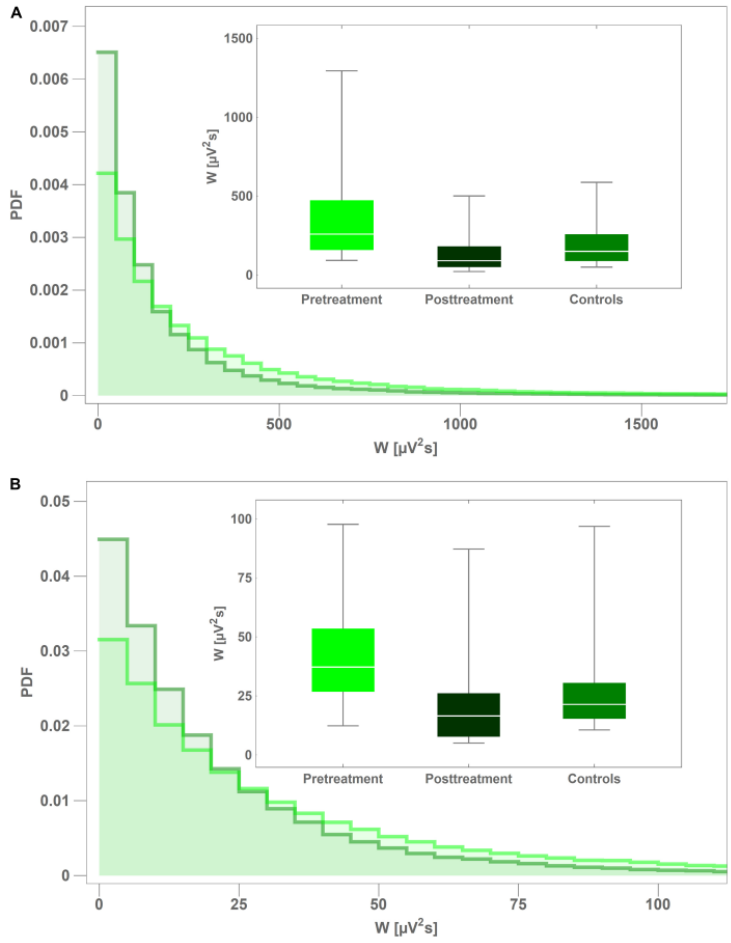

FIGURE 3 | Comparison of probability density function (PDF) of instantaneous wavelet power of interictal pretreatment EEG of CAE patients (light green) and the controls (dark green) for: theta **(A)** and beta **(B)** rhythms. PDFs were calculated from the closed-eyes segments extracted from C4 channel. The insets in both subplots show the boxplots of time-averaged values of the pretreatment and posttreatment wavelet power of as well as that of the controls.

Moreover, the theta wavelet power was positively correlated with the percentage of time in seizure. This result should not come as a surprise. In the late 1960s Doose et al. argued that strong rhythmic theta activity was an age-dependent electroencephalographic expression of a genetic disposition to convulsions, see a review paper (Doose and Baier, 1988) for a complete list of references. This hypothesis was noted, along with the opposing view, by the authors of the classic text on encephalography (Schomer and Lopes da Silva, 2018). To the best of our knowledge, initial observations have not been followed up on using quantitative EEG analysis (Doose et al., 2003). The more recent research provided new evidence for the role of theta rhythm in epilepsy. Clemens et al. (2012) using a Low Resolution Electromagnetic Tomography (LORETA) source localization found increased theta activity in the basal prefrontal and medial temporal limbic areas of CAE patients. Dömötör et al. (2017) observed reduced current source density in 0.5–8 Hz frequency range in CAE patients who responded to pharmacotherapy. Douw et al. (2010) in their MEG studies found that theta band brain connectivity and network topology is altered in epilepsy

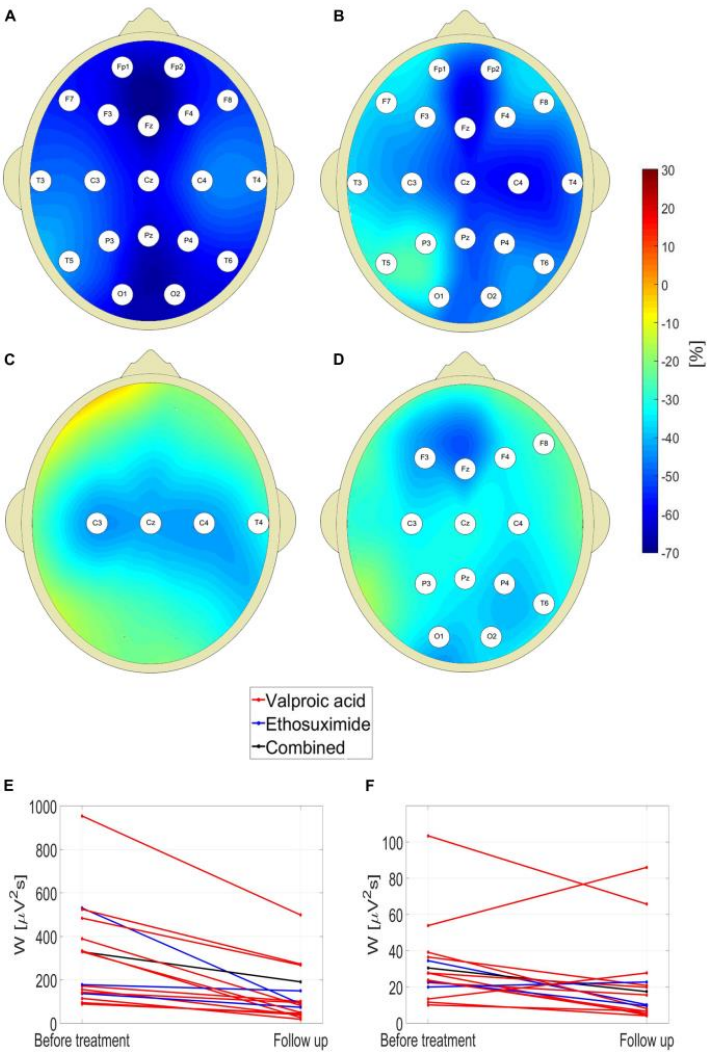

FIGURE 4 | Percentage change in posttreatment closed-eyes wavelet power of CAE patients with respect to the baseline for: delta **(A)**, theta **(B)**, alpha **(C)**, and beta **(D)** rhythms. The EEG channel labels indicate sites for which the differences were statistically significant. Effect of treatment on **(E)** theta and **(F)** beta wavelet power *W* in C4 channel.

which developed in brain tumor patients. Milikovsky et al. (2017) discussed the properties of theta dynamics in the animal model of postinjury epilepsy. Sitnikova and van Luijtelaar (2009) found that the increased delta and theta power preceded SWDs in WAG/Rij rats.

We interpret the results presented herein as evidence in support of the following postulates. We hypothesize that the increased theta rhythm power in CAE patients is a manifestation of cortical hyperexcitability (Vestal and Blumenfeld, 2010). Since strong theta rhythm may be found in up to 15% of healthy

children (Doose and Baier, 1988), cortical hyperexcitability may be a necessary but not a sufficient prerequisite for CAE. The increased beta power may reflect propensity for epileptic spikes generation – spikes that trigger absence seizures. This interpretation is corroborated by the recent work of Sorokin et al. (2016) who found that in rats absence seizure susceptibility correlates with pre-ictal beta oscillation. It is worth pointing out that as we detune the parameters of the analyzing wavelet away from the values optimal for spike detection, the differences in beta power between the pretreatment patients and controls disappear.

As with all epileptic syndromes, once the diagnosis of CAE is confirmed, only the absence or recurrence of seizures provides an indication as to whether anti-epileptic drugs (AEDs) have had any effect. We argue that the distinct features of CAE wavelet power spectrum may be used to define an EEG biomarker which could be used for diagnosis and long-term monitoring of patients. The most apparent applications of such monitoring would be in the assessment of the efficacy of pharmacotherapy and its duration.

Over the last three decades, transcranial magnetic stimulation (TMS) has become a principal tool for accessing cortical excitability associated with epilepsy (Bauer et al., 2014). However, there are essentially no TMS studies of drug-naive patients with CAE (Kessler, 2016). The barriers to the inclusion of children from such studies stem not only from the very nature of this experimental technique, e.g., its duration or immobilization of head during measurement, but also from a few fundamental reasons. For example, it is not clear whether the motor cortex physiology is a reliable marker of seizure susceptibility in children with less mature brain networks. Moreover, abnormalities in TMS markers of cortical excitability are not specific to epilepsy and may observed, among others, in ADHD, a common comorbid condition in children with epilepsy (Reilly et al., 2017). Future research should verify whether measurement of theta band power in CAE patients could be used in lieu of TMS. In particular, the previous TMS studies (Wright et al., 2006; Badawy et al., 2009) revealed that increased excitability preceded epileptic seizures. Thus, the question arises as to whether temporal changes in cortical excitability occur in CAE.

To use theta and beta wavelet power as biomarkers of CAE it needs to be proved that the observed changes between patient and controls are reproducible (which is important considering inherent variability of human EEG) and are not affected by the developmental changes of EEG which occur about the age of puberty. The main limitation of the study comes from its retrospective character. We analyzed the routine video EEGs that were used for diagnosis. We were able to demonstrate that the differences between patients and controls persisted throughout the EEG recordings. In particular, there were no differences in theta and beta wavelet power between the interictal segment (preceding the first observed seizure) and the preictal A, and postictal B segments. The data showed that the changes in wavelet power associated with absence seizure subsided within 30 s after its end. As we already mentioned, cortical excitability is known to vary with time. There is no doubt that future long-term EEG monitoring must verify our findings. The mean age of subjects was 7.4 ± 1.9 years. The follow-up EEGs were recorded on average one and a half year later. Puberty usually occurs in girls between the ages of 10 and 14, while in boys it generally occurs later. Thus, it is unlikely that the observed reduction of delta and theta power was merely effect of maturation and not brought about by pharmacotherapy. Moreover, there were no increases in alpha wavelet power in pretreatment and posttreatment EEGs which argues against the maturation effect.

Even though the analyzed pretreatment EEG segments were short, we were able to construct a balanced classifier which differentiated patients and controls with good accuracy using only several attributes. The assessment of applicability of such classifier in absence seizure diagnostics requires further studies with much larger datasets.

Pharmacological seizure control with acceptable side effects is achieved for slightly more than half of children with CAE. Herein we found that pharmacotherapy most effectively suppresses low-frequency EEG oscillations. Quantitative EEG analysis offers a unique opportunity to design a treatment which would more selectively attenuate the pathological theta and/or beta rhythms. The availability of low-cost, Internet connected personal EEG devices paves the way for home monitoring of patients which would facilitate drug titration and termination of pharmacotherapy.

DATA AVAILABILITY STATEMENT

The raw data supporting the conclusions of this article will be made available by the authors, without undue reservation, to any qualified researcher.

ETHICS STATEMENT

The studies involving human participants were reviewed and approved by the ethics committee of T. Marciniak Hospital in Wrocław, Poland. Written informed consent from the participants' legal guardian/next of kin was not required to participate in this study in accordance with the national legislation and the institutional requirements.

AUTHOR CONTRIBUTIONS

MJK, ML, and PG: conceptualization. PG, MK, MJK, and ML: investigation and original draft preparation. BW, WW, and WJ: review and editing. All authors contributed to methodology and formal analysis.

ACKNOWLEDGMENTS

MJK and ML dedicate this manuscript to the memory of our friend Andrzej Kozik who initiated this research project. This manuscript has been released as a Pre-Print at https://www.biorxiv.org/ (Glaba et al., 2019).

REFERENCES

Akman, O., Demiralp, T., Ates, N., and Onat, F. Y. (2010). Electroencephalographic differences between WAG/Rij and GAERS rat models of absence epilepsy. *Epilepsy Res.* 89, 185–193. doi: 10.1016/j.eplepsyres.2009.12.005

Badawy, R., MacDonell, R., Jackson, G., and Berkovic, S. (2009). The peri-ictal state: cortical excitability changes within 24 h of a seizure. *Brain* 132, 1013–1021. doi: 10.1093/brain/awp017

Bauer, P. R., Kalitzin, S., Zijlmans, M., Sander, J. W., and Visser, G. H. (2014). Cortical excitability as a potential clinical marker of epilepsy: a review of the clinical application of transcranial magnetic stimulation. *Int. J. Neural Syst.* 24:1430001. doi: 10.1142/S0129065714300010

Clemens, B., Puskás, S., Besenyei, M., Emri, M., Opposits, G., Kis, S. A., et al. (2012). EEG-LORETA endophenotypes of the common idiopathic generalized epilepsy syndromes. *Epilepsy Res.* 99, 281–292. doi: 10.1016/j.eplepsyres.2011.12.008

Covanis, A. (2010). "Childhood absence epilepsy," in *Atlas of Epilepsies*, ed. C. P. Panayiotopoulos (London: Springer), 1013–1023.

Dlugos, D., Shinnar, S., Cnaan, A., Hu, F., Moshé, S., Mizrahi, E., et al. (2013). Pretreatment EEG in childhood absence epilepsy: associations with attention and treatment outcome. *Neurology* 81, 150–156. doi: 10.1212/WNL.0b013e31829a3373

Dömötör, J., Clemens, B., Puskás, S., and Fekete, I. (2017). Decrease of global current source density predicts successful treatment in absence and juvenile myoclonic epilepsies. *Epilepsy Res.* 133, 1–5. doi: 10.1016/j.eplepsyres.2017.03.006

Doose, H., and Baier, W. K. (1988). Theta rhythms in the EEG: a genetic trait in childhood epilepsy. *Brain Dev.* 10, 347–354. doi: 10.1016/s0387-7604(88)80091-3

Doose, H., Neubauer, B. A., and Neuhäuser, G. (2003). *EEG in Childhood Epilepsy: Initial Presentation and Long-Term Follow-Up*. France: John Libbey Eurotext.

Douw, L., van Dellen, E., de Groot, M., Heimans, J. J., Klein, M., Stam, C. J., et al. (2010). Epilepsy is related to theta band brain connectivity and network topology in brain tumor patients. *BMC Neurosci.* 11:103. doi: 10.1186/1471-2202-11-103

Gallentine, W. B., and Mikati, M. A. (2012). Genetic generalized epilepsies. *J. Clin. Neurophysiol.* 29, 408–419. doi: 10.1097/WNP.0b013e31826bd92a

Glaba, P., Latka, M., Krause, M., Kuryło, M., Jernajczyk, W., Walas, W., et al. (2019). Changes in interictal pretreatment and posttreatment EEG in childhood absence epilepsy. *bioRxiv* [Preprint], doi: 10.1101/699868

Granert, O., Jansen, O., Stephani, U., Muhle, H., Wolff, S., Siniatchkin, M., et al. (2008). Simultaneous EEG-fMRI in drug-naive children with newly diagnosed absence epilepsy. *Epilepsia* 49, 1510–1519. doi: 10.1111/j.1528-1167.2008.01626.x

Kessler, S. K. (2016). "Non-invasive brain stimulation in pediatric epilepsy: diagnostic and therapeutic uses," in *Pediatric Brain Stimulation*, eds A. Kirton, and D. L. Gilbert (Amsterdam: Elsevier), 281–304. doi: 10.1016/b978-0-12-802001-2.00014-x

Latka, M., Was, Z., Kozik, A., and West, B. J. (2003). Wavelet analysis of epileptic spikes. *Phys. Rev. Eng.* 67:052902. doi: 10.1103/PhysRevE.67.052902

Lopes da Silva, F. H., Blanes, W., Kalitzin, S. N., Parra, J., Suffczynski, P., and Velis, D. N. (2003). Dynamical diseases of brain systems: different routes to epileptic seizures. *IEEE Trans. Biomed. Eng.* 50, 540–548. doi: 10.1109/TBME.2003.810703

Lüttjohann, A., and Van Luijtelaar, G. (2015). Dynamics of networks during absence seizure's on- and offset in rodents and man. *Front. Physiol.* 6:16. doi: 10.3389/fphys.2015.00016

Maris, E., and Oostenveld, R. (2007). Nonparametric statistical testing of EEG- and MEG-data. *J. Neurosci. Methods* 164, 177–190. doi: 10.1016/j.jneumeth.2007.03.024

Meeren, H., van Luijtelaar, G., Lopes da Silva, F., and Coenen, A. (2005). Evolving concepts on the pathophysiology of absence seizures: the cortical focus theory. *Arch. Neurol.* 62, 371–376. doi: 10.1001/archneur.62.3.371

Milikovsky, D. Z., Weissberg, I., Kamintsky, L., Lippmann, K., Schefenbauer, O., Frigerio, F., et al. (2017). Electrocorticographic dynamics as a novel biomarker in five models of epileptogenesis. *J. Neurosci.* 37, 4450–4461. doi: 10.1523/jneurosci.2446-16.2017

Moeller, F., Gotman, J., Dubeau, F., Siniatchkin, M., Muhle, H., LeVan, P., et al. (2010). Absence seizures: individual patterns revealed by EEG-fMRI. *Epilepsia* 51, 2000–2010. doi: 10.1111/j.1528-1167.2010.02698.x

Polack, P.-O., Mahon, S., Chavez, M., and Charpier, S. (2009). Inactivation of the somatosensory cortex prevents paroxysmal oscillations in cortical and related thalamic neurons in a genetic model of absence epilepsy. *Cereb. Cortex* 19, 2078–2091. doi: 10.1093/cercor/bhn237

Reilly, C., Atkinson, P., Das, K. B., Chin, R. F. M., Aylett, S. E., Burch, V., et al. (2017). Parent- and teacher-reported symptoms of ADHD in school-aged children with active epilepsy: a population-based study. *J. Atten. Disord.* 21, 887–897. doi: 10.1177/1087054714558117

Sadleir, L. G., Farrell, K., Smith, S., Connolly, M. B., and Scheffer, I. E. (2006). Electroclinical features of absence seizures in childhood absence epilepsy. *Neurology* 67, 413–418. doi: 10.1212/01.wnl.0000228257.60184.82

Schomer, D. L., and Lopes da Silva, F. H. (2018). *Niedermeyer's Electroencephalography: Basic Principles, Clinical Applications, and Related Fields*, 7th Edn. Oxford: Oxford University Press.

Sitnikova, E., and van Luijtelaar, G. (2009). Electroencephalographic precursors of spike-wave discharges in a genetic rat model of absence epilepsy: power spectrum and coherence EEG analyses. *Epilepsy Res.* 84, 159–171. doi: 10.1016/j.eplepsyres.2009.01.016

Sorokin, J., Paz, J. T., and Huguenard, J. R. (2016). Absence seizure susceptibility correlates with pre-ictal beta oscillations. *J. Physiol. Paris* 110, 372–381. doi: 10.1016/j.jphysparis.2017.05.004

Tenney, J. R., Fujiwara, H., Horn, P. S., Jacobson, S. E., Glauser, T. A., and Rose, D. F. (2013). Focal corticothalamic sources during generalized absence seizures: a MEG study. *Epilepsy Res.* 106, 113–122. doi: 10.1016/j.eplepsyres.2013.05.006

Vestal, M., and Blumenfeld, H. (2010). "Pathophysiology of absence seizures," in *Atlas of Epilepsies*, ed. C. P. Panayiotopoulos (London: Springer), 225–234. doi: 10.1007/978-1-84882-128-6-30

Westmijse, I., Ossenblok, P., Gunning, B., and van Luijtelaar, G. (2009). Onset and propagation of spike and slow wave discharges in human absence epilepsy: a MEG study. *Epilepsia* 50, 2538–2548. doi: 10.1111/j.1528-1167.2009.02162.x

Wright, M.-A. S. Y., Orth, M., Patsalos, P. N., Smith, S. J. M., and Richardson, M. P. (2006). Cortical excitability predicts seizures in acutely drug-reduced temporal lobe epilepsy patients. *Neurology* 67, 1646–1651. doi: 10.1212/01.wnl.0000242729.85335.a3

Conflict of Interest: The authors declare that the research was conducted in the absence of any commercial or financial relationships that could be construed as a potential conflict of interest.

9. Publikacja 2 – *Absence Seizure Detection Algorithm for Portable EEG Devices*

Druga praca została poświęcona problemowi automatycznej detekcji napadów nieświadomości. W ostatnich latach pojawiły się na rynku niedrogie, mobile urządzenia EEG, które wykorzystują zaledwie kilka elektrod. Celem pracy było sprawdzenie możliwości długoterminowego monitorowania pacjentów z CAE i JAE. Potencjalne korzyści z tego rodzaju monitoringu obejmują ułatwienie diagnozy, spersonalizowane miareczkowanie leku czy określenie długości farmakoterapii. Nowatorski algorytm detekcji napadów nieświadomości oparty jest na właściwościach ciągłej transformaty falkowej z funkcją bazową Morleta. Prezentowane w niniejszej pracy wyniki pokazały, że skuteczność zaproponowanego algorytmu jest wystarczająco duża do zastosowań klinicznych, a szybkość działania pozwala na implementację na powszechnie dostępnych smartfonach.

Podobnie jak w przypadku pierwszej publikacji mój wkład wynosi 60%. Zakres mojej pracy był analogiczny.

frontiers in Neurology

BRIEF RESEARCH REPORT
published: 29 June 2021
doi: 10.3389/fneur.2021.685814

Absence Seizure Detection Algorithm for Portable EEG Devices

Pawel Glaba[1], Miroslaw Latka[1], Małgorzata J. Krause[2], Sławomir Kroczka[3], Marta Kuryło[2], Magdalena Kaczorowska-Frontczak[4], Wojciech Walas[5], Wojciech Jernajczyk[6], Tadeusz Sebzda[7] and Bruce J. West[8]*

[1] Department of Biomedical Engineering, Wroclaw University of Science and Technology, Wroclaw, Poland, [2] Department of Pediatric Neurology, T. Marciniak Hospital, Wrocław, Poland, [3] Department of Child Neurology, Jagiellonian University Medical College, Krakow, Poland, [4] The Children's Memorial Health Institute, Warszawa, Poland, [5] Paediatric and Neonatal Intensive Care Unit, Institute of Medical Sciences, University of Opole, Opole, Poland, [6] Clinical Neurophysiology, Institute of Psychiatry and Neurology, Warszawa, Poland, [7] Department of Pathophysiology, Wroclaw Medical University, Wroclaw, Poland, [8] Office of the Director, Army Research Office, Research Triangle Park, Durham, NC, United States

Absence seizures are generalized nonmotor epileptic seizures with abrupt onset and termination. Transient impairment of consciousness and spike-slow wave discharges (SWDs) in EEG are their characteristic manifestations. This type of seizure is severe in two common pediatric syndromes: childhood (CAE) and juvenile (JAE) absence epilepsy. The appearance of low-cost, portable EEG devices has paved the way for long-term, remote monitoring of CAE and JAE patients. The potential benefits of this kind of monitoring include facilitating diagnosis, personalized drug titration, and determining the duration of pharmacotherapy. Herein, we present a novel absence detection algorithm based on the properties of the complex Morlet continuous wavelet transform of SWDs. We used a dataset containing EEGs from 64 patients (37 h of recordings with almost 400 seizures) and 30 age and sex-matched controls (9 h of recordings) for development and testing. For seizures lasting longer than 2 s, the detector, which analyzed two bipolar EEG channels (Fp1-T3 and Fp2-T4), achieved a sensitivity of 97.6% with 0.7/h detection rate. In the patients, all false detections were associated with epileptiform discharges, which did not yield clinical manifestations. When the duration threshold was raised to 3 s, the false detection rate fell to 0.5/h. The overlap of automatically detected seizures with the actual seizures was equal to ∼96%. For EEG recordings sampled at 250 Hz, the one-channel processing speed for midrange smartphones running Android 10 (about 0.2 s per 1 min of EEG) was high enough for real-time seizure detection.

Keywords: childhood absence epilepsy, EEG, wavelets, detector, portable device

OPEN ACCESS

Edited by:
Sharon Chiang,
University of California, San Francisco, United States

Reviewed by:
Kais Gadhoumi,
Duke University, United States
Jon Kleen,
University of California, San Francisco, United States

***Correspondence:**
Miroslaw Latka
miroslaw.latka@pwr.edu.pl

Specialty section:
This article was submitted to Epilepsy, a section of the journal Frontiers in Neurology

Received: *25 March 2021*
Accepted: *03 June 2021*
Published: *29 June 2021*

Citation:
Glaba P, Latka M, Krause MJ, Kroczka S, Kuryło M, Kaczorowska-Frontczak M, Walas W, Jernajczyk W, Sebzda T and West BJ (2021) Absence Seizure Detection Algorithm for Portable EEG Devices. Front. Neurol. 12:685814. doi: 10.3389/fneur.2021.685814

1. INTRODUCTION

Typical absence seizures are brief (lasting seconds) generalized nonmotor epileptic seizures with an abrupt onset and termination (1, 2). Transient impairment of consciousness and spike-slow wave discharges (SWDs) in electroencephalogram (EEG) are their characteristic manifestations. Typical absence seizures are severe in childhood (CAE) and juvenile (JAE) absence epilepsies but mild or inconspicuous in other syndromes such as juvenile myoclonic epilepsy (JME). Typical absence seizures are predominantly spontaneous, but in about 90% of untreated patients, they may be provoked by hyperventilation. Sleep deprivation, photostimulation, specific geometric

patterns, video games, and even thinking may also precipitate them. The pathophysiology of absence seizures is fundamentally different from other types of seizures, making their diagnosis and treatment unique.

CAE is the most common pediatric epileptic syndrome with an age of onset of around 6–8 years (3). It has a prevalence of 10–15% in childhood epilepsies. In children under the age of 16 years, the incidence rate is 1.3 to 6 per 100,000. The ictal EEG of a CAE seizure demonstrates rhythmic 3 Hz bilateral, synchronous, and symmetrical spike and wave discharges (SWDs) with a median duration of approximately 10 s, which on average appear several times per day. In pyknoleptic cases, hundreds of seizures may occur daily (4). The 2010 Childhood Absence Epilepsy Study showed that only 37% of all enrolled subjects were free from treatment failure on their first medication a year after diagnosis (5).

JAE typically begins between 10 and 16 years of age and is usually a life-long condition. JAE seizures tend to be longer than in CAE (lasting up to 45 s) and non-pyknoleptic (typically occurring less than daily).

While CAE and JAE are distinct epilepsy syndromes, there is considerable overlap between them, and the cut-off age remains controversial. During disease, patients with JAE or patients in the overlap group are more likely to develop generalized tonic-clonic seizures and myoclonic attacks. In the long-term follow-up (mean 26 years, range 3–69), only 58% of the patients with absence seizures were in remission (6).

The diagnosis of absence seizures is laborious since it requires analysis of long video-EEGs (on average around 30 minutes long) to detect seizures and their clinical manifestations (consciousness impairment, motor symptoms) and abnormal EEG background activity.

The appearance of low-cost, portable EEG devices (7) has paved the way for long-term, remote monitoring of patients with absence seizures. The potential benefits of this kind of monitoring include facilitation of diagnosis, personalized drug titration, and determining of duration of pharmacotherapy. The need for automatic and reliable detection of absence seizures has long been recognized (8). Diverse algorithms have been proposed so far to detect seizures in animal models of epilepsy (9–12) or in human EEG (13–21). Herein, we present a novel approach to absence seizure detection, which is applicable both to clinical EEGs and recordings made with portable EEG devices with a small number of channels. The algorithm's efficiency and robustness to motion artifacts enable its implementation on mobile devices.

2. MATERIALS AND METHODS

2.1. EEG Recordings

Wroclaw Medical University's Ethics Committee approved a retrospective analysis of routine anonymized video-EEG recordings of patients (36 with CAE and 28 with JAE) as well as 30 EEGs of age-matched controls. Epilepsy syndrome was established based on history, age at onset, clinical EEG findings, and neuroimaging. EEGs were acquired with Elmiko Digitrack (BRAINTRONICS B.V. ISO-1032CE amplifier) or Grass Comet Plus EEG (AS40-PLUS amplifier) using 200 or 250 Hz sampling frequency. The international 10-20 standard was used to arrange 19 Ag/AgCl electrodes (impedance below 5kΩ). Total EEG duration was equal to 37 and 9 h for the patients and controls, respectively.

We assigned patients' EEG to either training or testing datasets. In the first one, there were 34 recordings (22 CAE and 12 JAE) with 199 seizures (6 ± 4 per patient and averaged seizure duration equal to 12 ± 4 s). In the 30 recordings of the testing dataset (15 CAE and 15 JAE), there were 177 absence seizures (6 ± 5 per patient and averaged duration equal to 12 ± 6 s). An experienced neurologist carried out a visual EEG inspection and marked the seizures with a 1 s accuracy.

Figure 1 provides the rationale for using the longitudinal bipolar montage. The seizure detector was developed and tested for two channels: Fp1-T3 and Fp2-T4.

We used three filters for EEG preprocessing: a second-order infinite impulse response (IIR), 6th-order high-pass Butterworth with a cutoff frequency of 0.5 Hz, and 6th-order low-pass Butterworth with a cutoff frequency of 25 Hz. These filters remove 50 Hz power line noise, EEG baseline drift, and muscle artifacts, respectively.

2.2. Continuous Wavelet Transform

The continuous wavelet transform (CWT) of a signal $s(t)$ is an integral transform:

$$T[s](a,t_0)=\frac{1}{\sqrt{a}}\int_{-\infty}^{+\infty}s(t)\psi^*\left(\frac{t-t_0}{a}\right)dt \tag{1}$$

with the basis functions $\psi(a,t_0) = \psi(t-t_0/a)$, known as wavelets, that are translated and scaled version of the mother function $\psi(t)$ (22). Motivated by the results of the previous study (23), as a mother function, we use the complex Morlet wavelet (24, 25):

$$\psi(t)=\frac{1}{\pi^{1/4}}e^{2\pi i f_c t}e^{-t^2/2} \tag{2}$$

whose Fourier transform $\hat{\psi}(f)$ is given by

$$\hat{\psi}(f)=\sqrt{2}\sqrt[4]{\pi}e^{-2\pi^2(f-fc)^2}. \tag{3}$$

The real parameter f_c is called the center frequency since it is equal to the maximum point of the wavelet's Fourier power spectrum. The scale a corresponds to the following pseudofrequency:

$$f_a=\frac{f_c}{a}. \tag{4}$$

As we can see in Equations (2, 3), the wavelets are localized both in time and frequency domains. This dual localization makes CWT particularly applicable to the detection of transient events such as absence seizures.

Seizure detection is based on the properties of the instantaneous wavelet power $\left|T[s](a,t_0)\right|^2$ normalized by signal's variance σ^2:

$$w^{(n)}(f_a,t_0)=\left|T[s](a,t_0)\right|^2/\sigma^2. \tag{5}$$

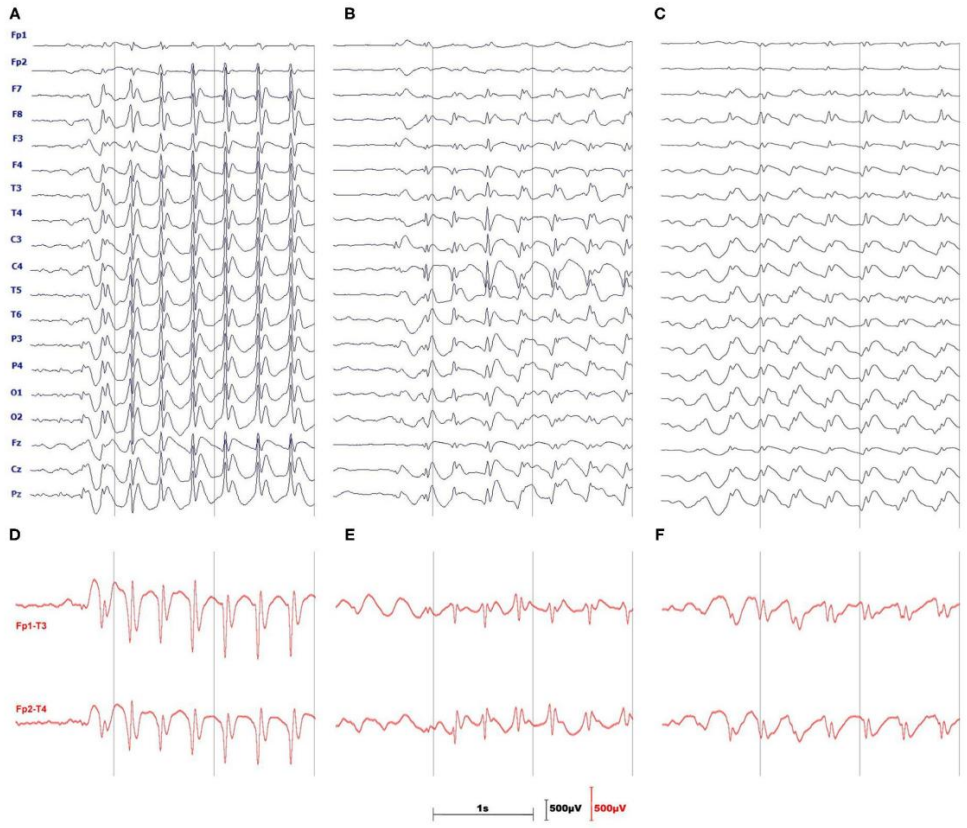

FIGURE 1 | Three monopolar EEGs illustrate the difficulties of absence seizure detection in a single channel. **(A)** is a textbook example of prominent, generalized SWDs. The amplitude of spikes **(B)** or slow waves **(C)** may be small and SWDs may be pronounced only in a handful of channels. **(D–F)** show the advantages of using the longitudinal, bipolar montage which in most cases augments both spikes and slow waves of SWDs.

If we apply the convolution theorem to Equation (1), then it is apparent that the Fourier transform of $T[s](a, t_0)$ is the pointwise product of the Fourier transforms of the signal and wavelet. Thus, it is possible to calculate CWT by taking the inverse Fourier transform of such a product. We used this approach in the MATLAB function, presented in **Supplementary Materials**, which calculates the complex Morlet CWT (25). We included the listing to facilitate the reproduction of the results and avoid confusion related to erroneous normalization of the most popular Python and MATLAB CWT implementations. We will discuss this problem in a forthcoming publication.

For the most commonly used wavelets, such as the complex Morlet, the analytical expression for their Fourier transform is known. Therefore, in the presented function, we calculate only the FFT of the signal and use Equation (3) to obtain the wavelet's FFT spectrum.

The complex Morlet CWT of the preprocessed Fp1-T3 and Fp2-T4 channels was calculated without signal partitioning.

2.3. Detection Algorithm

The detection of an absence seizure (**Figures 2A,E**), defined as an SWD lasting for more than 2 s (26), proceeds in two steps. First, we locate the train of slow waves and then verify that there are epileptic spikes embedded in it. One can see in the scalogram **Figure 2B** that when the wavelet's pseudofrequency is close to that of an absence ($\sim$ 3 Hz), then the wavelet power forms a prominent ridge. We refer to the time interval during which the power exceeds the chosen threshold T_E as the slow-wave

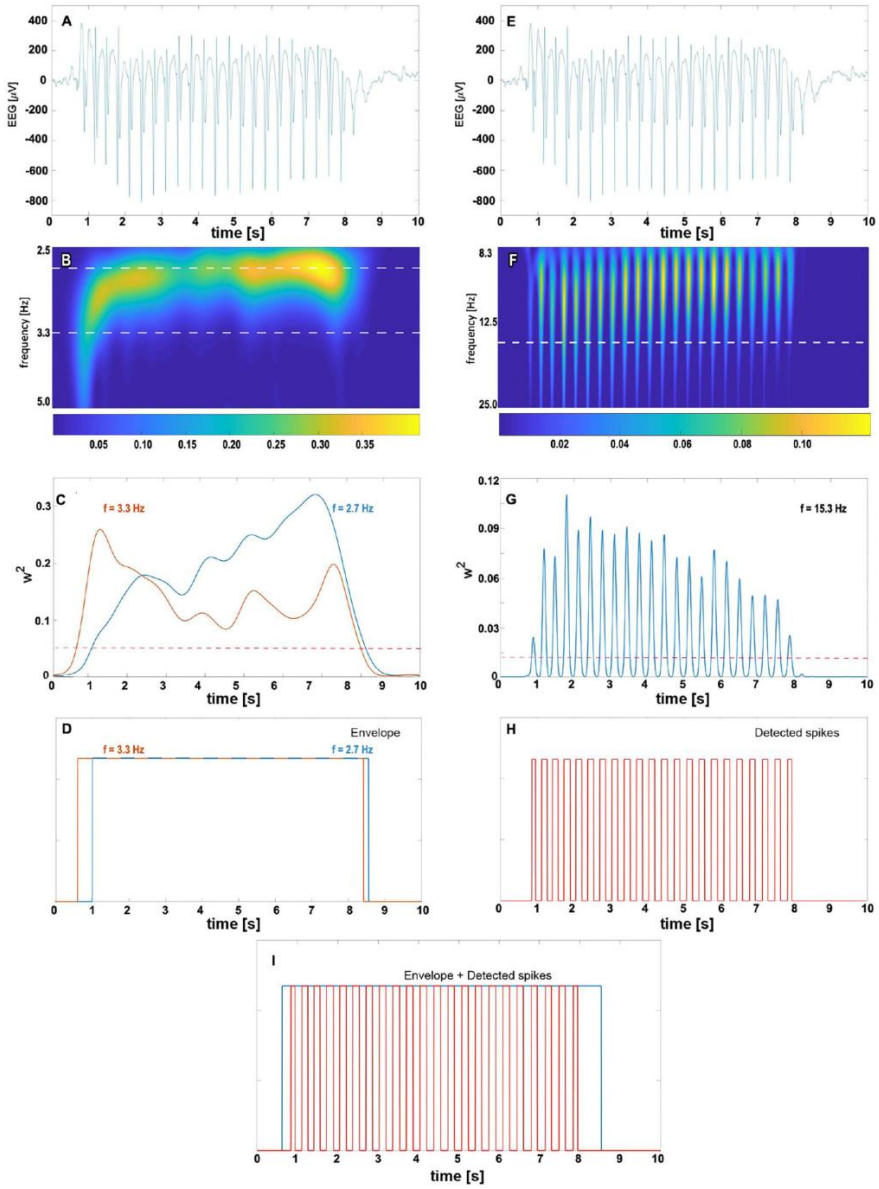

FIGURE 2 | The complex Morlet wavelet analysis of absence slow wave **(B–D)** and spikes **(F–H)**. For clarity, absence EEG is presented at the top of both columns (subplots **A,E**). The density map **(B)** shows the time evolution of normalized wavelet power for pseudo-frequencies in [2.5, 5] Hz range. The 2.7 and 3.3 Hz cuts

(Continued)

FIGURE 2 | (marked with the white horizontal dashed line) are plotted in subplot **(C)** with the blue and orange lines, respectively. We refer to time intervals during which the wavelet power for these frequencies exceeds the predetermined threshold (represented in **(C)** by the red dashed horizontal line) as the slow-wave envelopes. For a given seizure, the total envelope is obtained by merging 2.7 and 3.3 Hz envelopes as shown in **(D)**. The right column shows the complex Morlet analysis with parameters tuned to spike detection. The prominent ridges in wavelet power density map **(F)** and peaks in 15.3 Hz cut **(G)** are manifestations of seizure's spikes. The white horizontal dashed line in **(F)** corresponds to the spike frequency 15.3 Hz obtained in the grid search. The train of unit pulses in **(H)** indicates time intervals during which wavelet power for 15.3 Hz is greater than the spike threshold value (marked in subplot **(G)** with the red dashed horizontal line). An absence is detected whenever the epileptic spikes are found in the slow-wave envelope **(I)**.

envelope. This envelope is a unit boxcar function that takes on one whenever the power is greater than T_E. As the frequency of SWDs is subject-dependent and may even slightly vary during a seizure (15), we construct two envelopes with wavelet frequencies f_{low} and f_{high} (**Figure 2C**) and merge them as shown in **Figure 2D**. The merging amounts to a pointwise application of a logical OR function to both envelopes.

For a suitably chosen pseudofrequency f_{spike}, the wavelet power $w^{(n)}(f_{spike})$ peaks around the position of epileptic spikes (**Figure 2F**). If the percentage of samples PT within the final envelope for which the wavelet power is greater than T_S, we conclude that there are spikes (**Figure 2H**) within the envelope (**Figure 2I**). Such the envelope delineates the absence seizure.

In some cases, $w^{(n)}(f_{spike})$ may also be elevated for high-amplitude artifacts. To reduce the number of false positives, we modified the original algorithm. We do the following amplitude check and disregard all envelopes for which:

- More than 10% of the samples have amplitudes outside the range $[-500\ \mu V, 500\ \mu V]$ (in the differential montage epileptic spikes can have amplitudes of the order of hundreds μV).
- Any sample is outside the range [–1,000 μV, 1,000 μV].

For envelopes shorter than 5 s, we also calculate the variance of $w^{(n)}(f_{spike})$ to detect the wavelet power pulsatility of absence (**Figure 2G**). If such variance is greater than T_V, the detector flags the envelope as a seizure. We refer to such a comparison as the wavelet variance check.

Figure 3 shows the flowchart of the final absence seizure detection algorithm. The proposed algorithm may be used independently for channels Fp1-T3 and Fp2-T4. Alternatively, the seizure envelopes from these two channels may be superposed.

2.4. Determination of Algorithms' Parameters

We determine f_{low}, f_{high}, and T_E by maximizing the overlap of slow-wave envelopes with the absence seizures from a training dataset disregarding possible false detections.

Using these values, we search for the maximum of the following objective function:

$$O(f_{spike}, T_S, PT) = OVR_f - PERR - 0.5 \times FDET - FDET_C \quad (6)$$

to find f_{spike}, T_S, and PT_S – spike detection parameters. In Eq (6), OVR_f is the percentage overlap of slow-wave envelopes with seizures. $PERR$ is the percentage of the number of false positive samples in a given EEG. $FDET$ and $FDET_C$ are the number of false detections for the patients and controls, respectively.

The form of the objective function follows two requirements. The first is that we want to overlap the slow-wave envelope with the seizure as accurately as possible. The second is that in patients, false positives can be associated with epileptiform discharges with no clinical manifestations. Therefore, in Eq (6), the weight assigned to the patients' false detection penalty ($FDET$) is half of that given to the controls. We arbitrarily chose the 1:2 weight ratio.

T_V can be determined in the following way. We calculate the variance of $w^{(n)}(f_{spike})$ for the controls' EEGs. Then, we calculate the mean and standard deviation of the distribution. Finally, T_V is set to the mean increased by three standard deviations ($T_V = 0.05$).

We determined the slow-wave and spike detection parameters using the exhaustive grid search.

2.5. Software Implementation

The seizure detection software was implemented both in MATLAB (R2018a) and Java. In the latter case, we wrote a desktop version (which can be run on any computer with Java virtual machine) and a mobile version for Android smartphones. In Java software, we used the class FastFourierTransformer from Apache Commons Math Library (version 3.6.1). Testing and performance benchmarking was performed on a desktop PC with AMD Ryzen 7 3700X 8-Core processor running Windows 10 and Samsung S9 mobile phone (4GB of RAM and 2.8 GHz Samsung Exynos 9810 8-Core processor) with Android 10.

3. RESULTS

Using two-step (slow-wave envelope and spike detection) optimization on the training dataset, we obtained the following model parameters $f_{low} = 2.7$ Hz, $f_{high} = 3.3$ Hz, $T_E = 0.05$, $f_{spike} = 15.3$ Hz, $T_S = 0.012$, $PT_S = 12\%$. After the parameters were determined, we lowered the value of T_V from 0.05 to 0.008. This change is explained in Discussion section.

The seizure detector had 98.5% and 96.6% sensitivity for the training and testing datasets, respectively (see **Supplementary Tables 1, 2**). The corresponding false detection rates were equal to 0.9/h and 0.4/h. The overlap OVR of the detected and actual seizures was good for both datasets (97% ± 6% and 95% ± 10%). The percentage error $PERR$ that accounts for both false positives and erroneously extended slow-wave envelopes was equal to 0.9% ± 0.7% for both datasets.

Supplementary Table 3 shows that both the amplitude and wavelet variance checks contribute to the false detection reduction.

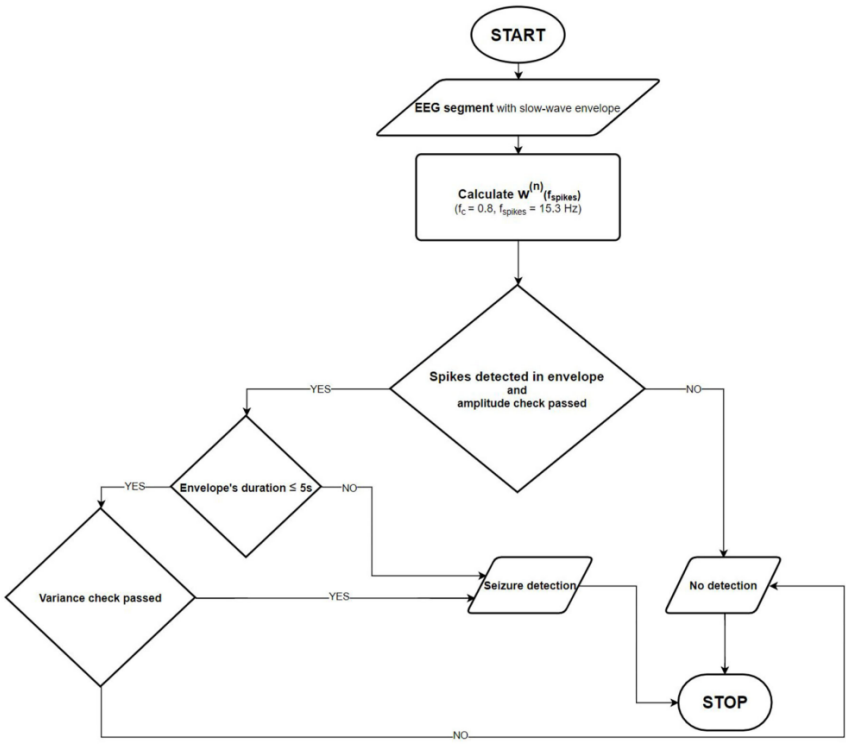

FIGURE 3 | Absence seizure detection flowchart. Once the slow-wave envelope is present in an analyzed EEG segment, the detector checks whether there are epileptic spikes embedded in it. The amplitude and the normalized wavelet power variance checks are also performed to eliminate artifacts.

In **Supplementary Table 4**, we compare the execution times of three absence seizure detector implementations. The execution time is determined by the efficiency of an FFT function, which is used to calculate the continuous wavelet transform. Matlab is renowned for its FFT implementation. Thus, it is not surprising that for the longest segment ($N = 2^{18}$), the Matlab version of the detector ran almost 16 and 19 times faster than the Java software running on Windows 10 and Android 10 (0.18 s vs. 2.79 s and 3.41 s). Interestingly enough, for shorter segments, the detector ran faster on the mid-range Android device than on the PC. Nevertheless, the single-channel Android processing speed of 0.2 s per minute of EEG is adequate for real-time seizure detection.

4. DISCUSSION

It has long been recognized that long-term EEG monitoring is the most reliable method for absence detection (27). Parents notice only about 6% of daytime seizures, and very often, teachers are the ones who recognize the CAE/JEA beginning (28). The 2010 Childhood Absence Epilepsy Study (5) has provided a compelling rationale for using portable EEG devices in the management of CAE/JEA patients. This randomized controlled trial showed that only 37% of all enrolled subjects were free from treatment failure on their first medication a year after diagnosis.

In the last two decades, many researchers have investigated absence seizure detection (13–17, 20). The datasets in these studies were small–the analyzed SWDs came from nine patients (range 2–20). On average, there were 70 seizures longer than 2 s (range 2–158). In all but one algorithm (20), discrete wavelet transform was used for signal preprocessing. Machine learning was used in 3 of 4 detectors. On average, 11 features were extracted from 15 EEG channels.

Kjaer et al. (19) used an experimental EEG setup with 3 electrodes for 24-h EEG monitoring of 6 patients (593 seizures). Their support vector machine detected 98.4% SWD's with 0.23/h false detection rate using 10 features of five-level db4 wavelet EEG decomposition.

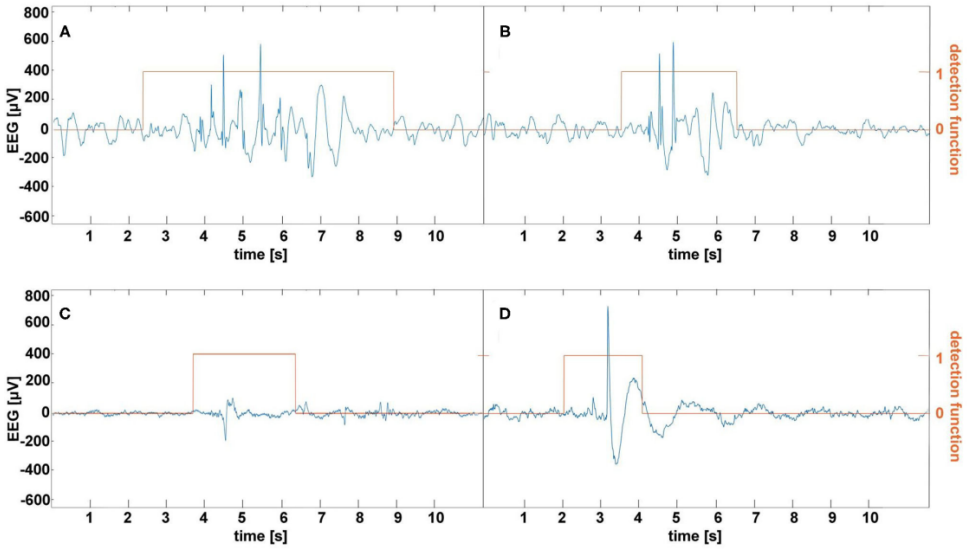

FIGURE 4 | Examples of false absence seizure detection in the EEG of the patients **(A,B)** and controls **(C,D)**. The epileptiform discharges in **(A,B)** were not accompanied by the clinical manifestations. **(C)** shows a rare example of a muscle artifact classified as an absence. A prominent spike-and-wave in **(D)** appeared in a healthy subject's EEG.

The absence seizure detection algorithm presented in this work is unique because it exploits the apparent traits of SWDs and EEG motion artifacts. Despite the simplicity, its 97.6% accuracy matches that of black-box machine learning classifiers.

Our experience indicates that frequent, albeit not excessively long, EEG home monitoring is feasible in pediatric patients as long as an EEG wearable is easy to put on and is comfortable. This study used the bipolar channels Fp1-T3 and Fp2-T4 for seizure detection because they approximately corresponded to the Muse headband electrode placement. On the one hand, this choice seems to be rational given absence seizures are usually well pronounced in the frontal regions (29) and the large spacing between the electrodes augments the characteristic features of SWDs as shown in **Figure 1**. On the other hand, Fp1 and Fp2 channels are prone to muscle and eyeblink artifacts. There were 26 and 8 false detections in the patients and controls, respectively. In the patients, all false detections were associated with epileptiform discharges, which did not yield clinical manifestations. Half of the errors in the control group were caused by the prominent SWDs. We show the examples of misclassified EEG segments in **Figure 4**. We used the stringent value $T_V = 0.05$ for the determination of the model parameters. Once we realized that false detections are not caused by motion artifacts, for classification, we lowered this parameter to 0.008 to maximize the detection sensitivity (for $T_V = 0.05$, the sensitivity was equal to 93% with the false detection rate 0.4/h). Some pediatricians agree that sensitivity of 90% and false detection rate of 1/h are clinically acceptable (19).

Unlike previous studies, the false detection rate was not determined by the motion artifacts. We would like to emphasize that the presented seizure detection was performed on clinical EEGs, which is the main limitation of this study. The question arises as to whether the amplitude and wavelet variance checks would be equally effective in eliminating motion artifacts in EEGs acquired with wearable devices in home settings. It is worth mentioning that the false detection rate can be reduced by using secondary electrodes for artifact cancellation (30) and employing different single-channel artifact detectors (31, 32). As most commercial EEG bands have MEMS accelerometers, one may also explore the possibility of incorporating head acceleration in the artifact removal algorithm. However, the connection between EEG artifacts and head movement is not always apparent (33).

In a recent study, Dan et al. presented an absence seizure detector based on a linear multichannel filter that was precomputed offline in a data-driven fashion based on the spatial-temporal signature of the seizure and peak interference statistics (21). The performance of this detector depends on the number of channels (from 3 to 18) used in the calculations. For the three channels, the accuracy was equal to 95% with a 0.4/h false detection rate. The authors set the minimum seizure length to 3 s (34). It is worth pointing out that for this absence duration threshold, the two-channel detector described in this work had

the false detection rate equal to 0.5/h (18 and 6 false detections for the patients, and controls, respectively.

To the best of our knowledge, we used the most diverse set of CAE/JAE EEGs (37 h of recordings from 64 patients) for development and testing. The overlap of automatically detected seizures with the actual seizures was high (about 96%). The poor overlap in some patients is predominantly caused by a very small amplitude of the epileptic spikes. Consequently, the detector does not classify such SWD trains as absence seizures. At the end of the seizure, the frequency of SWDs can decrease far below the canonical value of 3 Hz. In this case, the slow-wave envelope is shorter than expected. The frequency drop during the seizure leads to its sfragmentation.

For EEG recordings sampled at 250 Hz, the one-channel processing speed for midrange smartphones running Android 10 was high enough (about 0.2 s per 1 min of EEG) for real-time seizure detection. We found that the detection accuracy was highest for a sliding 30 s EEG buffer, which was shifted by 10 s.

Absence seizure manifestations are mild compared to other epileptic syndromes. Consequently, the rationale for using seizure detectors in CAE/JAE patients is different. Emphasis may be shifted from detection alerts to the facilitation of drug titration and side effects elimination. Unobtrusiveness and ease of use are particularly important for pediatric patients, who may be more willing to tolerate regular EEG measurements if they are incorporated into daily routines such as watching cartoons, playing mobile games, or listening to music.

It is worth pointing out that remote seizure monitoring will be one of the elements of personalized CAE/JAE treatment. There is a growing interest in the development of biomarkers of treatment response and side effects (35). These problems are the subject of our research (36).

DATA AVAILABILITY STATEMENT

The raw data supporting the conclusions of this article will be made available by the authors, without undue reservation.

ETHICS STATEMENT

The studies involving human participants were reviewed and approved by Wroclaw Medical University's Ethics Committee. Written informed consent for participation was not required for this study in accordance with the national legislation and the institutional requirements.

AUTHOR CONTRIBUTIONS

ML, PG, and MK: conceptualization and methodology. PG, ML and MJK: investigation original draft preparation. BW, WW, SK, TS, and WJ: review and editing. All authors contributed to formal analysis.

SUPPLEMENTARY MATERIAL

The Supplementary Material for this article can be found online at: https://www.frontiersin.org/articles/10.3389/fneur.2021.685814/full#supplementary-material

REFERENCES

1. Panayiotopoulos CP. *The Epilepsies: Seizures, Syndromes and management*. Oxfordshire (UK): Bladon Medical Publishing (2005).
2. Fisher RS, Cross JH, French JA, Higurashi N, Hirsch E, Jansen FE, et al. Operational classification of seizure types by the International league against epilepsy: position paper of the ILAE commission for classification and terminology. *Epilepsia*. (2017) 58:522–30. doi: 10.1111/epi.13670
3. Covanis A. *Childhood Absence Epilepsy*. Springer-Verlag: Atlas of epilepsies London (2010) p. 1013–23.
4. Schomer DL, da Silva FL. *Niedermeyer's Electroencephalography: Basic Principles, Clinical Applications, and Related Fields*. Oxford University Press (2018).
5. Glauser TA, Cnaan A, Shinnar S, Hirtz DG, Dlugos D, Masur D, et al. Ethosuximide, valproic acid, and lamotrigine in childhood absence epilepsy: initial monotherapy outcomes at 12 months. *Epilepsia*. (2013) 54:141–55. doi: 10.1111/epi.12028
6. Trinka E, Baumgartner S, Unterberger I, Unterrainer J, Luef G, Haberlandt E, et al. Long-term prognosis for childhood and juvenile absence epilepsy. *J Neurol*. (2004) 251:1235–41. doi: 10.1007/s00415-004-0521-1
7. Krigolson OE, Williams CC, Norton A, Hassall CD, Colino FL. Choosing MUSE: validation of a low-cost, portable EEG system for ERP research. *Front Neurosci*. (2017) 11:109. doi: 10.3389/fnins.2017.00109
8. Faust O, Acharya UR, Adeli H, Adeli A. Wavelet-based EEG processing for computer-aided seizure detection and epilepsy diagnosis. *Seizure*. (2015) 26:56–64. doi: 10.1016/j.seizure.2015.01.012
9. Sitnikova E, Hramov AE, Koronovsky AA, van Luijtelaar G. Sleep spindles and spike–wave discharges in EEG: their generic features, similarities and distinctions disclosed with Fourier transform and continuous wavelet analysis. *J Neurosci Methods*. (2009) 180:304–16. doi: 10.1016/j.jneumeth.2009.04.006
10. Ovchinnikov A, Lüttjohann A, Hramov A, Van Luijtelaar G. An algorithm for real-time detection of spike-wave discharges in rodents. *J Neurosci Methods*. (2010) 194:172–8. doi: 10.1016/j.jneumeth.2010.09.017
11. Bauquier SH, Lai A, Jiang JL, Sui Y, Cook MJ. Evaluation of an automated spike-and-wave complex detection algorithm in the EEG from a rat model of absence epilepsy. *Neurosci Bull*. (2015) 31:601–10. doi: 10.1007/s12264-015-1553-5
12. Grubov V, Sitnikova E, Pavlov A, Koronovskii A, Hramov A. Recognizing of stereotypic patterns in epileptic EEG using empirical modes and wavelets. *Phys A Stat Mech Appl*. (2017) 486:206–17. doi: 10.1016/j.physa.2017.05.091
13. Adeli H, Zhou Z, Dadmehr N. Analysis of EEG records in an epileptic patient using wavelet transform. *J Neurosci Methods*. (2003) 123:69–87. doi: 10.1016/S0165-0270(02)00340-0
14. Subasi A. Application of adaptive neuro-fuzzy inference system for epileptic seizure detection using wavelet feature extraction. *Comput Biol Med*. (2007) 37:227–44. doi: 10.1016/j.compbiomed.2005.12.003
15. Xanthopoulos P, Rebennack S, Liu CC, Zhang J, Holmes GL, Uthman BM, et al. A novel wavelet based algorithm for spike and wave detection in absence epilepsy. In: *2010 IEEE International Conference on BioInformatics and BioEngineering*. (Washington, DC: IEEE) (2010). p. 14–19.
16. Petersen EB, Duun-Henriksen J, Mazzaretto A, Kjær TW, Thomsen CE, Sorensen HB. Generic single-channel detection of absence seizures. In: *2011 Annual International Conference of the IEEE Engineering in Medicine and Biology Society*. (Boston, MA: IEEE) (2011). p. 4820–3.
17. Duun-Henriksen J, Madsen RE, Remvig LS, Thomsen CE, Sorensen HB, Kjaer TW. Automatic detection of childhood absence epilepsy seizures: toward a monitoring device. *Pediatr Neurol*. (2012) 46:287–92. doi: 10.1016/j.pediatrneurol.2012.02.018

18. Zeng K, Yan J, Wang Y, Sik A, Ouyang G, Li X. Automatic detection of absence seizures with compressive sensing EEG. *Neurocomputing*. (2016) 171:497–502. doi: 10.1016/j.neucom.2015.06.076
19. Kjaer TW, Sorensen HB, Groenborg S, Pedersen CR, Duun-Henriksen J. Detection of paroxysms in long-term, single-channel EEG-monitoring of patients with typical absence seizures. *IEEE J Transl Eng Health Med*. (2017) 5:1–8. doi: 10.1109/JTEHM.2017.2649491
20. Tenneti SV, Vaidyanathan P. Absence seizure detection using Ramanujan filter banks. In: *2018 52nd Asilomar Conference on Signals, Systems, and Computers*. (Danvers, MA: IEEE) (2018). p. 1913–7.
21. Dan J, Vandendriessche B, Paesschen WV, Weckhuysen D, Bertrand A. Computationally-Efficient Algorithm for Real-Time Absence Seizure Detection in Wearable Electroencephalography. *Int J Neural Syst*. (2020) 30:2050035. doi: 10.1142/S0129065720500355
22. Mallat S. *A Wavelet Tour of Signal Processing*. Burlington, MA: Elsevier (1999).
23. Latka M, Was Z, Kozik A, West BJ. Wavelet analysis of epileptic spikes. *Phys Rev E*. (2003) 67:052902. doi: 10.1103/PhysRevE.67.052902
24. Addison PS. *The Illustrated Wavelet Transform Handbook: Introductory Theory and Applications in Science, Engineering, Medicine and Finance*. Boca Raton, FL; London; New York, NY: CRC Press (2017).
25. Addison PS. Introduction to redundancy rules: the continuous wavelet transform comes of age. *Phil Trans R Soc A*. (2018) 376:20170258. doi: 10.1098/rsta.2017.0258
26. Szaflarski JP, DiFrancesco M, Hirschauer T, Banks C, Privitera MD, Gotman J, et al. Cortical and subcortical contributions to absence seizure onset examined with EEG/fMRI. *Epilepsy Behav*. (2010) 18:404–13. doi: 10.1016/j.yebeh.2010.05.009
27. Browne TR, Dreifuss FE, Penry JK, Porter RJ, White BG. Clinical and EEG estimates of absence seizure frequency. *Arch Neurol*. (1983) 40:469–72. doi: 10.1001/archneur.1983.04210070009004
28. Keilson MJ, Hauser WA, Magrill JP, Tepperberg J. Ambulatory cassette EEG in absence epilepsy. *Pediatr Neurol*. (1987) 3:273–6. doi: 10.1016/0887-8994(87)90067-1
29. Jun YH, Eom TH, Kim YH, Chung SY, Lee IG, Kim JM. Source localization of epileptiform discharges in childhood absence epilepsy using a distributed source model: a standardized, low-resolution, brain electromagnetic tomography (sLORETA) study. *Neurol Sci*. (2019) 40:993–1000. doi: 10.1007/s10072-019-03751-4
30. Nordin AD, Hairston WD, Ferris DP. Dual-electrode motion artifact cancellation for mobile electroencephalography. *J Neural Eng*. (2018) 15:056024. doi: 10.1088/1741-2552/aad7d7
31. Chen X, Liu A, Chiang J, Wang ZJ, McKeown MJ, Ward RK. Removing muscle artifacts from EEG data: multichannel or single-channel techniques? *IEEE Sensors J*. (2015) 16:1986–97. doi: 10.1109/JSEN.2015.2506982
32. Dhindsa K. Filter-bank artifact rejection: high performance real-time single-channel artifact detection for EEG. *Biomed Sig Proc Control*. (2017) 38:224–35. doi: 10.1016/j.bspc.2017.06.012
33. Kline JE, Huang HJ, Snyder KL, Ferris DP. Isolating gait-related movement artifacts in electroencephalography during human walking. *J Neural Eng*. (2015) 12:046022. doi: 10.1088/1741-2560/12/4/046022
34. Tenney JR, Glauser TA. The current state of absence epilepsy: can we have your attention? the current state of absence epilepsy. *Epilepsy Curr*. (2013) 13:135–40. doi: 10.5698/1535-7511-13.3.135
35. Kessler SK, McGinnis E. A practical guide to treatment of childhood absence epilepsy. *Pediatr Drugs*. (2019) 21:15–24. doi: 10.1007/s40272-019-00325-x
36. Glaba P, Latka M, Krause MJ, Kuryło M, Jernajczyk W, Walas W, et al. Changes in interictal pretreatment and posttreatment EEG in childhood absence epilepsy. *Front Neurosci*. (2020) 14:196. doi: 10.3389/fnins.2020.00196

Conflict of Interest: The authors declare that the research was conducted in the absence of any commercial or financial relationships that could be construed as a potential conflict of interest.

Supplementary Material

1 SUPPLEMENTARY DATA

Supplementary Listing L1. Matlab function that calculates the Complex Morlet continuous wavelet transform.

```
function [cwtm]=cmorletCWT(signal,avec,dt,fc)
% calculates complex Morlet continuous wavelet transform (cwt)
%
% signal is the input vector
% avec is the vector filled with the scales for which cwt is calculated
% dt is sampling period of the signal
% fc is the center frequency of the complex Morlet wavelet

   N=length(signal);
   Nas=length(avec);

   %%FFT of signal
   dfF=1/(N*dt);
   fftx=fft(signal);
   ff=(-(length(fftx)/2):(length(fftx)/2-1))*dfF;
   waveletMatrix = zeros(Nas,numel(ff));
   fcon=(pi^0.25)*(2^0.5);

   %%FFT of wavelet
   for i=1:Nas
      fftWavelet=sqrt(avec(i))*fcon*exp(-0.5*(((2*pi)*((avec(i)*ff-fc))).^2));
      waveletMatrix(i,:)=ifftshift(fftWavelet);
   end
   fftSigMatrix=repmat(fftx,Nas,1);
   combinedMatrix=fftSigMatrix.*waveletMatrix;
   cwtm=ifft(combinedMatrix,[],2);
end
```

Table S1. Seizure detection performance for the learning dataset. The absence characteristics are shown in the first four columns. The column labels are as follows: EEGD (EEG duration), NABS (numbers of absences), ADABS (average duration of absence), DET (number of detected seizures – true positives), OVR (overlap of the detected seizures with the actual ones), FDET (number of false detections – false positives), PERR (the percentage of false positive samples in a given EEG).

ID [-]	**EEGD** [s]	**NABS** [-]	**ADABS** [s]	**DET** [-]	**OVR** [%]	**FDET** [-]	**PERR** [%]
1 (CAE)	1800	6	10.50	6	100.00	0	0.51
2 (CAE)	1800	5	13.20	5	100.00	0	1.01
3 (CAE)	1920	10	10.33	10	99.22	1	2.07
4 (CAE)	3000	8	15.75	8	86.23	0	0.96
5 (CAE)	1800	11	11.00	11	100.00	0	1.93
6 (CAE)	3600	6	11.33	6	100.00	0	0.56
7 (CAE)	3300	2	13.50	2	100.00	0	0.15
8 (CAE)	1200	3	15.67	3	100.00	0	0.82
9 (CAE)	3600	7	15.00	7	98.90	1	0.54
10 (CAE)	2100	5	5.33	5	99.91	0	0.56
11 (CAE)	2400	5	8.75	5	98.91	1	0.84
12 (CAE)	2460	10	12.22	10	100.00	0	1.11
13 (CAE)	2100	3	14.33	3	100.00	1	0.43
14 (CAE)	730	2	7.67	2	100.00	0	0.39
15 (CAE)	2100	9	14.11	9	94.99	0	0.39
16 (CAE)	1020	1	5.00	1	100.00	0	0.23
17 (CAE)	1560	3	16.00	3	100.00	1	0.63
18 (CAE)	1200	5	23.20	5	99.94	0	1.20
19 (CAE)	1500	7	9.29	7	100.00	4	2.24
20 (CAE)	1800	2	4.33	2	90.62	2	0.76
21 (CAE)	1010	2	12.50	2	100.00	0	0.54
22 (CAE)	1240	7	16.86	7	99.88	0	1.48
23 (JAE)	1510	2	9.00	2	100.00	0	0.38
24 (JAE)	3200	6	14.19	6	70.23	5	1.52
25 (JAE)	1510	2	9.70	2	100.00	0	0.25
26 (JAE)	1802	3	13.30	3	100.00	0	0.16
27 (JAE)	2402	10	11.21	9	81.93	1	0.64
28 (JAE)	3380	8	13.43	8	100.00	2	1.08
29 (JAE)	3540	11	16.70	11	99.44	0	1.33
30 (JAE)	3000	8	12.44	8	100.00	0	1.13
31 (JAE)	3600	5	12.18	4	91.83	0	0.29
32 (JAE)	1800	17	14.02	16	95.73	0	3.46
33 (JAE)	3780	4	9.80	4	100.00	0	0.82
34 (JAE)	3660	4	14.25	4	100.00	0	0.22

Table S2. Seizure detection performance for the testing dataset. The absence characteristics are shown in the first four columns. The column labels are as follows: EEGD (EEG duration), NABS (numbers of absences), ADABS (average duration of absence), DET (number of detected seizure – true positives), OVR (overlap of the detected seizures with the actual ones), FDET (number of false detections – false positives), PERR (the percentage of false positive samples in a given EEG).

ID [-]	**EEGD** [s]	**NABS** [-]	**ADABS** [s]	**DET** [-]	**OVR** [%]	**FDET** [-]	**PERR** [%]
35 (CAE)	2700	4	12.25	3	68.09	0	0.12
36 (CAE)	3600	8	14.75	8	85.56	0	0.12
37 (CAE)	2700	14	11.14	14	99.66	1	1.00
38 (CAE)	2100	12	13.56	12	99.92	1	1.77
39 (CAE)	1020	3	19.67	3	100.00	0	0.55
40 (CAE)	1920	7	9.29	7	99.81	0	1.08
41 (CAE)	3640	3	11.00	3	100.00	1	0.94
42 (CAE)	1515	5	12.80	5	100.00	0	0.93
43 (CAE)	3010	16	6.36	14	92.91	2	1.07
44 (CAE)	2280	4	8.80	4	100.00	0	0.30
45 (CAE)	1970	12	7.00	12	90.72	0	1.94
46 (CAE)	2460	11	17.20	9	94.99	0	0.44
47 (CAE)	1360	2	13.50	2	100.00	0	0.87
48 (CAE)	1330	3	18.86	3	99.32	0	0.91
49 (CAE)	1300	6	6.80	6	98.39	0	2.30
50 (JAE)	1260	3	10.47	3	100.00	0	0.90
51 (JAE)	2050	1	8.50	1	100.00	1	0.27
52 (JAE)	920	1	8.70	1	100.00	0	0.12
53 (JAE)	1130	1	5.00	1	100.00	0	0.15
54 (JAE)	1290	4	8.22	4	100.00	0	0.77
55 (JAE)	1260	6	6.58	5	85.27	0	0.87
56 (JAE)	2100	2	10.70	2	99.48	0	0.15
57 (JAE)	2225	6	17.10	6	100.00	0	0.81
58 (JAE)	1200	7	13.80	7	84.36	0	3.05
59 (JAE)	1861	18	3.75	18	83.33	0	1.16
60 (JAE)	2340	4	13.25	4	100.00	0	1.08
61 (JAE)	2520	1	7.00	1	100.00	0	0.03
62 (JAE)	1460	3	35.67	3	55.99	0	1.96
63 (JAE)	1370	5	13.60	5	100.00	0	0.79
64 (JAE)	1360	5	8.93	5	99.17	1	0.82

Table S3. The amplitude and wavelet variance checks' contributions to false detection reduction. We present the number of false detections (in the learning and testing datasets) with the checks turned on (+) or off (-).

	$Fp_1 - T_3$				$Fp_2 - T_4$			
Amplitude check	-	+	-	+	-	+	-	+
Variance check	-	-	+	+	-	-	+	+
False Detections	102	89	53	15	152	105	58	19
PERR [%]	1.02	0.87	0.85	0.71	1.01	0.86	0.80	0.67

Table S4. Execution times for the Matlab and Java implementations of the absence seizure detector. We benchmarked the implementations for three EEG segment lengths. The mean values were calculated using the first 10 EEG recordings of the training dataset (Table S1). For the sampling frequency equal to 250 Hz, the segment length $N = 2^{18}$ corresponds to 17 min of EEG.

	Matlab 2018a Win 10			Java Win 10			Android 10		
N	2^{16}	2^{17}	2^{18}	2^{16}	2^{17}	2^{18}	2^{16}	2^{17}	2^{18}
Mean [s]	0.04	0.11	0.18	2.36	2.50	2.79	0.86	1.60	3.41
Std [s]	0.01	0.02	0.02	0.68	0.74	0.62	0.07	0.07	0.12

10. Publikacja 3 – *EEG phase synchronization during absence seizures*

Ostatnia publikacja prezentuje zmiany synchronizacji EEG podczas napadów nieświadomości. Wykorzystując synchronizację mocy falkowej w paśmie beta oraz znormalizowaną amplitudę sygnału EEG możliwym jest nie tylko wykrywać napady nieświadomości, ale również określać ich dezorganizację. Proponowany algorytm detekcji jest przystosowany do pracy w strumieniu danych. Według naszej wiedzy prezentowany w niniejszej pracy sposób opisu fragmentacji napadów jest pierwszą jakościową charakterystyką napadów nieświadomości. Dezorganizacja, która może być cechą szczególną u dzieci z JAE, może być wykorzystana do diagnozy różnicowej.

Mój wkład do tej pracy (60%) nie zmienił się w stosunku do poprzednich dwóch publikacji.

frontiers | Frontiers in Neuroinformatics

TYPE Original Research
PUBLISHED 19 June 2023
DOI 10.3389/fninf.2023.1169584

OPEN ACCESS

EDITED BY
Kais Gadhoumi,
Duke University, United States

REVIEWED BY
Edward M. Merricks,
Columbia University, United States
Aydin Akan,
Izmir University of Economics, Türkiye

*CORRESPONDENCE
Miroslaw Latka
✉ Miroslaw.Latka@pwr.edu.pl

RECEIVED 19 February 2023
ACCEPTED 25 May 2023
PUBLISHED 19 June 2023

CITATION
Glaba P, Latka M, Krause MJ, Kroczka S, Kuryło M, Kaczorowska-Frontczak M, Walas W, Jernajczyk W, Sebzda T and West BJ (2023) EEG phase synchronization during absence seizures. *Front. Neuroinform.* 17:1169584. doi: 10.3389/fninf.2023.1169584

EEG phase synchronization during absence seizures

Pawel Glaba[1], Miroslaw Latka[1]*, Małgorzata J. Krause[2], Sławomir Kroczka[3], Marta Kuryło[2], Magdalena Kaczorowska-Frontczak[4], Wojciech Walas[5], Wojciech Jernajczyk[6], Tadeusz Sebzda[7] and Bruce J. West[8]

[1]Department of Biomedical Engineering, Wroclaw University of Science and Technology, Wrocław, Poland, [2]Department of Pediatric Neurology, T. Marciniak Hospital, Wrocław, Poland, [3]Department of Child Neurology, Jagiellonian University Medical College, Kraków, Poland, [4]The Children's Memorial Health Institute, Warszawa, Poland, [5]Department of Anesthesiology, Intensive Care and Regional Extracorporeal Membrane Oxygenation (ECMO) Center, Institute of Medical Sciences, University of Opole, Opole, Poland, [6]Clinical Neurophysiology, Institute of Psychiatry and Neurology, Warszawa, Poland, [7]Department of Physiology and Pathophysiology, Medical University of Wroclaw, Wrocław, Poland, [8]Center for Nonlinear Science, University of North Texas, Denton, TX, United States

Absence seizures—generalized rhythmic spike-and-wave discharges (SWDs) are the defining property of childhood (CAE) and juvenile (JAE) absence epilepsies. Such seizures are the most compelling examples of pathological neuronal hypersynchrony. All the absence detection algorithms proposed so far have been derived from the properties of *individual* SWDs. In this work, we investigate EEG phase synchronization in patients with CAE/JAE and healthy subjects to explore the possibility of using the wavelet phase synchronization index to detect seizures and quantify their disorganization (fragmentation). The overlap of the ictal and interictal probability density functions was high enough to preclude effective seizure detection based solely on changes in EEG synchronization. We used a machine learning classifier with the phase synchronization index (calculated for 1 s data segments with 0.5 s overlap) and the normalized amplitude as features to detect generalized SWDs. Using 19 channels (10-20 setup), we identified 99.2% of absences. However, the overlap of the segments classified as ictal with seizures was only 83%. The analysis showed that seizures were disorganized in approximately half of the 65 subjects. On average, generalized SWDs lasted about 80% of the duration of abnormal EEG activity. The disruption of the ictal rhythm can manifest itself as the disappearance of epileptic spikes (with high-amplitude delta waves persisting), transient cessation of epileptic discharges, or loss of global synchronization. The detector can analyze a real-time data stream. Its performance is good for a six-channel setup (Fp1, Fp2, F7, F8, O1, O2), which can be implemented as an unobtrusive EEG headband. False detections are rare for controls and young adults (0.03% and 0.02%, respectively). In patients, they are more frequent (0.5%), but in approximately 82% cases, classification errors are caused by short epileptiform discharges. Most importantly, the proposed detector can be applied to parts of EEG with abnormal EEG activity to quantitatively determine seizure fragmentation. This property is important because a previous study reported that the probability of disorganized discharges is eight times higher in JAE than in CAE. Future research must establish whether seizure properties (frequency, length, fragmentation, etc.) and clinical characteristics can help distinguish CAE and JAE.

KEYWORDS

epilepsy, absence seizure, synchronization, wavelets, seizure detection, childhood absence epilepsy, juvenile absence epilepsy, seizure fragmentation

1. Introduction

Idiopathic generalized epilepsies (IGEs) are a subgroup of genetic generalized epilepsies (GGEs), composed of four syndromes: childhood absence epilepsy (CAE), juvenile absence epilepsy (JAE), juvenile myoclonic epilepsy (JME), and epilepsy with generalized tonic-clonic seizures alone (GTCA) (Hirsch et al., 2022). Absence seizures—generalized rhythmic (2.5–5.5 Hz) spike-and-wave discharges are the defining property of CAE and JAE. They can also be observed in about 33% of patients with JME.

CAE starts in otherwise normal children between 4 and 10 years of age and is more common in girls (60 to 75% of cases). It accounts for approximately 18% of epilepsy in school-aged children. Typical absence seizures begin suddenly and, in most children, lead to a deep loss of awareness and interruption of previously conducted activity. Seizures can be accompanied by staring, loss of facial expression, oral/manual automatism, blinking, or eye opening. Return to regular activity seems immediate, although children may initially be confused as they reorient themselves. The duration of seizures, which can occur multiple times a day, typically varies between 3 and 20 s, with a median of 10 s. CAE relapses in early adolescence in 60% of patients. In the rest, the disease can evolve into other IGE syndromes.

JAE is less common than CAE, accounting for 2.4–3.1% of new-onset epilepsy in children and adolescents, with a nearly equal distribution between men and women. However, it may be underdiagnosed as absences are less frequent (less than daily) and more subtle (less complete impairment of awareness). The age of onset is 12 ± 3 years (Asadi-Pooya et al., 2013). The ictal EEG is similar in CAE and JAE. However, disorganized (fragmented) discharges, defined as brief (<1 s) and transient interruptions in the ictal rhythm, are eight times more frequent in JAE (Sadleir et al., 2009). In most patients with JAE, lifelong seizure control pharmacotherapy is required.

The diagnosis of IGE requires the analysis of long video EEGs (on average about 30 min long) to detect seizures, their clinical manifestations (consciousness impairment, motor symptoms) and abnormal features in the interictal EEG. The 2010 Childhood Absence Epilepsy Study (Glauser et al., 2013) showed that after 1 year, the initial seizure-control pharmacotherapy was effective only in 37% of patients with CAE and JAE. Therefore, follow-up EEG recordings are necessary to ensure treatment efficacy and minimize potential side effects. It should be noted that parents notice only a small fraction (approximately 6%) of absences (Keilson et al., 1987), the estimate corroborated by a more recent study (Akman et al., 2009).

Low-cost portable EEG devices connected to the Internet (Krigolson et al., 2017) can be instrumental in personalizing pediatric epilepsy management. Children and adolescents may be more willing to tolerate regular EEG measurements if incorporated into daily routines, such as watching cartoons, playing mobile games, or listening to music. The potential benefits of remote long-term EEG monitoring include facilitation of diagnosis, personalized drug titration, and determining the duration of pharmacotherapy. Consequently, there is a strong demand for fast and accurate computer seizure detection that can be used on devices with as few EEG channels as possible. Global synchronization is the most conspicuous property of EEG dynamics during absence seizure. However, all the absence detection algorithms proposed so far (Adeli et al., 2003; Subasi, 2007; Sitnikova et al., 2009; Ovchinnikov et al., 2010; Xanthopoulos et al., 2010; Petersen et al., 2011; Duun-Henriksen et al., 2012; Bauquier et al., 2015; Zeng et al., 2016; Grubov et al., 2017; Kjaer et al., 2017; Tenneti and Vaidyanathan, 2018; Dan et al., 2020; Glaba et al., 2021; Japaridze et al., 2022) exploit only the properties of SWD complexes. In this work, we investigate EEG phase synchronization in patients with CAE/JAE and healthy subjects to explore the possibility of using the phase synchronization index to detect seizures and characterize their disorganization. The qualitative assessment of absence fragmentation could be used to discriminate between CAE and JAE, an important clinical problem.

2. Materials and methods

2.1. EEG recordings

The data set used in our previous study (Glaba et al., 2021) was slightly modified and expanded by routine EEG of healthy young adults (12 women and 7 men, mean age 22 years, range 20–24 years). For these adults, the EEG was recorded for 8 min, the first half in closed eyes and the second in open eyes condition. The recordings were made with Elmiko Digitrack (BRAINTRONICS B.V. ISO-1032CE amplifier, 250 Hz sampling frequency, impedance below 5kΩ). The ethics committee of the Warsaw Institute of Psychiatry and Neurology approved the reanalysis of the data. Subjects gave their informed consent.

The ethics committee of Wroclaw Medical University approved a retrospective analysis of routine anonymized video EEG recordings of patients (36 with CAE and 29 with JAE) as well as 30 EEGs of controls of the same age (Glaba et al., 2021). Epilepsy syndrome was established based on age of onset, the properties of the first video-EEG, and neuroimaging. Consequently, diagnosis should be considered as preliminary. EEGs were acquired with Elmiko Digitrack (BRAINTRONICS B.V. ISO-1032CE amplifier) or Grass Comet Plus EEG (AS40-PLUS amplifier) using a sampling frequency of 200 or 250 Hz. The international 10-20 standard was used to arrange 19 Ag/AgCl electrodes (impedance below 5kΩ). The total duration of the EEG was equal to 37 and 9 h for the patients and controls, respectively.

All EEGs were acquired with the reference electrode mounted on the subject's forehead.

We used two filters for EEG preprocessing: a second-order infinite impulse response (IIR) and a 6th-order high-pass Butterworth with a cutoff frequency of 0.5 Hz. These filters remove 50-Hz power line noise and EEG baseline drift, respectively.

2.2. Synchronization matrix

We quantify the EEG synchronization using a matrix made up of pairwise frequency-dependent synchronization coefficients $\gamma(k,l)$ calculated for EEG channels k and l ($k,l = 1..19$). $\gamma(k,l)$ can be defined with the help of the complex continuous wavelet

transform (CWT) (Lachaux et al., 1999):

$$T[s](a,t_0)=\frac{1}{\sqrt{a}}\int_{-\infty}^{+\infty}s(t)\psi^*\left(\frac{t-t_0}{a}\right)dt \quad (1)$$

which is the convolution of the signal $s(t)$ with wavelets $\psi(a,t_0)$. Such wavelets are generated from the mother function ψ by translation and scaling: $\psi(a,t_0)=\psi(t-t_0/a)$ (Mallat, 1999). Motivated by the results of the previous study (Glaba et al., 2021), we used the complex Morlet wavelet (Addison, 2017, 2018):

$$\psi(t)=\frac{1}{\pi^{1/4}}e^{2\pi i f_c t}e^{-t^2/2} \quad (2)$$

whose Fourier transform $\hat{\psi}(f)$ is given by

$$\hat{\psi}(f)=\sqrt{2}\sqrt[4]{\pi}e^{-2\pi^2(f-f_c)^2}. \quad (3)$$

The real parameter f_c is called the center frequency, since it equals the maximum point of the wavelet's Fourier power spectrum. The scale a corresponds to the following pseudo-frequency:

$$f_a=\frac{f_c}{a}. \quad (4)$$

The instantaneous phase of a signal s can be defined as

$$\phi(t_0,f_a)=-i\log\left[\frac{T[s](a,t_0)}{|T[s](a,t_0)|}\right], \quad (5)$$

where i is an imaginary number. The distribution $P[\Delta\phi(k,l)]$ of the phase difference $\Delta\phi(k,l)=\phi_k-\phi_l$ can be used to characterize the synchronization between two EEG channels. A uniform distribution corresponds to the absence of synchronization (two signals are statistically independent). In contrast, a well-pronounced peak in the distribution is a manifestation of phase locking, which means that one time series tracks the dynamics of the other. The stability of the phase difference $\Delta\phi$ is quantified with the index $\gamma(k,l)$ (Quiroga et al., 2002; Latka et al., 2005)

$$\gamma(k,l)=\langle\sin\Delta\phi(k,l)\rangle^2+\langle\cos\Delta\phi(k,l)\rangle^2. \quad (6)$$

The angle brackets in the above equation denote the temporal average of the phase-difference fluctuations. The synchronization index can have values between 0 and 1, and in the case of human EEG, it is frequency dependent. When the distribution of phase differences is uniform, the time averages of both trigonometric functions in Equation (6) are zero which in turn makes the synchronization index equal to zero. From the trigonometric identity, it follows that $\gamma=1$ corresponds to perfect synchronization (phase locking of two EEG channels).

The average synchronization index γ is the average value of the non-diagonal elements of the synchronization matrix:

$$\gamma=\sum_{k\in S_N}\sum_{l\in S_N,k>l}\gamma(k,l), \quad (7)$$

where S_N denotes subsets of 10-20 channels. We calculate γ for all 19 channels ($N=19$) and for three subsets ($N<19$):

- S_4 (Fp1, Fp2, T5, T6)
- S_6 (Fp1, Fp2, F7, F8, O1, O2)
- S_{12} (Fp1, Fp2, F7, F8, F3, F4, P3, P4, T5, T6, O1, O2).

The electrode arrangement in the above subsets is similar, but not always identical, to the low-cost EEG headsets currently available on the market (Pu et al., 2021). The applicability of such headsets to home monitoring of pediatric patients was the main reason for testing different S_N.

The channel synchronization index is defined as follows:

$$\gamma(k)=\sum_{k,l\in S_N,k>l}\gamma(k,l). \quad (8)$$

We calculate phase synchronization for 1-s intervals using a half-second overlap. We use the overlap to simulate live data stream analysis. For patients, there were 7,270 ictal and 266,653 interictal data segments. 1,540 windows partially overlapped absence seizures. The partitioning of the controls' EEG yielded 58,460 segments. For students, we obtained the 9,064 and 9,121 intervals for closed and open eyes, respectively.

The value of the synchronization index γ depends on the center frequency of the Morlet wavelet f_c and the pseudofrequency f_a. We use a grid search to determine optimal values for absence detection. In particular, we search for f_c and f_a that maximize the difference between ictal and interictal synchronization.

We would like to emphasize that the synchronization properties depend on the choice of reference electrode (Dominguez et al., 2005).

In this work, we used short EEG data segments. Consequently, when calculating the CWT with the help of a fast Fourier transform, boundary effects must be considered.

2.3. Absence seizure classifier

Prominent SWD and global EEG synchronization are hallmarks of absence seizures (Figure 1). Therefore, we decided to detect seizures using the normalized amplitude of the EEG $A_m^{(n)}$ and the synchronization index γ_m as machine learning features. The former is defined as

$$A_m^{(n)}=\frac{A_m}{A_{ref}}, \quad (9)$$

where A_m is the average absolute value of the EEG signal in segment m (we average across all channels). A_{ref} is the mean absolute value calculated for the 30 s segment taken from the interictal beginning of the EEG recording. Normalization by A_{ref} was necessary because the amplitude of EEG in children can decrease significantly with age and depends on the impedance of the electrodes.

We use the k-nearest neighbor (k-NN) classifier implemented in Matlab R2022a (MATLAB, 2022) Machine Learning Toolbox for absence detection. We accept the default values of the model parameters (10 neighbors, the Euclidean distance, data point scaling, and no weighting function). We employ leave-one-out cross-validation (LOOCV)—the number of folds equals the number of patients (65). For each patient, k-NN is built using the features extracted from the other 64 patients and applied to their

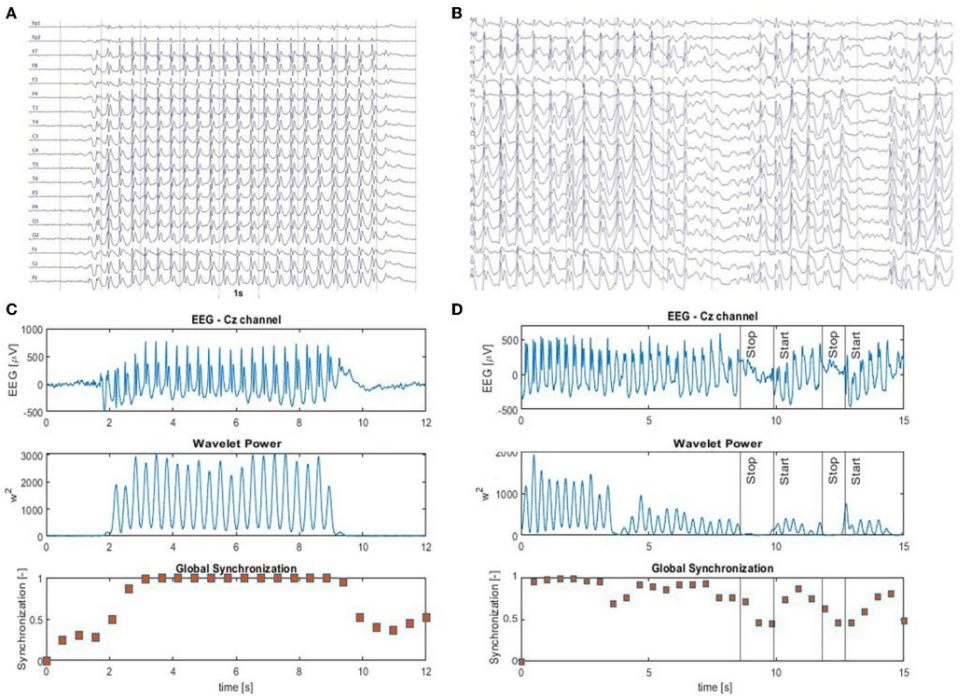

FIGURE 1
(A) Archetype of high-amplitude, continuous generalized spike and wave discharges with prominent epileptic spikes. The absence seizure in **(B)** is briefly interrupted two times. Panels **(C, D)** show the EEG from Cz channel (top panel) as well as the corresponding time series of the wavelet power (middle panel) and the global synchronization index (bottom panel). The wavelet power and synchronization index were calculated using $f_c = 1$ Hz and $f_a = 12$ Hz. These case studies demonstrate that global synchronization decreases when epileptic activity subsides.

segmented EEG (1 s windows with 0.5 s overlap). We prepare the training set as follows. We select only those ictal windows whose mean γ is greater than a threshold determined from the interictal synchronization distribution. In particular, for this threshold, 95% of interictal segments have a smaller mean γ. We disregard all data windows that partially overlap absence seizures. The sets of ictal and interictal segments are highly unbalanced (7,270 vs. 266,653). Therefore, we randomly select only a small fraction of the interictal segments for the training set. We use the 1:3 ratio of the ictal and interictal windows.

We evaluated the performance of the detector in the same way as in our previous article (Glaba et al., 2021) using the relative overlap (OVR) of segments classified as ictal with absence seizures and relative duration of false positives (PERR). During the PERR computation, we apply the logical OR function to determine the status of the common part of two consecutive EEG data segments. In other words, the common part is ictal if any segment is ictal. We also report the number of false positives (FP) and the number of different trains of misclassified segments (MT).

Supplementary Figure 1 elucidates the relationship between the number of erroneously classified EEG segments and PERR. For overlapping segments, this relationship can sometimes be counterintuitive.

Short (<2 s) epileptiform discharges, quite common in patients with CAE/JAE, usually do not produce clinical manifestations (Szaflarski et al., 2010). Therefore, we also tested the possibility of reducing the number of false positives by post-processing the k-NN classification results. In particular, we labeled any isolated ictal segment as non-ictal. In other words, the shortest possible ictal interval can have a length of 1.5 s (two consecutive segments).

2.4. Seizure fragmentation

We apply the absence detector described in Section 2.3 (with the post-processing turned off) to the parts of the EEG marked by neurologists as abnormal activity. Then, we calculate the percentage overlap of the segments classified as ictal with the analyzed fragment. As before, the common part of the adjacent segments is considered ictal if at least one of the segments is ictal. Seizure fragmentation

is defined as

$$SFRAG = 100\% - OVR. \quad (10)$$

3. Results

3.1. Synchronization

When calculating γ, we used $f_c = 1$ Hz and $f_a = 12$ Hz. For these values, the percentage difference between ictal and interictal synchronization was highest (168%). In the same vein, we determined these parameters for each patient. The median values were similar: $f_c = 0.8$ Hz and $f_a = 13$ Hz. Supplementary Figures 2, 3 elucidate the determination of the wavelet parameters.

Figure 1A shows an archetypal absence seizure with continuous high-amplitude generalized SWDs. In contrast, the seizure in Figure 1B was briefly interrupted twice. For both absences, for the chosen f_c and f_a, the power $|T|^2$ peaks at the location of epileptic spikes (Figures 1C, D). It is apparent that wavelet power and global synchronization are low when epileptic activity subsides. In Figure 2, we compare the ictal synchronization matrices calculated for the EEG segments presented in Figures 1A, B.

Figures 3A, B show that γ increases at the beginning and on average gradually subsides towards the end of the seizure. For the eight types of data segments (labeled from 0 to 7) presented in these figures, the average γ was equal to 0.28 ± 0.09, 0.46 ± 0.17, 0.62 ± 0.19, 0.79 ± 0.18, 0.75 ± 0.19, 0.58 ± 0.19, 0.44 ± 0.16, 0.36 ± 0.12. γ in ictal segments (1 to 7) was significantly higher than the interictal baseline 0.28 ± 0.09 ($p < 0.0001$ for the Mann–Whitney test).

The probability density function (PDF) of γ for the interictal and ictal segments strongly overlaps. In Figure 3C, PDF was calculated using global synchronization for the 19 channels (S_{19}) while Figure 3D shows PDF for the four-channel subset S_4 (Fp1, Fp2, T5, T6). The cut-off value for which 95% of the interictal segments had smaller synchronization was equal to 0.49, 0.65, 0.45, and 0.48 for S_{19}, S_{12}, S_6, and S_4, respectively.

3.2. Seizure detection

We detected absences with the k-NN classifier using synchronization and normalized amplitude as features. Supplementary Table 1 shows that the accuracy of other classifiers, such as neural networks or decision trees, is comparable. In actual implementations, these classifiers would be preferable because they do not require the attachment of training samples (feature vectors with the corresponding labels). We chose k-NN because of its short training time, which speeds up cross-validation.

Figure 4 elucidates the building of a seizure detector for patient P1, who had six absences with a mean duration of 10.5 s. One of the absences of P1 is presented in Figure 1A. The training set was created using data from the other 64 patients using the 19 channels (S_{19}) or the four-channel subset S_4. The scatter plots in Figures 4A, C show the spread of the synchronization and the normalized amplitude for S_{19} and S_4, respectively. Patient P1's EEG was partitioned into 3,598 windows. 108 were fully embedded in the seizures, while 24 partially overlapped them. Please note that for testing purposes, we consider any data segment that even partially overlaps a seizure as ictal. Of the 132 ictal windows, 14 (FN = 10.6%) and 17 (FN = 12.9%) were misclassified for S_{19} and S_4, respectively. For both subsets, all 3,464 interictal segments were correctly labeled.

Supplementary Figure 4 shows the construction of a seizure detector for patient P18. One of his absences is presented in Figure 1B.

The overlap OVR was the largest for S_{19} ($82.90 \pm 20.83\%$) and the smallest for S_4 ($69.31 \pm 25.09\%$) (Table 1). For S_{19}, PERR was equal to $0.87 \pm 1.23\%$, $0.12 \pm 0.26\%$, $0.07 \pm 0.14\%$ for patients, controls, and young adults, respectively. The corresponding values for S_4 were $0.68 \pm 1.32\%$, $0.03 \pm 0.07\%$, and $0.02 \pm 0.06\%$.

The false detection rate of the patients was five times higher than that of controls (0.5 vs. 0.1%) for S_{19} setup (Table 1). For smaller subsets, the detector performance was markedly better. For S_6, the false detection rate was equal to 0.5, 0.03, and 0.04% for patients, controls, and young adults, respectively. Comparison of the number of distinct trains of misclassified segments with the number of false positives reveals that parts of the EEG marked incorrectly as ictal are, on average, shorter than 2 s. We found by visual inspection that about 82% of the false positives were caused by short epileptiform discharges, which are quite common in epilepsy patients and rare in controls and young adults. The EEG artifacts comprise the rest: 7% were caused by spike-like high-amplitude artifacts and 7% by artifacts of more complicated morphology. The seizure detection performance for each patient is presented in Supplementary Table 2. The post-processing cuts approximately in half the number of FP (Table 1).

For two patients, P1 and P18, we built the detector for different combinations of wavelet parameters f_c and f_a. OVR, PERR, and FP for these calculations are presented in Supplementary Tables 3, 4. The results show that the detector performance is weakly affected by small changes in the wavelet parameters. For example, for P1, the grid search yielded $f_c = 0.8$ Hz and $f_a = 10$ Hz. For these values $OVR = 99.17\%$, $PERR = 0.30\%$, and $FP = 1$. For the standard parameters $f_c = 1.0$ Hz and $f_a = 12$ Hz (used for all subjects), we obtained $OVR = 99.15\%$, $PERR = 0.22\%$, and $FP = 0$. For P1, for 10 runs, we obtained the following average values: $OVR = 99.16 \pm 0.00\%$, $PERR = 0.22 \pm 0.01$, and $FP = 1 \pm 0$. For P18, the corresponding values were equal to $98.38 \pm 0.15\%$, 1.25 ± 0.02, and $FP = 33 \pm 1$.

Supplementary Table 5 shows the group average characteristics of seizure detection for different combinations of wavelet parameters. There are a number of combinations (e.g., $f_a = 11$ Hz and $f_c = 1$ Hz or $f_a = 14$ Hz and $f_c = 1.4$ Hz) for which the detection performance is comparable (the trade-off between the overlap and the number of false positives) with $f_a = 12$ Hz and $f_c = 1$ Hz used in this study. We chose the latter parameters because they have a clear physical interpretation (the difference between interictal and ictal synchronization is highest) and the number of false positives for the controls is acceptable (Supplementary Table 6).

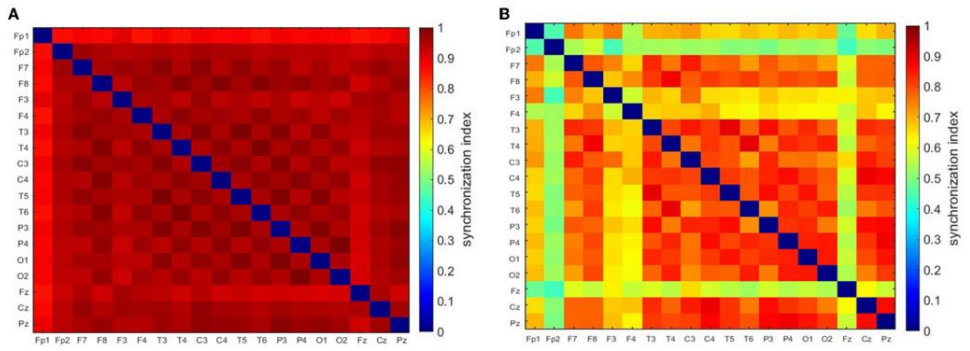

FIGURE 2
Synchronization matrices for the regular **(A)** and disorganized **(B)** seizure. These seizures are shown in Figure 1.

3.3. Seizure fragmentation

In Figure 5, we compare the EEG dynamics with the classifier output (detection function). SWDs do not emerge simultaneously from the background EEG in all channels. At the end of the seizure, ictal activity gradually subsides: epileptic spikes disappear, the amplitude of the EEG decreases, and global synchronization is lost. However, the initial and final transients were very short (< 0.5 s), and consequently, the first and last segments were classified as ictal. Two segments during which the ictal rhythm was interrupted were correctly identified. For the absence seizure presented, *SFRAG* was equal to 6.4%. Two EEG intervals in Figure 5 were marked blue to draw attention to the limitations of fragmentation analysis. First, seizure disorganizations shorter than 0.5 s are, in most cases, undetected. Second, the duration of the disorganization can be underestimated because of the size of the data window used to calculate the synchronization.

We analyzed all EEG segments classified as noictal that were fully embedded in seizures to find that in approximately 98% of these segments, seizure activity was disorganized or SWDs were simply absent. The other 2% contained artifacts.

For S_{19} set-up, the group-averaged *SFRAG* was equal to 20 ± 24%. For 46 patients (71%), the average fragmentation of seizures was less than 25% (Figure 6A). Of the 385 absences, 280 (73%) had *SFRAG* smaller than 25% (Figure 6B). Disorganization did not occur in 120 cases. For such seizures, $SFRAG < 5\%$.

SFRAG was equal to 18 ± 24%, 24 ± 26%, and 30 ± 29% for S_{12}, S_6, and S_4, respectively.

4. Discussion

An epileptic seizure is "a transient occurrence of signs and/or symptoms due to abnormal excessive or synchronous neuronal activity in the brain" (Fisher et al., 2005). Childhood and juvenile absences are the most compelling examples of pathological neuronal synchrony. Interestingly enough, all the absence detection algorithms proposed so far (Adeli et al., 2003; Subasi, 2007; Sitnikova et al., 2009; Ovchinnikov et al., 2010; Xanthopoulos et al., 2010; Petersen et al., 2011; Duun-Henriksen et al., 2012; Bauquier et al., 2015; Zeng et al., 2016; Grubov et al., 2017; Kjaer et al., 2017; Tenneti and Vaidyanathan, 2018; Dan et al., 2020; Glaba et al., 2021; Japaridze et al., 2022) have been derived from the properties of *individual* SWD complexes. Figures 3C, D provide an explanation, the overlap of the ictal and interictal probability density functions is so large that it precludes seizure detection based solely on changes in EEG synchronization. This conclusion agrees with previous studies on epileptic synchronization (Altenburg et al., 2003; Slooter et al., 2006).

This paper used the phase-synchronization index and the normalized amplitude as classification features. False detections are rare in controls and young adults. Although the PERR for the patients (0.55% for S_6) was even lower than that of the detector we had presented earlier (Glaba et al., 2021), the false detection rate per hour (8/h) was an order of magnitude higher. However, visual inspection of the EEG showed that 82% of the false positives corresponded to epileptiform discharges.

Of 385 absences, all but three were identified (accuracy (99.2%). Misclassified seizures were highly disorganized. The group-average overlap of EEG segments classified as ictal with seizures never exceeded 83%. There are two reasons for such a low value. The first is trivial, since we calculate γ for 1-s sliding windows. For windows that only partially cover the absences, γ is inevitably lower, which can lead to errors. The second reason is more fundamental and can be traced back to the disorganization of absences. Non-ictal classification within abnormal EEG activity was always associated with such disorganization. Apart from the segments that partially overlap seizures, we did not find a convincing example of a false negative.

The detection algorithm employs short data segments, making it suitable for real-time EEG analysis as several algorithms described previously (Xanthopoulos et al., 2010; Petersen et al., 2011; Duun-Henriksen et al., 2012; Kjaer et al., 2017; Dan et al., 2020; Japaridze et al., 2022). It is computationally more expensive

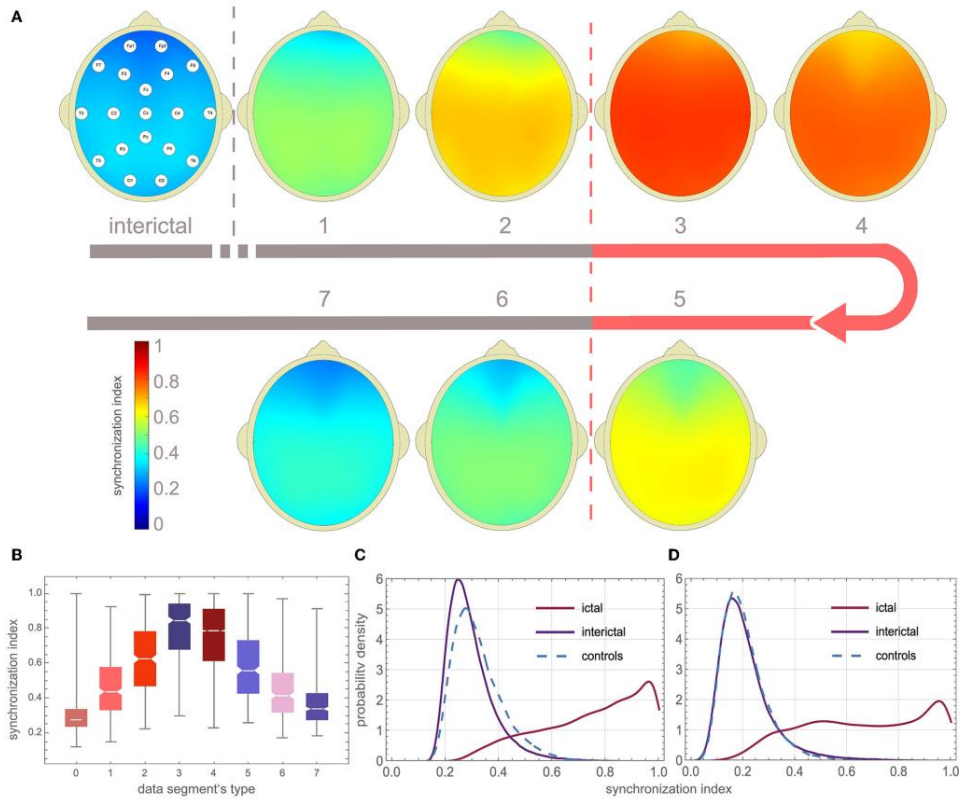

FIGURE 3
EEG synchronization during absence seizures. **(A)** Topographic map of channel synchronization (cohort average) for all interictal segments (0), the first window that partially overlaps seizures (1), the second partially overlapping (2), the first fully embedded in the seizure (3), all embedded without the first and last (4), the last embedded (5), the last but one overlapping (6) and last overlapping (7). **(B)** Global synchronization boxplots for data segments 0–7 (segments from all patients were used). **(C, D)** Probability density function (PDF) of the average synchronization index for the 19 channels (S_{19}) and the four-channel subset S_4 (Fp1, Fp2, T5, T6), respectively. One can see that global synchronization is high during seizures and that there is a strong overlap of the interictal and ictal distributions of the synchronization index.

than those derived from the properties of SWDs. This drawback is largely irrelevant today, except for portable EEGs with severely limited computing power. It should be noted that while the spectral and amplitude properties of EEG change significantly during maturation (Schomer and da Silva, 2018), the detector works equally well in children, juveniles, and young adults. The classification accuracy is good for a six-channel setup (Fp1, Fp2, F7, F8, O1, O2), which can be implemented as an unobtrusive EEG headband—a crucial requirement from the point of view of pediatric applications.

In the previous paper (Glaba et al., 2021), we used a delta frequency envelope to identify abnormal EEG activity. However, to detect absence seizures, we had to use two arbitrarily chosen heuristic criteria. First, we checked whether there were epileptic spikes in the envelope by calculating the percentage of EEG samples for which the beta wavelet power was greater than the threshold value. Second, if the envelope was shorter than 5 s, we also calculated the variance of the beta wavelet power. Although this algorithm was very fast and worked well, the approach presented here is not only more elegant, but it also allows quantifying seizure fragmentation.

The proposed detector cannot determine the fragmentation of the seizure in the live data stream. This can only be accomplished retrospectively when the detector (with post-processing turned off) is applied to EEG segments with abnormal EEG activity. Such segments can be marked by a neurologist or by building a delta wave envelope as demonstrated in Glaba et al. (2021). To our knowledge, we present the first qualitative characterization of absence seizure fragmentation. The analysis showed that seizures were disorganized in approximately half

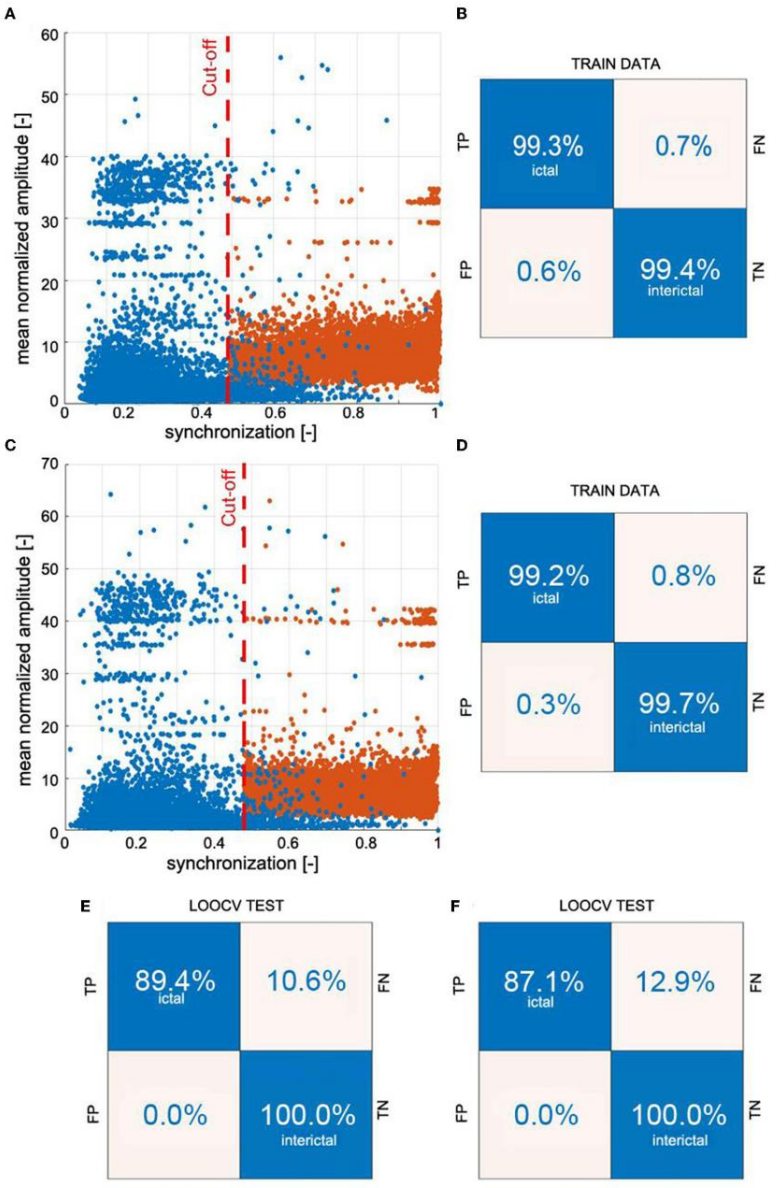

FIGURE 4
Example of building a k-NN seizure detector with the leave-one-out cross-validation (LOOCV) for patient P1. We used the global synchronization index and mean normalized EEG amplitude as the features. The learning set comprised randomly chosen interictal and segments fully embedded in absences with average synchronization greater than the cut-off value. We used 3:1 ratio of interictal to ictal windows. Panels **(A, C)** show the spread of the data generated for all 19 channels of 10-20 EEG setup (S_{19}) and the subset S_4 (channels Fp1, Fp2, T5, and T6), respectively. The confusion matrices in **(B, D)** show the results of 10-fold cross-validation. The classifiers were applied to the segmented EEG of patient P1 (1 s windows with 0.5 s overlap). Panels **(E, F)** show P1's confusion matrices for S_{19} and S_4, respectively.

TABLE 1 Seizure detection characteristics for the 19 channels (S_{19}) and three subsets with a smaller number of electrodes.

EEG SETUP	OVR [%]	PERR (FP, MT) [%, -, -]			
		P	C	Y	T
Synchronization and normalized amplitude					
S_{19}	82.9	0.87 (1437, 832)	0.12 (44, 32)	0.07 (7, 6)	0.36 (1488, 870)
S_{12}	78.01	0.71 (1147, 735)	0.23 (77, 58)	0.13 (13, 11)	0.36 (1237, 804)
S_6	79.36	0.86 (1282, 775)	0.05 (18, 14)	0.04 (4, 4)	0.32 (1304, 793)
S_4	69.31	0.68 (1196, 743)	0.03 (11, 9)	0.02 (2, 2)	0.25 (1209, 754)
Synchronization and normalized amplitude with post-processing					
S_{19}	80.93	0.57 (985, 381)	0.13 (21, 9)	0.03 (4, 2)	0.24 (1010, 392)
S_{12}	75.56	0.40 (652, 267)	0.22 (35, 15)	0.03 (4, 2)	0.22 (691, 284)
S_6	76.85	0.55 (868, 311)	0.06 (5, 2)	0.00 (0, 0)	0.21 (873, 313)
S_4	65.10	0.38 (746, 278)	0.03 (4, 2)	0.00 (0, 0)	0.13 (750, 280)

We used a k-nearest neighbor classifier with the synchronization index and normalized amplitude as the features. The overlap (OVR) of segments classified as ictal with absence seizures and relative duration of false positives (PERR) are presented for patients (P), controls (C), young adults (Y), and for segments from all cohorts (T). In parentheses, we give the number of distinct trains of misclassified windows (MT) and false positives (FP). In patients, false detections are predominantly caused by short (< 2 s) epileptiform discharges. Therefore, we also tested the possibility of reducing the number of false positives by post-processing the k-nearest neighbors classification. In particular, any isolated ictal segment was labeled non-ictal.

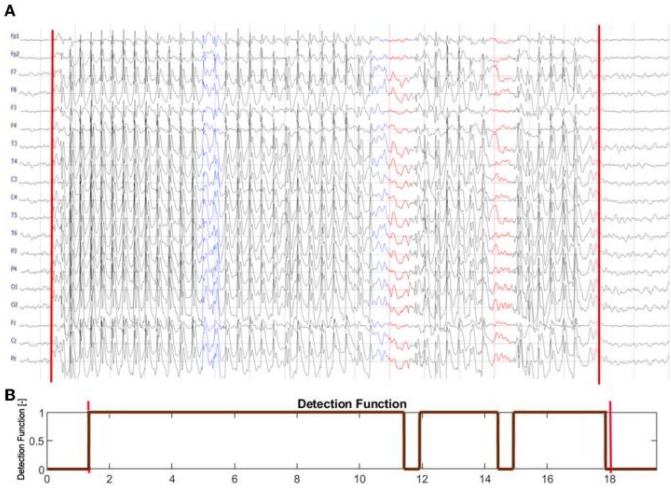

FIGURE 5
(A) Seizure from Figure 1B is shown with the leading and trailing interictal segments. **(B)** The output of the seizure detector. The detection function equals 1 for the segments classified as ictal and 0 otherwise. The red vertical lines in both subplots delineate the abnormal EEG activity marked by a neurologist. Note that SWDs do not simultaneously emerge from the background EEG in all channels. At the end of the seizure, ictal activity gradually subsides: epileptic spikes disappear, the amplitude of the EEG decreases, and global synchronization is lost. The initial and final transients are shorter than 0.5 s. The detector correctly identified the two interruptions in the ictal rhythm, marked in **(A)** in red. Two EEG intervals were marked blue to draw attention to the limitations of fragmentation analysis. Seizure disorganization shorter than about 0.5 s are, in most cases, undetected. Due to the finite size of the data window used to calculate phase synchronization, the fragmentation can be underestimated.

of the 65 subjects. On average, generalized SWDs lasted about 80% of the duration of abnormal EEG activity. The disruption of the ictal rhythm can manifest itself as the disappearance of epileptic spikes (with high-amplitude delta waves persisting), transient (about 1 s) cessation of epileptic discharges, or loss of global synchronization.

Although CAE and JAE are distinct epilepsy syndromes, there is considerable age overlap between them. Consequently, the diagnosis is not always obvious. This is an important clinical problem, as JAE is a lifelong disease. Sadleir et al. reported that disorganized discharges are eight times more frequent in JAE (Sadleir et al., 2009). For most patients, we

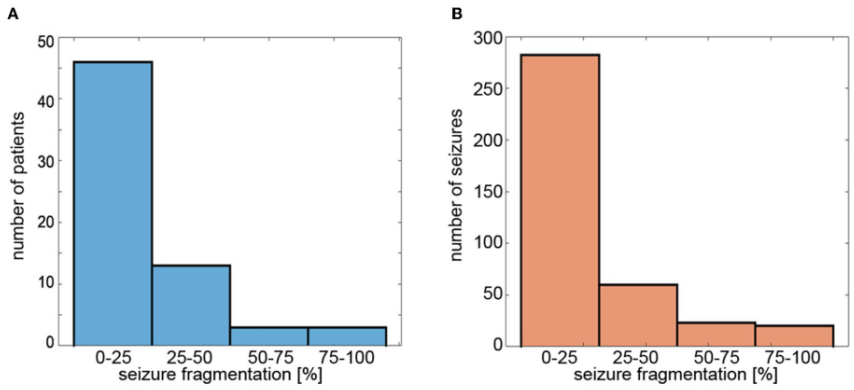

FIGURE 6
Histograms of **(A)** average fragmentation of the patient's seizures and **(B)** fragmentation of individual seizures. Seizure fragmentation is defined as the duration of segments classified as non-ictal embedded in the abnormal EEG activity interval divided by the length of such an interval.

only had the electroencephalogram recorded before the onset of pharmacotherapy. Therefore, future research must establish whether seizure properties (frequency, length, fragmentation, etc.) and clinical characteristics can distinguish CAE and JAE.

It should be noted that some EEG synchronization properties are unique to absence seizures. Figure 3B shows that γ peaks at the beginning of the seizure and is approximately twice the mean interictal value, in agreement with the recent study of (Zhong et al., 2022). However, Majmundar et al. argue that for most focal-onset seizures, synchronization occurs toward the end of the seizure rather than at the time of onset (Majumdar et al., 2014). Absence seizures exhibit longer-range synchrony than generalized tonic motor seizures of secondary (symptomatic) generalized epilepsy or frontal lobe epilepsy (Dominguez et al., 2005).

Epilepsy has historically been perceived as a functional brain disorder associated with hypersynchronization. Interestingly, desynchronization can precede seizures (Aarabi et al., 2008; Jiruska et al., 2013; Zeng et al., 2016). Figure 3C shows that the peak of the interictal distribution of γ is shifted to low values relative to the controls. Therefore, the question arises of whether this shift is a manifestation of desynchronization in patients with CAE / JAE. We will present a detailed analysis of interictal EEG synchronization properties elsewhere.

Data availability statement

The raw data supporting the conclusions of this article will be made available by the authors, without undue reservation.

Ethics statement

The studies involving human participants were reviewed and approved by Wroclaw Medical University's and Warsaw Institute of Psychiatry and Neurology Ethics Committees. Written informed consent from the participants' legal guardian/next of kin was not required to participate in this study in accordance with the national legislation and the institutional requirements.

Author contributions

ML, PG, and MK: conceptualization and methodology. PG, ML, and MJK: investigation original draft preparation. BW, WW, SK, TS, and WJ: review and editing. All authors contributed to formal analysis. All authors contributed to the article and approved the submitted version.

Funding

This research was supported by the grand of Wroclaw Medical University (SUBZ.A422.22.014).

Acknowledgments

We thank Łukasz Bratos for the help with the numerical calculations.

Conflict of interest

The authors declare that the research was conducted in the absence of any commercial or financial relationships that could be construed as a potential conflict of interest.

Publisher's note

All claims expressed in this article are solely those of the authors and do not necessarily represent those of their affiliated organizations, or those of the publisher, the editors and the reviewers. Any product that may be evaluated in this article, or claim that may be made by its manufacturer, is not guaranteed or endorsed by the publisher.

Supplementary material

The Supplementary Material for this article can be found online at: https://www.frontiersin.org/articles/10.3389/fninf.2023.1169584/full#supplementary-material

References

Aarabi, A., Wallois, F., and Grebe, R. (2008). Does spatiotemporal synchronization of EEG change prior to absence seizures? *Brain Res.* 1188, 207–221. doi: 10.1016/j.brainres.2007.10.048

Addison, P. S. (2017). *The Illustrated Wavelet Transform Handbook: Introductory Theory and Applications in Science, Engineering, Medicine and Finance*. Boca Raton, FL: CRC Press.

Addison, P. S. (2018). Introduction to redundancy rules: the continuous wavelet transform comes of age. *Philos. Trans. R. Soc. A Math. Phys. Eng. Sci.* 376, 20170258. doi: 10.1098/rsta.2017.0258

Adeli, H., Zhou, Z., and Dadmehr, N. (2003). Analysis of EEG records in an epileptic patient using wavelet transform. *J. Neurosci. Methods* 123, 69–87. doi: 10.1016/S0165-0270(02)00340-0

Akman, C. I., Montenegro, M. A., Jacob, S., Eck, K., Chiriboga, C., and Gilliam, F. (2009). Seizure frequency in children with epilepsy: factors influencing accuracy and parental awareness. *Seizure* 18, 524–529. doi: 10.1016/j.seizure.2009.05.009

Altenburg, J., Vermeulen, R. J., Strijers, R. L., Fetter, W. P., and Stam, C. J. (2003). Seizure detection in the neonatal EEG with synchronization likelihood. *Clin. Neurophysiol.* 114, 50–55. doi: 10.1016/S1388-2457(02)00322-X

Asadi-Pooya, A. A., Emami, M., and Sperling, M. R. (2013). A clinical study of syndromes of idiopathic (genetic) generalized epilepsy. *J. Neurol. Sci.* 324, 113–117. doi: 10.1016/j.jns.2012.10.014

Bauquier, S. H., Lai, A., Jiang, J. L., Sui, Y., and Cook, M. J. (2015). Evaluation of an automated spike-and-wave complex detection algorithm in the EEG from a rat model of absence epilepsy. *Neurosci. Bull.* 31, 601–610. doi: 10.1007/s12264-015-1553-5

Dan, J., Vandendriessche, B., Paesschen, W. V., Weckhuysen, D., and Bertrand, A. (2020). Computationally-efficient algorithm for real-time absence seizure detection in wearable electroencephalography. *Int. J. Neural Syst.* 30, 2050035. doi: 10.1142/S0129065720500355

Dominguez, L. G., Wennberg, R. A., Gaetz, W., Cheyne, D., Snead, O. C., and Velazquez, J. L. P. (2005). Enhanced synchrony in epileptiform activity? Local versus distant phase synchronization in generalized seizures. *J. Neurosci.* 25, 8077–8084. doi: 10.1523/JNEUROSCI.1046-05.2005

Duun-Henriksen, J., Madsen, R. E., Remvig, L. S., Thomsen, C. E., Sorensen, H. B., and Kjaer, T. W. (2012). Automatic detection of childhood absence epilepsy seizures: toward a monitoring device. *Pediatr. Neurol.* 46, 287–292. doi: 10.1016/j.pediatrneurol.2012.02.018

Fisher, R. S., Boas, W. V. E., Blume, W., Elger, C., Genton, P., Lee, P., et al. (2005). Epileptic seizures and epilepsy: definitions proposed by the international league against epilepsy (ILAE) and the international bureau for epilepsy (IBE). *Epilepsia* 46, 470–472. doi: 10.1111/j.0013-9580.2005.66104.x

Glaba, P., Latka, M., Krause, M. J., Kroczka, S., Kuryło, M., Kaczorowska-Frontczak, M., et al. (2021). Absence seizure detection algorithm for portable EEG devices. *Front. Neurol.* 12, 685814. doi: 10.3389/fneur.2021.685814

Glauser, T. A., Cnaan, A., Shinnar, S., Hirtz, D. G., Dlugos, D., Masur, D., et al. (2013). Ethosuximide, valproic acid, and lamotrigine in childhood absence epilepsy: initial monotherapy outcomes at 12 months. *Epilepsia.* 54, 141–155.

Grubov, V., Sitnikova, E., Pavlov, A., Koronovskii, A., and Hramov, A. (2017). Recognizing of stereotypic patterns in epileptic EEG using empirical modes and wavelets. *Phys. A Stat. Mech. Appl.* 486, 206–217. doi: 10.1016/j.physa.2017.05.091

Hirsch, E., French, J., Scheffer, I. E., Bogacz, A., Alsaadi, T., Sperling, M. R., et al. (2022). Ilae definition of the idiopathic generalized epilepsy syndromes: position statement by the ILAE task force on nosology and definitions. *Epilepsia* 63, 1475–1499. doi: 10.1111/epi.17236

Japaridze, G., Loeckx, D., Buckinx, T., Armand Larsen, S., Proost, R., Jansen, K., et al. (2022). Automated detection of absence seizures using a wearable electroencephalographic device: a phase 3 validation study and feasibility of automated behavioral testing. *Epilepsia*. doi: 10.1111/epi.17200

Jiruska, P., De Curtis, M., Jefferys, J. G., Schevon, C. A., Schiff, S. J., and Schindler, K. (2013). Synchronization and desynchronization in epilepsy: controversies and hypotheses. *J. Physiol.* 591, 787–797. doi: 10.1113/jphysiol.2012.239590

Keilson, M. J., Hauser, W. A., Magrill, J. P., and Tepperberg, J. (1987). Ambulatory cassette EEG in absence epilepsy. *Pediatr. Neurol.* 3, 273–276.

Kjaer, T. W., Sorensen, H. B., Groenborg, S., Pedersen, C. R., and Duun-Henriksen, J. (2017). Detection of paroxysms in long-term, single-channel EEG-monitoring of patients with typical absence seizures. *IEEE J. Transl. Eng. Health Med.* 5, 1–8. doi: 10.1109/JTEHM.2017.2649491

Krigolson, O. E., Williams, C. C., Norton, A., Hassall, C. D., and Colino, F. L. (2017). Choosing muse: validation of a low-cost, portable EEG system for erp research. *Front. Neurosci.* 11, 109. doi: 10.3389/fnins.2017.00109

Lachaux, J.-P., Rodriguez, E., Martinerie, J., and Varela, F. J. (1999). Measuring phase synchrony in brain signals. *Hum. Brain Mapp.* 8, 194–208.

Latka, M., Turalska, M., Glaubic-Latka, M., Kolodziej, W., Latka, D., and West, B. J. (2005). Phase dynamics in cerebral autoregulation. *Am. J. Physiol. Heart Circ. Physiol.* 289, H2272–H2279. doi: 10.1152/ajpheart.01307.2004

Majumdar, K., Prasad, P. D., and Verma, S. (2014). Synchronization implies seizure or seizure implies synchronization? *Brain Topogr.* 27, 112–122. doi: 10.1007/s10548-013-0284-z

Mallat, S. (1999). *A Wavelet Tour of Signal Processing*. San Diego, CA: Elsevier.

MATLAB (2022). *version 9.13.0.2049777 (R2022a)*. The MathWorks Inc., Natick, MA.

Ovchinnikov, A., Lüttjohann, A., Hramov, A., and Van Luijtelaar, G. (2010). An algorithm for real-time detection of spike-wave discharges in rodents. *J. Neurosci. Methods* 194, 172–178. doi: 10.1016/j.jneumeth.2010.09.017

Petersen, E. B., Duun-Henriksen, J., Mazzaretto, A., Kjær, T. W., Thomsen, C. E., and Sorensen, H. B. (2011). "Generic single-channel detection of absence seizures," in *2011 Annual International Conference of the IEEE Engineering in Medicine and Biology Society* (Boston, MA: IEEE), 4820–4823.

Pu, L., Lion, K. M., Todorovic, M., and Moyle, W. (2021). Portable EEG monitoring for older adults with dementia and chronic pain-a feasibility study. *Geriatr. Nurs.* 42, 124–128. doi: 10.1016/j.gerinurse.2020.12.008

Quiroga, R. Q., Kraskov, A., Kreuz, T., and Grassberger, P. (2002). Performance of different synchronization measures in real data: a case study on electroencephalographic signals. *Phys. Rev. E* 65, 041903. doi: 10.1103/PhysRevE.65.041903

Sadleir, L. G., Scheffer, I. E., Smith, S., Carstensen, B., Farrell, K., and Connolly, M. B. (2009). EEG features of absence seizures in idiopathic generalized epilepsy: impact of syndrome, age, and state. *Epilepsia* 50, 1572–1578. doi: 10.1111/j.1528-1167.2008.02001.x

Schomer, D. L. and da Silva, F. L. (2018). *Niedermeyer's Electroencephalography: Basic Principles, Clinical Applications, and Related Fields*. Oxford: Oxford University Press.

Sitnikova, E., Hramov, A. E., Koronovsky, A. A., and van Luijtelaar, G. (2009). Sleep spindles and spike–wave discharges in EEG: their generic features, similarities

and distinctions disclosed with fourier transform and continuous wavelet analysis. *J. Neurosci. Methods* 180, 304–316. doi: 10.1016/j.jneumeth.2009.04.006

Slooter, A., Vriens, E., Leijten, F., Spijkstra, J., Girbes, A., van Huffelen, A., et al. (2006). Seizure detection in adult ICU patients based on changes in EEG synchronization likelihood. *Neurocrit. Care* 5, 186–192. doi: 10.1385/NCC:5:3:186

Subasi, A. (2007). Application of adaptive neuro-fuzzy inference system for epileptic seizure detection using wavelet feature extraction. *Comput. Biol. Med.* 37, 227–244. doi: 10.1016/j.compbiomed.2005.12.003

Szaflarski, J. P., DiFrancesco, M., Hirschauer, T., Banks, C., Privitera, M. D., Gotman, J., et al. (2010). Cortical and subcortical contributions to absence seizure onset examined with EEG/fMRI. *Epilepsy Behav.* 18, 404–413. doi: 10.1016/j.yebeh.2010.05.009

Tenneti, S. V., and Vaidyanathan, P. (2018). "Absence seizure detection using ramanujan filter banks," in *2018 52nd Asilomar Conference on Signals, Systems, and Computers* (Pacific Grove, CA: IEEE), 1913–1917.

Xanthopoulos, P., Rebennack, S., Liu, C.-C., Zhang, J., Holmes, G. L., Uthman, B. M., et al. (2010). "A novel wavelet based algorithm for spike and wave detection in absence epilepsy," in *2010 IEEE International Conference on BioInformatics and BioEngineering* (Philadelphia, PA: IEEE), 14–19.

Zeng, K., Yan, J., Wang, Y., Sik, A., Ouyang, G., and Li, X. (2016). Automatic detection of absence seizures with compressive sensing EEG. *Neurocomputing* 171, 497–502. doi: 10.1016/j.neucom.2015.06.076

Zhong, L., Wan, J., Wu, J., He, S., Zhong, X., Huang, Z., and Li, Z. (2022). Temporal and spatial dynamic propagation of electroencephalogram by combining power spectral and synchronization in childhood absence epilepsy. *Front. Neuroinform.* 16, 962466. doi: 10.3389/fninf.2022.962466

Supplementary Material

1 SUPPLEMENTARY DATA

1.1 Figures

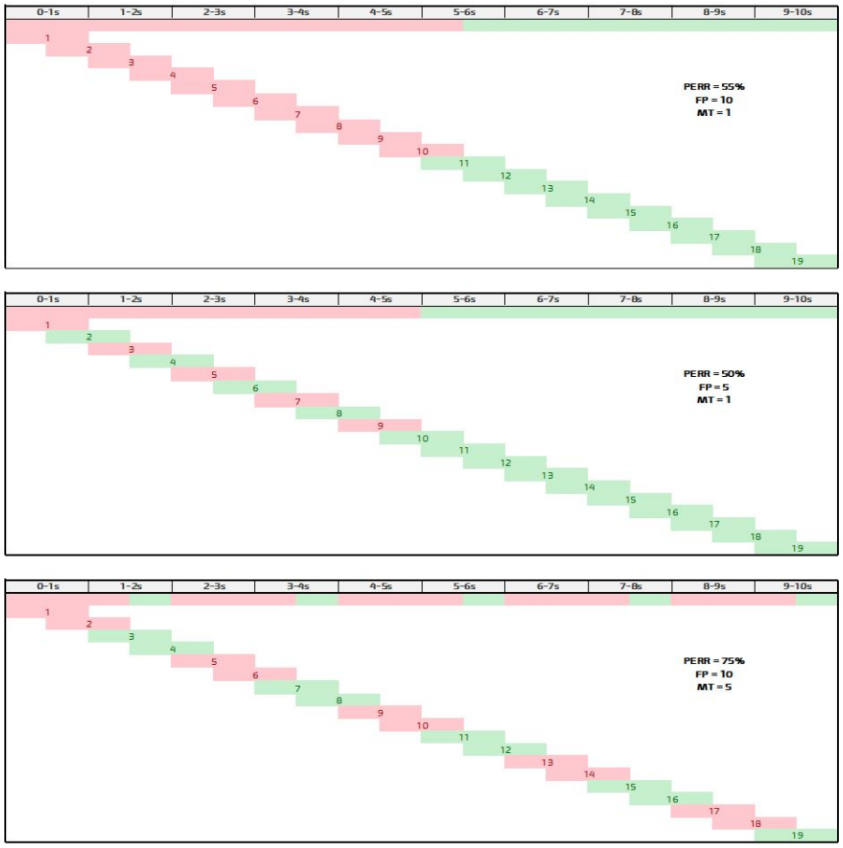

Figure S1: Three theoretical examples elucidate the relationship between the number of erroneously (red) and correctly (green) classified EEG segments and the relative duration of false positives (PERR). MT stands for the number of different trains of misclassified EEG segments. The top bar in each subplot shows the result of classification for 10-s EEG. As in the actual calculations, we used 1 s windows with 0.5 s overlap in this diagram.

A

f_a [Hz] \ f_c [Hz]	0.7	0.8	0.9	1	1.1	1.2	1.3	1.4	1.5
10	0.69	0.73	0.75	0.77	0.79	0.80	0.81	0.82	0.83
11	0.68	0.72	0.75	0.78	0.79	0.81	0.82	0.83	0.83
12	0.65	0.69	0.72	0.75	0.77	0.79	0.80	0.81	0.82
13	0.60	0.65	0.69	0.72	0.74	0.76	0.78	0.79	0.80
14	0.56	0.61	0.65	0.69	0.72	0.74	0.76	0.78	0.79
15	0.52	0.57	0.62	0.66	0.69	0.71	0.74	0.75	0.77

B

f_a [Hz] \ f_c [Hz]	0.7	0.8	0.9	1	1.1	1.2	1.3	1.4	1.5
10	0.31	0.32	0.33	0.34	0.36	0.37	0.38	0.39	0.40
11	0.28	0.29	0.30	0.31	0.32	0.33	0.34	0.35	0.36
12	0.26	0.27	0.28	0.28	0.29	0.31	0.32	0.33	0.34
13	0.24	0.25	0.26	0.27	0.28	0.30	0.31	0.32	0.33
14	0.23	0.24	0.25	0.27	0.28	0.29	0.30	0.31	0.33
15	0.23	0.24	0.25	0.26	0.27	0.29	0.30	0.31	0.32

synchronization [-]: 1.0, 0.9, 0.8, 0.7, 0.6, 0.5, 0.4, 0.3, 0.2, 0.1, 0.0

C

f_a [Hz] \ f_c [Hz]	0.7	0.8	0.9	1	1.1	1.2	1.3	1.4	1.5
10	122.58	128.13	127.27	126.47	119.44	116.22	113.16	110.26	107.50
11	142.86	148.28	150.00	151.61	146.88	145.45	141.18	137.14	130.56
12	150.00	155.56	157.14	167.86	165.52	154.84	150.00	145.45	141.18
13	150.00	160.00	165.38	166.67	164.29	153.33	151.61	146.88	142.42
14	143.48	154.17	160.00	155.56	157.14	155.17	153.33	151.61	139.39
15	128.42	137.50	148.00	153.85	155.56	144.83	146.67	141.94	140.63

difference [%]: 170, 160, 150, 140, 130, 120, 110

Figure S2: We performed the grid search to determine the values of the wavelet parameters f_c and f_a appropriate for seizure detection. The average value of the synchronization index for the interictal and ictal segments is shown in (A) and (B), respectively. (C) shows the relative percentage difference (with respect to the interictal EEG).

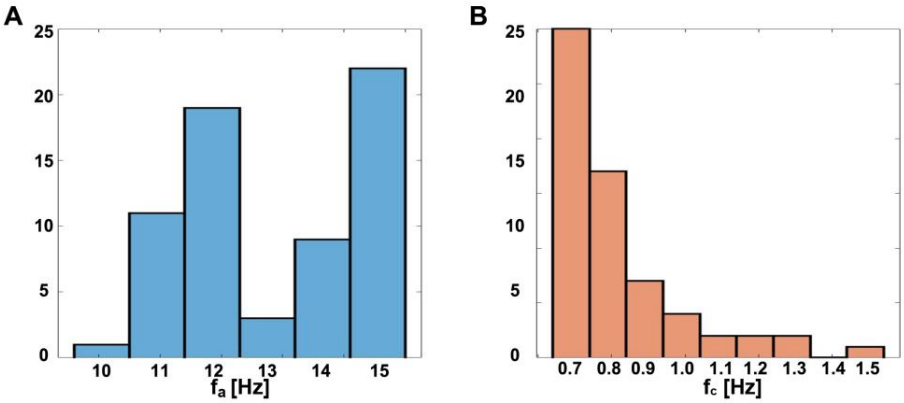

Figure S3: Histograms of: (A) f_a and (B) f_c. The parameters of the complex Morlet wavelets were determined for each patient in the same way as in the calculations from Fig. S2.

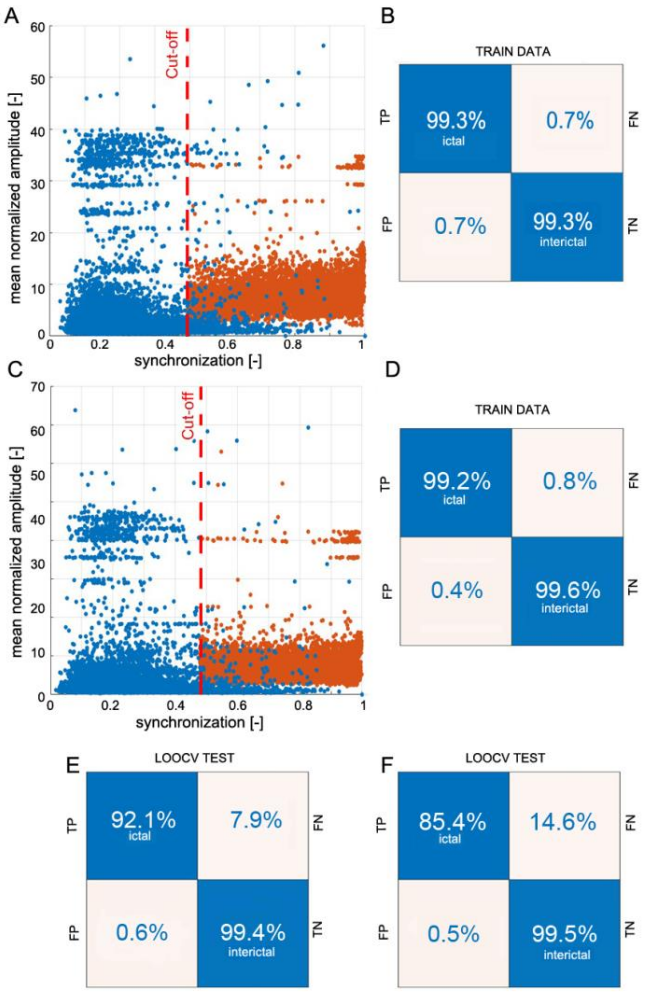

Figure S4: Example of the building of a k-NN seizure detector with the Leave-One-Out Cross Validation (LOOCV) for patient P18. We used the global synchronization index and the mean normalized EEG amplitude as the features. The learning set consisted of randomly chosen interictal segments and segments fully embedded in absences with average synchronization greater than the cutoff value. We used 3:1 ratio of interictal to ictal windows. (A) and (C) show the spread of the data generated for all 19 channels of 10-20 EEG setup (S_{19}) and the subset S_4 (channels Fp1, Fp2, T5, and T6), respectively. The confusion matrices in (B) and (D) show the results of a 10-fold cross-validation. The classifiers were applied to the segmented EEG of patient P18 (1 s windows with 0.5 s overlap). (E) and (F) show the confusion matrices of P18 for S_{19} and S_4, respectively.

1.2 Tables

Table S1. Comparison of the performance of machine learning classifiers used for absence seizure detection. ACC - accuracy; TCV - total cost of validations (number of misclassified windows); PS - prediction speed; TT - training time. For each family of classifiers, we averaged performance metrics generated by the Classification Learner package across different variants.

Class Type	ACC [%]	TCV [-]	PS [obs/s]	TT [s]
Neural Network	98.34	164	188 000	99.2
Nearest Neighbor	98.25	179	94 600	2.60
Decissions Trees	98.23	181	106 000	3.28
SVM	97.68	231	90 500	9.26
Naive Bayes	97.65	290	240 000	1.37
Ensemble	96.66	333	25 400	9.76
Discriminant Analysis	96.30	371	225 000	1.33
Logistic Regression	96.10	384	200 000	2.77

Table S2. Seizure detection performance for each patient. Column labels are as follows: NABS (numbers of absences), ADABS (average duration of absence seizure), DET (number of detected seizures), OVR (overlap of the detected seizures with the actual ones), PERR (the relative duration of false positives), FP (number of false positives), MT (number of distinct trains of misclassified windows)

ID	NABS [-]	ADABS [s]	DET [-]	OVR [%]	PERR [%]	FP [-]	MT [-]
1	6	10.50	6	99.15	0.22	0	0
2	5	13.20	5	96.84	0.22	0	0
3	10	10.33	10	71.82	1.25	20	15
4	8	15.75	8	92.87	0.33	5	4
5	11	11.00	11	92.95	0.78	10	7
6	6	11.33	6	99.20	0.28	5	4
7	2	13.50	2	99.98	0.03	0	0
8	3	15.67	3	98.84	0.54	5	4
9	7	15.00	7	97.40	0.15	2	1
10	5	5.33	4	77.31	0.79	20	9
11	5	8.75	5	78.38	6.89	228	101
12	10	12.22	10	96.72	1.57	43	25
13	3	14.33	3	99.99	0.31	8	3
14	2	7.67	2	96.62	0.35	2	2
15	9	14.11	9	98.36	2.70	67	39
16	4	12.25	4	98.92	0.15	3	3
17	8	14.75	8	56.54	3.42	161	85
18	14	11.14	14	98.15	1.32	35	19
19	12	13.56	12	78.06	0.50	0	0
20	3	19.67	3	99.99	0.34	2	2
21	7	9.29	7	98.46	0.62	10	6
22	4	11.00	4	91.10	0.12	4	3
23	5	12.80	5	96.09	0.10	1	1
24	16	6.36	16	78.98	2.93	105	64
25	4	8.80	4	54.52	0.04	1	1
26	12	7.00	12	62.07	0.79	17	12
27	11	17.20	11	87.20	1.98	56	35
28	1	13.50	1	80.02	0.10	1	1
29	3	18.86	3	95.75	0.61	13	5
30	5	23.20	5	97.00	0.54	5	4
31	3	10.47	3	40.41	0.00	0	0
32	1	8.50	1	78.64	0.41	0	0
33	1	8.70	1	87.56	0.60	4	4
34	1	5.00	1	72.23	0.35	2	2
35	4	8.22	4	63.19	1.28	11	10
36	6	6.58	6	11.46	0.36	4	2
37	3	14.67	3	54.59	0.53	7	3
38	2	9.00	2	70.67	0.33	2	1
39	6	14.19	6	57.59	0.68	41	15
40	2	8.50	2	23.59	0.56	11	6
41	2	10.00	2	92.48	0.12	3	2
42	6	17.10	6	99.99	1.82	47	26
43	7	13.80	7	82.18	1.29	18	9
44	18	3.75	18	89.76	1.37	24	11
45	3	13.00	3	93.60	0.08	1	1
46	10	10.50	10	89.04	0.48	11	8
47	8	11.50	8	69.62	0.21	4	4
48	11	15.18	11	90.74	0.80	32	21
49	8	11.12	8	95.53	0.47	9	6
50	5	9.80	5	76.57	2.41	107	64
51	16	8.82	16	85.08	1.75	22	10
52	4	8.50	4	82.38	0.12	3	3
53	2	35.67	2	98.14	0.03	0	0
54	4	13.50	4	98.88	0.26	6	2
55	4	11.25	4	92.80	0.02	0	0
56	3	7.00	1	11.57	0.00	0	0
57	5	21.66	5	99.17	0.11	1	1
58	5	13.60	5	52.42	0.11	0	0
59	7	9.29	7	99.29	2.24	50	27
60	2	12.50	2	99.94	1.58	34	20
61	2	4.33	2	97.48	0.00	0	0
62	7	16.86	7	99.07	0.57	2	2
63	2	13.50	2	97.34	0.15	2	1
64	9	7.90	9	77.56	5.44	150	116
65	6	6.80	6	88.91	0.12	0	0

Table S3. Seizure detection characteristics for different combinations of wavelet parameters f_a and f_c. The overlap (OVR) of the segments classified as ictal with the absence seizures, the relative duration of false positives (PERR), and the number of false positives (FP) were calculated for patient P1 (all 19 channels were used). The individual grid search for this patient yielded $f_c = 1.3$ Hz and $f_a = 15$ Hz.

	fc [Hz]											
	0.7			0.8			0.9			1.0		
f [Hz]	OVR [%]	PERR [%]	FP [-]	OVR [%]	PERR [%]	FP [-]	OVR [%]	PERR [%]	FP [-]	OVR [%]	PERR [%]	FP [-]
10	98.34	0.28	1	99.17	0.30	1	99.17	0.30	1	99.17	0.33	1
11	98.34	0.28	1	99.16	0.28	1	99.17	0.28	1	99.17	0.31	1
12	98.33	0.22	1	99.16	0.22	1	99.16	0.25	1	**99.15**	**0.22**	**0**
13	98.33	0.22	1	99.16	0.22	1	99.16	0.22	1	99.99	0.22	0
14	97.50	0.22	1	99.16	0.22	1	99.98	0.22	1	99.99	0.22	0
15	95.83	0.20	0	98.32	0.20	0	98.32	0.22	1	99.15	0.22	1
	1.1			**1.2**			**1.3**			**1.4**		
10	99.17	0.31	1	99.99	0.31	1	99.99	0.33	1	99.99	0.33	1
11	99.17	0.33	1	99.17	0.33	1	99.17	0.39	1	99.17	0.39	1
12	99.16	0.22	1	99.15	0.22	1	99.98	0.28	2	99.98	0.28	2
13	99.98	0.22	1	99.99	0.22	1	99.99	0.25	1	99.98	0.25	1
14	99.99	0.22	1	99.98	0.22	1	99.99	0.25	2	99.99	0.25	1
15	99.15	0.22	1	99.99	0.25	2	99.15	0.22	1	99.15	0.22	1

Table S4. Seizure detection characteristics for different combinations of wavelet parameters f_a and f_c. The overlap (OVR) of the segments classified as ictal with the absence seizures, the relative duration of false positives (PERR), and the number of false positives (FP) were calculated for patient P18 (all 19 channels were used). The individual grid search for this patient yielded $f_c = 1.3$ Hz and $f_a = 15$ Hz.

	fc [Hz]											
	0.7			0.8			0.9			1.0		
f [Hz]	OVR [%]	PERR [%]	FP [-]	OVR [%]	PERR [%]	FP [-]	OVR [%]	PERR [%]	FP [-]	OVR [%]	PERR [%]	FP [-]
10	98.99	0.91	17	98.98	1.02	24	98.98	1.00	23	99.31	1.24	31
11	98.65	0.91	20	99.31	1.00	21	99.32	1.13	27	99.31	1.24	30
12	97.99	0.78	19	98.98	0.97	23	98.98	1.02	25	**98.15**	**1.32**	**35**
13	95.66	0.65	16	96.99	0.85	22	97.99	1.10	29	98.65	1.10	28
14	93.00	0.61	17	95.99	0.72	19	96.66	0.87	22	97.32	1.08	28
15	91.01	0.61	17	94.99	0.67	18	96.00	0.76	21	96.99	0.87	24
	1.1			**1.2**			**1.3**			**1.4**		
10	99.65	1.34	35	99.65	1.49	40	99.65	1.50	40	99.65	1.71	46
11	99.65	1.32	32	99.65	1.34	35	99.65	1.69	46	99.65	1.78	48
12	98.99	1.43	37	99.32	1.58	44	99.32	1.71	48	99.32	1.69	48
13	98.65	1.26	34	98.65	1.30	36	98.65	1.43	39	98.32	1.48	42
14	97.99	0.97	24	98.32	1.10	28	98.32	1.23	31	97.99	1.24	33
15	98.32	1.02	26	98.65	1.08	28	98.66	1.24	33	98.99	1.28	34

Table S5. Seizure detection characteristics for different combinations of wavelet parameters f_a and f_c. The overlap (OVR) of the segments classified as ictal with the absence seizures, the relative duration of false positives (PERR), and the number of false positives (FP) were calculated for all patients (19 channels were used). The values are presented as mean ± standard deviation. The grid search presented in Fig. S2 yielded $f_c = 1$ Hz and $f_a = 12$ Hz.

	fc [Hz]											
	0.7			**0.8**			**0.9**			**1.0**		
f [Hz]	**OVR [%]**	**PERR [%]**	**FP [-]**	**OVR [%]**	**PERR [%]**	**FP [-]**	**OVR [%]**	**PERR [%]**	**FP [-]**	**OVR [%]**	**PERR [%]**	**FP [-]**
10	76.09 ± 28.91	0.77 ± 1.14	1251	79.16 ± 27.31	0.87 ± 1.22	1410	81.61 ± 25.20	1.01 ± 1.46	1696	83.77 ± 22.78	1.11 ± 1.57	1859
11	76.28 ± 27.80	0.65 ± 0.99	1026	80.02 ± 24.94	0.75 ± 1.13	1214	82.19 ± 23.60	0.87 ± 1.27	1436	84.22 ± 21.73	1.02 ± 1.45	1683
12	74.30 ± 28.78	0.57 ± 0.90	900	78.17 ± 26.10	0.67 ± 0.97	1080	80.93 ± 23.30	0.76 ± 1.11	1254	**82.90 ± 20.83**	**0.87 ± 1.23**	**1437**
13	69.58 ± 29.65	0.51 ± 0.84	830	75.33 ± 26.87	0.60 ± 0.91	956	78.30 ± 24.70	0.68 ± 0.98	1090	80.39 ± 23.67	0.80 ± 1.14	1298
14	63.54 ± 31.39	0.44 ± 0.74	719	69.87 ± 29.30	0.53 ± 0.84	847	73.84 ± 27.25	0.61 ± 0.89	970	77.52 ± 25.48	0.68 ± 0.97	1107
15	55.87 ± 32.11	0.40 ± 0.69	659	62.90 ± 31.61	0.47 ± 0.75	748	68.62 ± 30.23	0.53 ± 0.81	842	72.94 ± 28.65	0.60 ± 0.88	964
	1.1			**1.2**			**1.3**			**1.4**		
10	85.08 ± 21,81	1.29 ± 1.88	2213	86.30 ± 20.86	1.43 ± 2.07	2469	86.76 ± 20.70	1.57 ± 2.23	2697	87.15 ± 20.49	1.76 ± 2.60	3073
11	85.43 ± 20.30	1.10 ± 1.59	1844	86.64 ± 19.30	1.23 ± 1.84	2098	87.57 ± 18.56	1.39 ± 2.09	2397	87.85 ± 18.48	1.52 ± 2.28	2632
12	84.23 ± 20.49	1.00 ± 1.40	1659	85.14 ± 19.70	1.11 ± 1.58	1874	85.98 ± 19.75	1.24 ± 1.76	2094	86.74 ± 19.64	1.37 ± 1.95	2342
13	82.04 ± 22.85	0.89 ± 1.23	1473	83.47 ± 22.13	0.97 ± 1.34	1615	84.01 ± 22.49	1.12 ± 1.56	1864	85.20 ± 20.78	1.22 ± 1.65	2027
14	79.54 ± 23.82	0.77 ± 1.05	1227	81.78 ± 22.14	0.86 ± 1.16	1400	83.42 ± 20.54	0.94 ± 1.26	1548	84.19 ± 20.54	1.04 ± 1.44	1736
15	76.39 ± 25.86	0.67 ± 0.94	1065	79.12 ± 23.04	0.75 ± 1.00	1213	80.34 ± 22.22	0.82 ± 1.08	1330	81.28 ± 21.52	0.91 ± 1.21	1495

Table S6. False positives detection characteristics for different combinations of wavelet parameters f_a and f_c. The relative duration of false positives (PERR), and the number of false positives (FP) were calculated for all controls (19 channels were used). The values are presented as mean $\pm$ standard deviation. The grid search presented in Fig. S2 yielded $f_c = 1$ Hz and $f_a = 12$ Hz.

	f_c **[Hz]**							
	0.7		**0.8**		**0.9**		**1**	
f_a **[Hz]**	**PERR [%]**	**FP [-]**	**PERR [%]**	**FP [-]**	**PERR [%]**	**FP [-]**	**PERR [%]**	**FP [-]**
10	0.12 ± 0.26	44	0.15 ± 0.26	54	0.21 ± 0.36	74	0.24 ± 0.39	83
11	0.12 ± 0.25	40	0.16 ± 0.31	53	0.17 ± 0.31	57	0.22± 0.36	72
12	0.08 ± 0.14	26	0.10 ± 0.17	32	0.11 ± 0.21	39	**0.12 ± 0.27**	**44**
13	0.05 ± 0.12	18	0.06 ± 0.15	21	0.07 ± 0.16	25	0.09 ± 0.17	31
14	0.04 ± 0.11	13	0.05 ± 0.12	16	0.05 ± 0.13	19	0.07 ± 0.17	25
15	0.03 ± 0.09	11	0.05 ± 0.14	16	0.05 ± 0.13	18	0.07 ± 0.18	25
	1.1		**1.2**		**1.3**		**1.4**	
10	0.25 ± 0.42	93	0.34 ± 0.51	119	0.36 ± 0.54	128	0.44 ± 0.62	153
11	0.22 ± 0.40	77	0.23 ± 0.42	81	0.30± 0.44	104	0.34 ± 0.53	119
12	0.15 ± 0.28	53	0.14 ± 0.27	51	0.18 ± 0.34	68	0.20 ± 0.75	75
13	0.11 ± 0.21	42	0.14 ± 0.22	49	0.25 ± 0.15	55	0.20 ± 0.34	69
14	0.09 ± 0.23	32	0.11 ± 0.24	38	0.13 ± 0.25	45	0.15 ± 0.27	50
15	0.09 ± 0.23	33	0.12 ± 0.27	40	0.13 ± 0.28	44	0.17 ± 0.37	61

11. Podsumowanie i kierunek przyszłych badań

Publikacje wchodzące w skład cyklu odnoszą się bezpośrednio do problemów badawczych przedstawionych w niniejszej rozprawie doktorskiej. Zaproponowane w naszych publikacjach [2, 3] algorytmy detekcji napadów nieświadomości są na tyle skuteczne, że mogą być zastosowane zarówno w rutynowej praktyce klinicznej jak i do monitorowania pacjentów w warunkach domowych. Zostały one przetestowane na największej, w porównaniu do wcześniejszych badań, bazie zapisów EEG. Walidacja algorytmów stanowi pierwszy, najważniejszy krok do implementacji na urządzeniach mobilnych. Długoterminowe monitorowanie EEG jest widocznym trendem w badaniach naukowych poświęconych epilepsji i wpisuje się w koncepcję medycyny spersonalizowanej. Prezentowane wyniki pokazują, że detekcja napadów nieświadomości jest możliwa w warunkach domowych za pomocą nieskomplikowanych, tanich przenośnych aparatów EEG, które współpracują z powszechnie dostępnymi w chwili obecnej smartfonami. Implementuję obecnie system telemedyczny, który umożliwi lekarzom ocenę skuteczności farmakoterapii, precyzyjne miareczkowanie leków w celu minimalizacji efektów ubocznych oraz wyznaczenie momentu przerwania farmakoterapii.

Głównym ograniczeniem wcześniejszych prac poświęconych biomarkerom oraz detekcji napadów nieświadomości jest zbyt mały, niezróżnicowany zbiór zapisów EEG. Opracowanie wiarygodnego biomarkera i wprowadzenie go do procesu diagnozy jest możliwe tylko w wyniku starannie przeprowadzonych badań wieloośrodkowych. Próba opracowania modelu zindywidualizowanej farmakoterapii wymaga regularnych badań EEG w określonych interwałach czasowych z kontrolą przyjmowanych przez pacjenta leków. Potwierdzenie użyteczności zaproponowanych biomarkerów napadów nieświadomości wymaga więc dalszych systematycznych badań.

Kolejnym, naturalnym krokiem badań będzie zbadanie międzynapadowej synchronizacji EEG. Wstępna analiza pozwala na sformułowanie hipotezy mówiącej, że jest ona niższa u pacjentów z napadami nieświadomości w porównaniu do grupy kontrolnej. Wyjaśnienie tego efektu i możliwości jego wykorzystania jako predyktora reakcji na farmakoterapię jest przedmiotem badań, w których uczestniczę.

Napisane podczas studiów doktoranckich oprogramowanie pozwala szybko i efektywnie analizować sygnały EEG pod kątem szukania cech szczególnych dla danej jednostki chorobowej. W przyszłości planuję badania EEG pacjentów z chorobą Wilsona jak również cierpiących na chorobę afektywną jedno- i dwubiegunową.

12. Bibliografia

Aarabi, A., Wallois, F., and Grebe, R. (2008). Does spatiotemporal synchronization of EEG change prior to absence seizures? *Brain Res.* 1188, 207–221.

Abarrategui, B., Parejo-Carbonell, B., García García, M. E., Di Capua, D., and García-Morales, I. (2018). The cognitive phenotype of idiopathic generalized epilepsy. *Epilepsy Behav.* 89, 99–104. doi: 10.1016/j.yebeh.2018.10.007.

Abualsaud, K., Mohamed, A., Khattab, T., Yaacoub, E., Hasna, M., and Guizani, M. (2018). Classification for Imperfect EEG Epileptic Seizure in IoT applications: A Comparative Study. *2018 14th Int. Wirel. Commun. Mob. Comput. Conf. IWCMC 2018*, 364–369. doi: 10.1109/IWCMC.2018.8450279.

Ahmadi, N., Pei, Y., Carrette, E., Aldenkamp, A. P., and Pechenizkiy, M. (2020). EEG-based classification of epilepsy and PNES: EEG microstate and functional brain network features. *Brain Informatics* 7. doi: 10.1186/s40708-020-00107-z.

Akman, C. I., Montenegro, M. A., Jacob, S., Eck, K., Chiriboga, C., and Gilliam, F. (2009). Seizure frequency in children with epilepsy: factors influencing accuracy and parental awareness. *Seizure* 18, 524–529.

Beghi, E., Giussani, G., Nichols, E., Abd-Allah, F., Abdela, J., Abdelalim, A., et al. (2019). Global, regional, and national burden of epilepsy, 1990--2016: a systematic analysis for the Global Burden of Disease Study 2016. *Lancet Neurol.* 18, 357–375.

Bouma, P. A. D., Westendorp, R. G. J., Van Dijk, J. G., Peters, A. C. B., and Brouwer, O. F. (1996). The outcome of absence epilepsy: A meta-analysis. *Neurology* 47, 802–808. doi: 10.1212/WNL.47.3.802.

Camfield, P., and Camfield, C. (2015). Incidence, prevalence and aetiology of seizures and epilepsy in children. *Epileptic Disord.* 17, 117–123.

Casson, A. J. (2019). Wearable EEG and beyond. *Biomed. Eng. Lett.* 9, 53–71. doi: 10.1007/s13534-018-00093-6.

Cavazzuti, G. B. (1980). Epidemiology of Different Types of Epilepsy in School Age Children of Modena, Italy. *Epilepsia* 21, 57–62. doi: 10.1111/j.1528-1157.1980.tb04044.x.

Chavez, M., Le Van Quyen, M., Navarro, V., Baulac, M., and Martinerie, J. (2003). Spatio-temporal dynamic prior to neocortical seizures: amplitude vs. phase couplings. *IEEE Trans. Biomed. Eng.* 50, 571–583. Available at: papers3://publication/uuid/314487F0-0C52-4C59-A5C8-A0B84FB1C03B.

Covanis, A. (2010). "Childhood Absence Epilepsy," in *Atlas of Epilepsies*, eds. Panayiotopoulos and C.P. (London: Springer), 1013–1023.

Dlugos, D., Shinnar, S., Cnaan, A., Hu, F., Moshé, S., Mizrahi, E., et al. (2013). Pretreatment EEG in childhood absence epilepsy: associations with attention and treatment outcome. *Neurology* 81, 150–6. doi: 10.1212/WNL.0b013e31829a3373.

Dümpelmann, M. (2019). Early seizure detection for closed loop direct neurostimulation devices in epilepsy. *J. Neural Eng.* 16, 041001. doi: 10.1088/1741-2552/ab094a.

Ein Shoka, A. A., Dessouky, M. M., El-Sayed, A., and Hemdan, E. E. D. (2023). EEG seizure detection: concepts, techniques, challenges, and future trends. *Multimed. Tools Appl.* doi: 10.1007/s11042-023-15052-2.

Elmali, A. D., Auvin, S., Bast, T., Rubboli, G., and Koutroumanidis, M. (2020). How to diagnose and classify idiopathic (genetic) generalized epilepsies. *Epileptic Disord.* 22, 399–420. doi: 10.1684/epd.2020.1192.

Engel, J., Bragin, A., and Staba, R. (2018). Nonictal EEG biomarkers for diagnosis and treatment. *Epilepsia Open* 3, 120–126. doi: 10.1002/epi4.12233.

Engel, J., and da Silva, F. L. (2012). High-frequency oscillations - where we are and where we need to go. *Prog. Neurobiol.* 98, 316–318. doi: 10.1016/J.PNEUROBIO.2012.02.001.

Faust, O., Acharya, U. R., Adeli, H., and Adeli, A. (2015). Wavelet-based EEG processing for computer-aided seizure detection and epilepsy diagnosis. *Seizure* 26, 56–64.

Fedio, P., and Mirsky, A. F. (1969). Selective intellectual deficits in children with temporal lobe or centrencephalic epilepsy. *Neuropsychologia* 7, 287–300. doi: 10.1016/0028-3932(69)90054-2.

Fisher, R. S., Boas, W. V. E., Blume, W., Elger, C., Genton, P., Lee, P., et al. (2005). Epileptic seizures and epilepsy: definitions proposed by the International League Against Epilepsy (ILAE) and the International Bureau for Epilepsy (IBE). *Epilepsia* 46, 470–472.

Fisher, R. S., and Velasco, A. L. (2014). Electrical brain stimulation for epilepsy. *Nat. Rev. Neurol.* 10, 261–270. doi: 10.1038/nrneurol.2014.59.

Gallotto, S., and Seeck, M. (2023). EEG biomarker candidates for the identification of epilepsy. *Clin. Neurophysiol. Pract.* 8, 32–41. doi: 10.1016/j.cnp.2022.11.004.

Glauser, T. A., Cnaan, A., Shinnar, S., Hirtz, D. G., Dlugos, D., Masur, D., et al. (2013). Ethosuximide, valproic acid, and lamotrigine in childhood absence epilepsy: initial monotherapy outcomes at 12 months. *Epilepsia* 54, 141–155.

Gruenbaum, B. F., Sandhu, M. R. S., Bertasi, R. A. O., Bertasi, T. G. O., Schonwald, A., Kurup, A., et al. (2021). Absence seizures and their relationship to depression and anxiety: Evidence for bidirectionality. *Epilepsia* 62, 1041–1056. doi: 10.1111/epi.16862.

Guerrini, R. (2006). Epilepsy in children. *Lancet* 367, 499–524. doi: 10.1016/S0140-6736(06)68182-8.

Henkin, Y., Sadeh, M., Kivity, S., Shabtai, E., Kishon-Rabin, L., and Gadoth, N. (2005). Cognitive function in idiopathic generalized epilepsy of childhood. *Dev. Med. Child Neurol.* 47, 126–132. doi: 10.1017/S0012162205000228.

Hirsch, E., French, J., Scheffer, I. E., Bogacz, A., Alsaadi, T., Sperling, M. R., et al. (2022).

ILAE definition of the idiopathic generalized epilepsy syndromes: Position Statement by the ILAE Task Force on Nosology and Definitions. *Epilepsia*.

Inouye, T., Sakamoto, H., Shinosaki, K., Toi, S., and Ukai, S. (1990). Analysis of rapidly changing EEGs before generalized spike and wave complexes. *Electroencephalogr. Clin. Neurophysiol.* 76, 205–221. doi: 10.1016/0013-4694(90)90016-D.

Jacobs, J., LeVan, P., Châtillon, C.-É., Olivier, A., Dubeau, F., and Gotman, J. (2009). High frequency oscillations in intracranial EEGs mark epileptogenicity rather than lesion type. *Brain* 132, 1022–1037. doi: 10.1093/brain/awn351.

Jallon, P., and Latour, P. (2005). Epidemiology of idiopathic generalized epilepsies. *Epilepsia* 46, 10–14. doi: 10.1111/j.1528-1167.2005.00309.x.

Jambaqué, I., Dellatolas, G., Dulac, O., Ponsot, G., and Signoret, J. L. (1993). Verbal and visual memory impairment in childrem with epilepsy. *Neuropsychologia* 31, 1321–1337. doi: 10.1016/0028-3932(93)90101-5.

Keilson, M. J., Hauser, W. A., Magrill, J. P., and Tepperberg, J. (1987). Ambulatory cassette EEG in absence epilepsy. *Pediatr. Neurol.* 3, 273–276.

Khanna, A., Pascual-Leone, A., Michel, C. M., and Farzan, F. (2015). Microstates in resting-state EEG: Current status and future directions. *Neurosci. Biobehav. Rev.* 49, 105–113. doi: 10.1016/J.NEUBIOREV.2014.12.010.

Krigolson, O. E., Williams, C. C., Norton, A., Hassall, C. D., and Colino, F. L. (2017). Choosing MUSE: Validation of a low-cost, portable EEG system for ERP research. *Front. Neurosci.* 11, 109.

Krumholz, A. (2009). Driving Issues in Epilepsy: Past, Present, and Future. *Epilepsy Curr.* 9, 31–35. doi: 10.1111/j.1535-7511.2008.01283.x.

Le Van Quyen, M., Adam, C., Baulac, M., Martinerie, J., and Varela, F. J. (1998). Nonlinear interdependencies of EEG signals in human intracranially recorded temporal lobe seizures. *Brain Res.* 792, 24–40. doi: 10.1016/S0006-8993(98)00102-4.

Li, F., Liang, Y., Zhang, L., Yi, C., Liao, Y., Jiang, Y., et al. (2019). Transition of brain networks from an interictal to a preictal state preceding a seizure revealed by scalp EEG network analysis. *Cogn. Neurodyn.* 13, 175–181. doi: 10.1007/s11571-018-09517-6.

Liu, S., Gurses, C., Sha, Z., Quach, M. M., Sencer, A., Bebek, N., et al. (2018). Stereotyped high-frequency oscillations discriminate seizure onset zones and critical functional cortex in focal epilepsy. *Brain* 141, 713–730. doi: 10.1093/brain/awx374.

Lopes da Silva, F. H., Blanes, W., Kalitzin, S. N., Parra, J., Suffczynski, P., and Velis, D. N. (2003a). Dynamical diseases of brain systems: different routes to epileptic seizures. *IEEE Trans. Biomed. Eng.* 50, 540–548. doi: 10.1109/TBME.2003.810703.

Lopes da Silva, F. H., Blanes, W., Parra, J., Velis, D. N., Kalitzin, S. N., and Suffczynski, P. (2003b). Dynamical Diseases of Brain Systems: Different Routes to Epileptic Seizures. *IEEE Trans. Biomed. Eng.* 50, 540–548. doi: 10.1109/TBME.2003.810703.

Majumdar, K., Prasad, P. D., and Verma, S. (2014). Synchronization implies seizure or

seizure implies synchronization? *Brain Topogr.* 27, 112–122.

Marini, C., King, M. A., Archer, J. S., Newton, M. R., and Berkovic, S. F. (2003). Idiopathic generalised epilepsy of adult onset: Clinical syndromes and genetics. *J. Neurol. Neurosurg. Psychiatry* 74, 192–196. doi: 10.1136/jnnp.74.2.192.

Martinerie, J., Adam, C., Le Van Quyen, M., Baulac, M., Clemenceau, S., Renault, B., et al. (1998). Epileptic seizures can be anticipated by non-linear analysis. *Nat. Med.* 4, 1173–1176. doi: 10.1038/2667.

Mormann, F., Andrzejak, R. G., Elger, C. E., and Lehnertz, K. (2007). Seizure prediction: The long and winding road. *Brain* 130, 314–333. doi: 10.1093/brain/awl241.

Mormann, F., Kreuz, T., Andrzejak, R. G., David, P., Lehnertz, K., and Elger, C. E. (2003). Epileptic seizures are preceded by a decrease in synchronization. *Epilepsy Res.* 53, 173–185. doi: 10.1016/S0920-1211(03)00002-0.

Morse, E., Giblin, K., Chung, M. H., Dohle, C., Berg, A. T., and Blumenfeld, H. (2019). Historical trend toward improved long-term outcome in childhood absence epilepsy. *Epilepsy Res.* 152, 7–10. doi: 10.1016/j.eplepsyres.2019.02.013.

Orsini, A., Esposito, M., Perna, D., Bonuccelli, A., Peroni, D., and Striano, P. (2018). Personalized medicine in epilepsy patients. *J. Transl. Genet. Genomics*, 1–18. doi: 10.20517/jtgg.2018.14.

Panayiotopoulos, C. P. (2005). *The epilepsies: seizures, syndromes and management*. Bladon Medical Publishing, Oxfordshire (UK).

Pavone, P., Bianchini, R., Trifiletti, R. R., Incorpora, G., Pavone, A., and Parano, E. (2001). Neuropsychological assessment in children with absence epilepsy. *Neurology* 56, 1047–1051. doi: 10.1212/WNL.56.8.1047.

Pediaditis, M., Tsiknakis, M., Koumakis, L., Karachaliou, M., Voutoufianakis, S., and Vorgia, P. (2012). Vision-based absence seizure detection. in *2012 Annual International Conference of the IEEE Engineering in Medicine and Biology Society* (IEEE), 65–68.

Rozenblat, T., Kraus, D., Mahajnah, M., Goldberg-Stern, H., and Watemberg, N. (2020). Absence seizure provocation during routine EEG: Does position of the child during hyperventilation affect the diagnostic yield? *Seizure* 79, 86–89. doi: 10.1016/j.seizure.2020.03.013.

Sadleir, L. G., Farrell, K., Smith, S., Connolly, M. B., and Scheffer, I. E. (2006). Electroclinical features of absence seizures in childhood absence epilepsy. *Neurology* 67, 413–418. doi: 10.1212/01.wnl.0000228257.60184.82.

Sadleir, L. G., Scheffer, I. E., Smith, S., Carstensen, B., Farrell, K., and Connolly, M. B. (2009). EEG features of absence seizures in idiopathic generalized epilepsy: impact of syndrome, age, and state. *Epilepsia* 50, 1572–1578.

Schomer, D. L., and Lopes da Silva, F. H. (2018). *Niedermeyer's Electroencephalography: Basic Principles, Clinical Applications, and Related Fields*. 7th ed. Oxford University Press.

Singh, K., and Malhotra, J. (2019). IoT and cloud computing based automatic epileptic seizure detection using HOS features based random forest classification. *J. Ambient Intell. Humaniz. Comput.* doi: 10.1007/s12652-019-01613-7.

Siren, A., Eriksson, K., Jalava, H., Kilpinen-Loisa, P., and Koivikko, M. (2002). Idiopathic generalised epilepsies with 3 Hz and faster spike wave discharges: A population-based study with evaluation and long-term follow-up in 71 patients. *Epileptic Disord.* 4, 209–16. Available at: https://www.jle.com/fr/revues/epd/e-docs/idiopathic_generalised_epilepsies_with_3_hz_and_faster_spike_wave_discharges_a_population_based_study_with_evaluation_and_long_term_follow_up_in_71_patients_110017/article.phtml?tab=texte [Accessed June 9, 2023].

Sirén, A., Kylliäinen, A., Tenhunen, M., Hirvonen, K., Riita, T., and Koivikko, M. (2007). Beneficial effects of antiepileptic medication on absence seizures and cognitive functioning in children. *Epilepsy Behav.* 11, 85–91. doi: 10.1016/j.yebeh.2007.04.009.

Sugden, R. J., Pham-kim-nghiem-phu, V. L., Campbell, I., and Leon, A. (2023). Remote collection of electrophysiological data with brain wearables : opportunities and challenges.

van Luijtelaar, G., Lüttjohann, A., Makarov, V. V., Maksimenko, V. A., Koronovskii, A. A., and Hramov, A. E. (2016). Methods of automated absence seizure detection, interference by stimulation, and possibilities for prediction in genetic absence models. *J. Neurosci. Methods* 260, 144–158. doi: 10.1016/J.JNEUMETH.2015.07.010.

van Mierlo, P., Höller, Y., Focke, N. K., and Vulliemoz, S. (2019). Network perspectives on epilepsy using EEG/MEG source connectivity. *Front. Neurol.* 10, 1–13. doi: 10.3389/fneur.2019.00721.

Verhoeven, T., Coito, A., Plomp, G., Thomschewski, A., Pittau, F., Trinka, E., et al. (2018). Automated diagnosis of temporal lobe epilepsy in the absence of interictal spikes. *NeuroImage Clin.* 17, 10–15. doi: 10.1016/j.nicl.2017.09.021.

Vorderwülbecke, B. J., Kowski, A. B., Kirschbaum, A., Merkle, H., Senf, P., Janz, D., et al. (2017). Long-term outcome in adolescent-onset generalized genetic epilepsies. *Epilepsia* 58, 1244–1250. doi: 10.1111/epi.13761.

Walker, L. E., Mirza, N., Yip, V. L. M., Marson, A. G., and Pirmohamed, M. (2015). Personalized medicine approaches in epilepsy. *J. Intern. Med.* 277, 218–234. doi: 10.1111/joim.12322.

Wang, L., Wang, C., Fu, F., Yu, X., Guo, H., Xu, C., et al. (2011). Temporal lobe seizure prediction based on a complex Gaussian wavelet. *Clin. Neurophysiol.* 122, 656–663. doi: 10.1016/J.CLINPH.2010.09.018.

Wilke, C., Worrell, G., and He, B. (2011). Graph analysis of epileptogenic networks in human partial epilepsy. *Epilepsia* 52, 84–93. doi: 10.1111/j.1528-1167.2010.02785.x.

Wirrell, E. C., Grossardt, B. R., Wong-Kisiel, L. C. L., and Nickels, K. C. (2011). Incidence and classification of new-onset epilepsy and epilepsy syndromes in children in Olmsted County, Minnesota from 1980 to 2004: a population-based study. *Epilepsy Res.* 95, 110–

118.

YIN, Y., Zeng, Y., Chen, X., and Fan, Y. (2016). The internet of things in healthcare: An overview. *J. Ind. Inf. Integr.* 1, 3–13. doi: 10.1016/J.JII.2016.03.004.

Yuan, Y., Xun, G., Jia, K., and Zhang, A. (2019). A multi-view deep learning framework for EEG seizure detection. *IEEE J. Biomed. Heal. Informatics* 23, 83–94. doi: 10.1109/JBHI.2018.2871678.

Zenteno, J. F. T. (2007). Generalized Seizures: From Clinical Phenomenology to Underlying Systems and Networks. First Edition. 2006. Edited by Edouard Hirsch, Frederick Andermann, Patrick Chauvel, Jerome Engel, Fernando Lopes da Silva. Published by John Libbey Eurotext Limited. 320 pages. Price C$120. *Can. J. Neurol. Sci.* 34, 1–320. doi: 10.1017/S0317167100116725.

Zheng, Y., Wang, G., Li, K., Bao, G., and Wang, J. (2014). Epileptic seizure prediction using phase synchronization based on bivariate empirical mode decomposition. *Clin. Neurophysiol.* 125, 1104–1111.

Zijlmans, M., Jacobs, J., Zelmann, R., Dubeau, F., and Gotman, J. (2009). High-frequency oscillations mirror disease activity in patients with epilepsy. *Neurology* 72, 979 LP – 986. doi: 10.1212/01.wnl.0000344402.20334.81.

13. Dorobek naukowy

13.1 Publikacje

[1] Glaba P, Latka M, Krause MJ, Kuryło M, Jernajczyk W, Walas W and West BJ (2020) *Changes in Interictal Pretreatment and Posttreatment EEG in Childhood Absence Epilepsy*. Front. Neurosci. 14:196.
doi: 10.3389/fnins.2020.00196

[2] Glaba P, Latka M, Krause MJ, Kroczka S, Kuryło M, Kaczorowska-Frontczak M, Walas W, Jernajczyk W, Sebzda T and West BJ (2021) *Absence Seizure Detection Algorithm for Portable EEG Devices. Front*. Neurol. 12:685814.
doi: 10.3389/fneur.2021.685814

[3] Glaba P, Latka M, Krause MJ, Kroczka S, Kuryło M, Kaczorowska-Frontczak M, Walas W, Jernajczyk W, Sebzda T and West BJ (2023) *EEG Phase Synchronization During Absence Seizures*. Front. Neuroinform. Volume 17 -2023.
doi: 10.3389/fninf.2023.1169584

13.2 Konferencje

epiXchange 2018, Brussels, Belgium, 23rd May 2018r, poster: *EEG connectivity in patients with absence seizures*.

13th European Congress on Epileptology Vienna, Austria, 26th-30th August 2018, poster: *EEG functional connectivity during absence seizure*.

4th International Congress on Mobile Health and Digital Technology in Epilepsy, Lausanne, Switzerland, 11st-13rd October 2023, poster: *Absence seizure detection and characterization* (Accepted on May 16th, 2023).